

Alma Mater Studiorum – Università di Bologna

DOTTORATO DI RICERCA IN ONCOLOGIA E PATOLOGIA SPERIMENTALE  
XXIX Ciclo

Settore Concorsuale di afferenza: 06/A2  
Settore Scientifico disciplinare: MED/04

CHARACTERIZATION AND CYTOTOXIC MECHANISMS  
OF TOXIC AND NON-TOXIC TYPE 2 RIBOSOME-  
INACTIVATING PROTEINS

Presentata da: **Dott.ssa Stefania Maiello**

Coordinatore Dottorato

**Prof. Pier-Luigi Lollini**

Relatore

**Prof. Andrea Bolognesi**

DIPARTIMENTO DI MEDICINA SPECIALISTICA, DIAGNOSTICA E SPERIMENTALE  
-DIMES  
Esame finale anno 2017



## INDEX

<b><u>Chapter 1: INTRODUCTION</u></b> .....	1
<b>1.1 General properties</b> .....	3
1.1.1 Ribosome-inactivating proteins (RIPs) .....	3
1.1.2 Classification of RIPs.....	4
1.1.3 RIP tridimensional structure .....	8
1.1.4 Interaction of RIPs with cells: mechanism of entry .....	11
<b>1.2 Biological activities of RIPs</b> .....	13
1.2.1 RNA N- glycosylase activity .....	13
1.2.2 Polynucleotide:adenosine glycosylase activity (PNAG) .....	14
1.2.3 Effects on laboratory animals and humans .....	15
1.2.4 Retrograde axonal transport .....	16
1.2.5 RIPs and cell death mechanisms .....	17
1.2.6 Antiviral activity .....	21
<b>1.3 Toxic and non-toxic type 2 RIPs</b> .....	22
1.3.1 Type 2 toxic RIPs from <i>Adenia</i> .....	22
1.3.2 Type 2 non-toxic RIPs from <i>Sambucus</i> .....	24
<b>1.4 RIP employment in experimental and clinical medicine</b> .....	27
1.4.1 Immunotoxins .....	27
1.4.2 Anti-tumor therapy.....	29
1.4.3 Immune disorders.....	30
<b><u>Chapter 2: KIRKIIN: A NEW TOXIC TYPE 2 RIP FROM THE CAUDEX OF ADENIA KIRKII</u></b> .....	33
<b>AIM OF THE PROJECT</b> .....	35
<b>RESULTS AND DISCUSSION</b> .....	38
<b>2.1 Partial purification and characterization of <i>Adenia</i> lectins</b> .....	38
2.1.1 Purification of <i>A. kirkii</i> lectins .....	40
2.1.2 Enzymatic properties .....	42
2.1.2.1 Effects on protein synthesis .....	42
2.1.2.2 rRNA glycosylase activity .....	44
2.1.2.3 Polynucleotide:adenosine glycosylase activity.....	46
2.1.2.4 Endonuclease activity on supercoiled plasmid DNA .....	48
2.1.3 Isoelectric focusing .....	49
2.1.4 Immunological properties .....	50

<b>2.2 Cytotoxic effects in cell cultures</b> .....	53
2.2.1 Inhibition of protein synthesis .....	53
2.2.2 Cell viability assay .....	54
2.2.3 Time-response experiments on NB100 cell line.....	56
<b>2.3. Assessment of apoptosis</b> .....	57
2.3.1. Microscopic analysis .....	57
2.3.2 Cytofluorimetric analysis .....	59
2.3.3 Caspase 3/7 activation .....	60
<b>2.4 Kirkiin amino acid sequence</b> .....	62
2.4.1 Isolation and cloning of the kirkiin gene .....	62
2.4.1.1 Selection of the oligonucleotides for PCR amplification .....	62
2.4.1.2 Molecular cloning and sequencing of genomic DNA frags encoding kirkiin ....	63
2.4.1.3 Molecular cloning and sequencing of a cDNA encoding kirkiin A-chain .....	65
2.4.2. Sequence analysis .....	69
<b>CONCLUSION</b> .....	83

## **Chapter 3: CELL DEATH PATHWAYS INDUCED BY NON-TOXIC TYPE 2 RIPs FROM SAMBUCUS**.....85

<b>AIM OF THE PROJECT</b> .....	87
<b>RESULTS AND DISCUSSION</b> .....	89
<b>3.1. Cell viability assay</b> .....	90
<b>3.2. Assessment of apoptosis</b> .....	91
3.2.1. Microscopic analysis with phase-contrast .....	91
3.2.2 Cytofluorimetric analysis .....	92
3.2.3 Caspase 3/7 activation .....	94
<b>3.3 Evaluation of cytotoxicity by inhibitors of specific cell death pathways</b> 96	
3.3.1. Caspase-dependent apoptosis inhibition by Z-VAD-fmk.....	96
3.3.2 Evaluation of the involvement of necroptosis .....	100
<b>3.4 Cell cycle analysis</b> .....	101
<b>3.5 Assessment of autophagy</b> .....	102
<b>CONCLUSION</b> .....	104

<b><u>Chapter 4: MATERIALS AND METHODS</u></b> .....	105
<b>4.1 Materials</b> .....	107
<b>4.2 Methods</b> .....	111
4.2.1 <i>Adenia</i> lectin purification .....	111
4.2.2. <i>Adenia kirkii</i> lectin purification .....	111
4.2.3. Chemico-physical characterization of lectins .....	112
4.2.4. Haemagglutinating activity .....	112
4.2.5 Enzyme-linked immunosorbent assay (ELISA) .....	112
4.2.6 rRNA glycosylase activity .....	113
4.2.7 Polynucleotide:adenosine glycosylase (PNAG) activity assay .....	114
4.2.8 Endonuclease activity on supercoiled plasmid DNA .....	115
4.2.9 Synthesis of DNA .....	115
4.2.10 Synthesis of cDNA via reverse transcription (RT).....	115
4.2.11 Selection of the oligonucleotides for PCR amplification .....	116
4.2.12 Kirkiin gene amplification .....	117
4.2.13 cDNA and DNA cloning.....	118
4.2.14 Purification of the plasmids .....	119
4.2.15 DNA sequence .....	120
4.2.16 Protein synthesis inhibition assay .....	120
4.2.17 Cell viability assay .....	121
4.2.18 Cell and nuclear morphology.....	123
4.2.19 Analysis of the mitochondrial membrane electrical potential gradient .....	123
4.2.20 Assessment of apoptosis .....	123
4.2.21 Cell cycle analysis by flow cytometry with PI .....	124
4.2.22 Assessment of autophagy.....	125
4.2.23 SDS- PAGE .....	126
4.2.24 RNA electrophoresis on 5% polyacrylamide-7M urea gel.....	126
4.2.25 DNA electrophoresis on agarose gel .....	126
<b><u>BIBLIOGRAPHY</u></b> .....	127



## ABSTRACT

Ribosome inactivating proteins (RIPs) are a family of plant proteins that irreversibly arrest protein synthesis through depurination of rRNA. The anticancer, antiviral and neurotoxic properties allow RIPs to have useful applications in agriculture and in many biomedical fields, including clinical drug development.

Galactose-binding lectins contained in caudices of four *Adenia* species were purified by affinity chromatography on CL Sepharose 6B. All lectins agglutinate human erythrocytes. The lectin from *A. kirkii*, called kirkiin, had the highest toxicity, inhibiting protein synthesis both by cell-free system and by whole cells, and deadenylates mammalian and yeast ribosomes. Kirkiin is highly toxic to cells, in which it induces apoptosis with  $EC_{50}$  (concentration reducing viability by 50%) of  $10^{-14}M$  after 72h. Analysis of the genomic clones encoding kirkiin reveals a high degree of sequence similarity to other type 2 RIPs. Molecular modeling confirmed that kirkiin have a similar structure to ricin. Thus, kirkiin shows all the properties of a toxic type 2 RIP and is amongst the most potent plant toxins.

The pathogenesis of cell intoxication induced by the non-toxic type 2 RIPs from *Sambucus*, ebulin 1 and nigrin b, was investigated in a neuroblastoma-derived cell line (NB100), which showed to be very sensitive to RIPs. Despite the high translational inhibition activity in cell-free systems, both RIPs showed a low cytotoxicity in NB100 cells with respect to both type 1 and type 2 RIPs. The results revealed that the mechanism of cell death induced by *Sambucus* RIPs ( $10^{-8}M$ ) is partly due to caspase-dependent apoptosis and suggest the existence of a further cell death pathway that would be prevalent at the early 24h of intoxication and that is different from necrosis, necroptosis and autophagy. A block of cell cycle can be excluded. After 24h, the apoptotic pathway becomes the main route of cell death.



*Chapter 1*

# **Introduction**



## 1.1 General properties

### 1.1.1 Ribosome-inactivating proteins (RIPs)

Ribosome-inactivating proteins (RIPs) are a family of proteins widely spread in the plant kingdom, purified from different angiosperms, monocots and dicots, but also present in some fungal and bacterial species (Stirpe, 2013). More than 50 species of plants belonging to 17 families have been reported to contain RIPs. The designation RIPs is related to their rRNA N-glycosidase activity, which makes them able to inactivate eukaryotic ribosomes through the removal of one or more adenines from rRNA and other nucleotide substrates, irreversibly blocking the cell protein synthesis and causing death (Barbieri *et al.*, 2003; Walsh *et al.*, 2013).

The biological effects of RIPs have been known since ancient times, such as the abortifacient activity of *Trichosanthes kirillowii* and *Mormordica charantia*. Ricin, extracted from the seeds of *Ricinus communis*, was one of the first RIPs to be discovered in 1888 by Stillmark, who found that the toxin caused erythrocyte agglutination and precipitation of serum proteins (Stillmark, 1888). Subsequently, other plant toxins with similar properties have been identified, such as abrin from *Abrus precatorius* seeds (Martin, 1887). In 1970, Lin and co-workers discovered that these toxins showed a higher toxicity against tumor cells compared to normal cells (Lin *et al.*, 1970). Years later, Stirpe introduced the term RIP for plant proteins able to inactivate animal ribosomes, when enzymatic activity and structure were still unknown (Stirpe, 1982). When their enzymatic activity was clarified, the term RIP was attributed only to proteins capable of catalyzing the endohydrolysis of the N-glycosidic bond at a specific adenine of the 28S rRNA of the large 60S ribosomal subunit (Endo *et al.*, 1987). Other proteins can inactivate or damage ribosomes with different mechanisms, but they are not called RIPs. Later, it has been found that some RIPs can remove more than one adenine residue per ribosome (Barbieri *et al.*, 1994) and even from DNA and other polynucleotides. As a consequence, the name adenine: polynucleotide glycosylase was proposed for these proteins (Barbieri *et al.*, 2001).

The expression level of RIPs in plant tissues is highly variable, ranging from traces to hundreds of milligrams per 100 grams of tissue. In some plants these proteins are expressed in many of examined tissues (roots, leaves, buds, flowers, fruits, seeds, bark, latex, plant cells in culture), while in other plants they are present in a single tissue

(Ferrerias *et al.*, 1993; Girbes *et al.*, 2003). In other cases, RIPs may have a specific localization. Moreover, the expression seems to increase during senescence, in unfavorable conditions (Stirpe *et al.*, 1996) and in virally infected cells (Barbieri *et al.*, 2001).

Despite their wide distribution among plants, the physiological role of RIPs is still unclear. It has been hypothesized a possible defensive mechanism of plants against biotic and abiotic stresses (Nielsen *et al.*, 2001; Polito *et al.*, 2013).

RIPs are not limited to the plant kingdom. Bacterial RIPs include Shiga and Shiga-like toxins are produced by gram-negative pathogenic bacteria as virulence factors (Walsh *et al.*, 2013). RIPs have been also identified in mushrooms, such as  $\alpha$ -sarcin, purified from *Aspergillus giganteus* (Xu *et al.*, 2011).

### **1.1.2 Classification of RIPs**

Studies on the structure and genetics of RIPs allowed identifying their primary structure, as well as information on the mechanism of action. According to their physical characteristics and the presence or absence of a lectin-like chain, RIPs are divided into two groups: type 1 and type 2.

The first group consists of proteins characterized by a single polypeptide chain of about 30 kDa with enzymatic activity. Instead, the second group includes toxins with molecular weight of 60-65 kDa, consisting of two polypeptide chains: an enzymatically active A-chain, with properties similar to type 1 RIPs, linked to a B-chain with lectin properties. The B-chain has strong affinity for sugar moieties of cell surface and can facilitate the entry of the toxin into the cell (Walsh *et al.*, 2013). The two chains are linked by hydrophobic interactions and by at least one disulfide bridge (Girbes *et al.*, 2003).

A third group of RIPs has been identified, which consist of an active chain linked by peptide bond to a second chain whose function is not yet known (Peumans *et al.*, 2001). This group includes only two proteins, b-32 from *Zea mays* (corn) (Walsh *et al.*, 1991) and JIP60 from *Hordeum vulgare* (barley) (Reinbothe *et al.*, 1994) (figure 1.1).

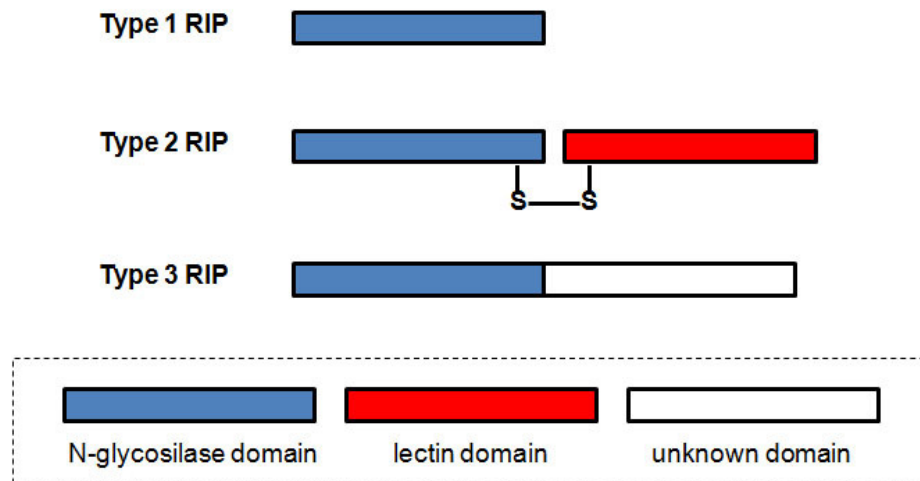


**Fig. 1.1.** RIPs structural classification.

### Type 1 RIPs

These enzymes are widely distributed in nature and have been extracted from plants belonging to families even phylogenetically distant from each other (table 1.1). Notably examples are pokeweed antiviral protein (PAP), saporin (*Saponaria officinalis*), dianthin (*Dianthus caryophyllus*) and momordin (*Momordica charantia*). Type 1 RIPs are basic proteins (usually with a  $pI \geq 9.5$ ). Most of them, with the exception of those from Poaceae, are synthesized from intron-less genes as pre-proteins with a signal peptide, the mature protein and a C-terminal extension (Nielsen *et al.*, 2001). They are synthesized on ER and then follow the secretory pathway to be finally secreted from the cell or targeted to the vacuoles (Hartley and Lord, 2004). For example, PAP is located in the cell wall matrix and in some vacuoles (Ready *et al.*, 1986), while saporin is present in the intercellular spaces, in the paramural region between the primary wall and plasmalemma and within the vacuole of the periplasmic cells (Carzaniga *et al.*, 1994).

**Table 1.1.** Some type 1 RIPs. Data from Schrot *et al.*, 2015.

<b>Caryophyllaceae</b>		
<i>Agrostemma githago</i>	Agrostin 2,5 e 6	seeds
<i>Dianthus barbatus</i>	Dianthin 29	leaves
<i>Dianthus caryophyllus</i>	Dianthin 30 e 32	leaves
<i>Dianthus sinensis</i>	RIP 1,2,3	leaves
<i>Lychnis chalcedonica</i>	Lychnin	seeds
<i>Saponaria ocymoides</i>	Ocymoidine	seeds
<i>Saponaria officinalis</i>	Saporin S5, S6, S8, S9	seeds
	Saporin L1, L2	leaves
	Saporin R1, R2, R3	roots
<i>Vaccaria pyramidata</i>	Pyramidatine	seeds
<b>Cucurbitaceae</b>		
<i>Benincasa hispida</i> var. <i>chieh-qua</i>	Hyspidin	seeds
<i>Bryonia dioica</i>	Bryodin-L	leaves
	Bryodin 1 e 2	roots
<i>Luffa acutangula</i>	Luffaculin	seeds
<i>Luffa aegyptiaca</i>	LRIP (Luffin c)	seeds
<i>Luffa cykubdruca</i>	Luffin a e b	seeds
<i>Luffa cylindrica</i>	Luffin S	seeds
	Luffacilina	seeds
<i>Momordica balsamina</i>	Momordin II	
<i>Momordica charantia</i>	Momordin I	seeds
	$\alpha$ , $\beta$ MMC	seeds
	Charantin	seeds
<i>Momordica cochinchinensis</i>	Momorcochin S	seeds
	Momorcochin R	roots
<i>Trichosanthes cucumerina</i>	Trichoanguin	seeds
<i>Trichosanthes cucumeroides</i>	B trichosanthin	roots
<i>Trichosanthes kirilowii</i>	S-Trichokirin	seeds
	Trichosanthin TAP29	roots
	TCS $\alpha$ , $\beta$ , $\gamma$	roots
<b>Euphorbiaceae</b>		
<i>Croton tiglium</i>	Croton I e II (2, 3)	seeds
<i>Gelonium multiflorum</i>	Gelonin (GAP)	
<i>Jatropha curcas</i>	Curcin 2	seeds
<i>Manihot palmat</i>	Mapalmin	seeds
<i>Manihot utulissima</i>	Manutin 1 e 2	seeds
<b>Phytolaccaceae</b>		
<i>Phytolacca americana</i>	PAP I, PAP II	leaves
	PAP-S1 e S2	seeds
	PAP-R	roots
<i>Phytolacca dioica</i>	PD-S1, S2, S3	seeds
	PD-L1, L2, L3, L4	leaves
<i>Phytolacca dodecera</i>	Dodecandrin	leaves
<i>Phytolacca acinosa</i>	PAP	
<i>Phytolacca insularis</i>	PIP	leaves
	PIP 2	cdna
<b>Lauraceae</b>		
<i>Cinnamomun camphora</i>	Camphorin	seeds

### Type 2 RIPs

These enzymes can be heterodimeric or tetrameric, with a molecular mass of 60 kDa or 120 kDa, respectively. The majority of type 2 RIPs known are heterodimers composed of an A-chain linked to a B-chain, like abrin, modeccin, ricin, volkensin and stenodactylin. The tetrameric protein is the result of the union of two heterodimers by another disulfide bond between the two B-chains, such as Ricinus agglutinin (RCA) (Van Damme *et al.*, 2001).

Ricin is the best-characterized RIP in terms of gene structure. Genomic and transcriptomic analyses show that ricin is synthesized in the developing endosperm of *R. communis* seeds from a single mRNA that encodes a preprotein known as preproricin, which contains the A- and B-chains. The first 35 amino acids of preproricin correspond to the signal peptide important for translocation of the protein to the endoplasmic reticulum (ER) lumen. (Lamb *et al.*, 1985). Here the signal peptide is cleaved and four exposed asparagine residues are N-glycosylated, and five disulfide bridges are formed to obtain the proricin. The linker peptide between the two chain sequences is a signal for vacuolar sorting (Frigerio *et al.*, 2001). Therefore, the proricin is transported via the ER and the Golgi complex into protein storage vacuoles, where the proteolytical removal of the linker peptide occur to form the mature ricin (Lord *et al.*, 1994). It seems that all type 2 RIPs are synthesized in a similar way.

The presence of a lectin B-chain, which facilitates the translocation of the A-chain into the cytosol by interaction with galactosyl residues of membrane glycoproteins and/or glycolipids, makes type 2 RIPs highly toxic. In fact, these RIPs are  $10^4$  - $10^5$  times more toxic than their type 1 counterparts in cultured cells and  $10^3$  times more toxic in animals (Ready *et al.*, 1984; Battelli, 2004). However, a number of type 2 RIPs display low or no cytotoxicity despite possessing the lectin B-chain and strongly inhibiting protein synthesis in free-cell systems. Their low toxicity may be due to low affinity for membrane galactosyl residues which alter their intracellular routing (Girbes *et al.*, 2003; Ferreras *et al.*, 2011).

Toxic type 2 RIPs have only been identified in six plants, which are members of Euphorbiaceae, Fabaceae, Passifloraceae, and Viscaceae, while non-toxic type 2 RIPs have been identified in Euphorbiaceae, Sambucaceae, Lauraceae, Ranunculaceae, Liliaceae and Iridaceae (table 1.2).

**Table 1.2.** Type 2 RIPs. Data from Schrot *et al.*, 2015.

<b>Euphorbiaceae</b>		
<i>Ricinus communis</i>	Ricin (D, E) RCA (Ricinus communis agglutinin)	Seeds
<b>Fabaceae</b>		
<i>Abrus precatorius</i>	Abrin a, b, c, d	Seeds
<i>Abrus pulchellus</i>	Pulchellins	Seeds
<b>Iridaceae</b>		
<i>Iris holleica</i>	IRA-b e IRA-r	bulbs
<b>Lauraceae</b>		
<i>Cinnamomum, camphora</i>	cinnamomin	seeds
<i>Cinnamomum porrectum</i>	porrectin	seeds
<b>Liliaceae</b>		
<i>Poligonatum multiflorum</i>	PMRIPm e PMRIPt	leaves
<b>Passifloraceae</b>		
<i>Adenia volkensis</i>	Volkensin	roots
<i>Adenia stenodactyla</i>	Stenodactylin	caudex
<i>Adenia digitata</i>	Modeccin 4B and 6B	roots
<b>Ranunculaceae</b>		
<i>Eranthis hyemalis</i>	EHL, <i>Eranthis hyemalis lectin</i>	bulbs
<b>Sambucaceae</b>		
<i>Sambucus ebulus</i>	Ebulin I	leaves
	Ebulin r1 e r2	rizhome
	Ebulin f	fruits
<i>Sambucus nigra</i>	Nigrin f, SNA-If	fruits
	Nigrin b, SNAI, SNAI', Basic Nigrin b, SNLRP1 2	barks
	Nigrin I1 e I2, SNAId	leaves
	Nigrin s, SNAIII	seeds
<i>Sambucus racemosa</i>	Basic racemosin	barks
<i>Sambucus sieboldiana</i>	Sieboldin b and SSA	barks
<b>Viscaceae</b>		
<i>Phoradendron californicum</i>	PCL, <i>Phoradendron californicum lectin</i>	leaves
<i>Viscum album</i>	MLI (viscumin), II, III	leaves

### 1.1.3 RIP tridimensional structure

Despite RIPs have been object of a large number of studies, their biological role has never been ascertained. Structure and sequence analyses of RIPs have been performed to better understand the protein function and the relationship between structure and cytotoxicity.

N-terminal sequence of many RIPs are known and the complete sequence and the three-dimensional structure of several RIPs are available. A comparison of amino acid sequences shows similarity between the type 1 and the A-chains of type 2 RIPs and among the B-chains of type 2 RIPs. However, the homology among N-terminal amino acid sequences is higher than C-terminal sequences (Hartley *et al.*, 1996). Ricin was the first RIP analyzed by X-ray diffraction and its structure was published in 1987 (Montfort *et al.*, 1987; Rutenber *et al.*, 1991). The X-ray diffraction data revealed it is composed of two polypeptide chains, an A-chain (RTA) with the enzymatic activity of inactivating ribosomes, linked by a disulphide bond to a lectinic B-chain (RTB) with a galactose-specificity, which allows it to bind to cells (Olsnes and Pihl, 1973). RTA was found to be a globular protein of 267 amino acids folded into three domains with eight  $\alpha$ -helical and six  $\beta$ -strand structures. RTB consists of two homologues globular domains, characterized by twelve antiparallel  $\beta$ -strands connected by  $\beta$ -turns and  $\Omega$  loops. Each domain is organized around two disulfide bridges in a trefoil structure with three lobes arranged in a symmetrical manner (beta trefoil structure) (Villafranca and Robertus, 1981) and is composed of three subdomains ( $1\alpha$ ,  $1\beta$  and  $1\gamma$  for the domain 1 and  $2\alpha$ ,  $2\beta$  and  $2\gamma$  for the domain 2). Only  $1\alpha$  and  $2\gamma$  subdomains show galactoside-binding activity (Rutember *et al.*, 1987).

Despite the amino acid sequence may highly vary, the superimposition of the crystallized structures of RIPs have been shown to share a common fold and the catalytic mechanism of RTA (de Virgilio *et al.*, 2010). To date, the crystal structures reported in Protein Data Bank (PDB) are 153, including same RIPs with amino acid substitutions or different binding compounds (i.e. active site substrates and sugar binding molecules). The structure of type 1 and the A-chains of type 2 RIPs is very similar with the exception of N- and C-terminal, which can vary in length and therefore, assume different conformations (Robertus and Monzingo, 2004). Although the high variability, several amino acid residues are highly conserved among type 1 and the A-chains of type 2 RIPs and seem to be important for the catalytic activity. Based on ricin A-chain sequence, Tyr80, Tyr123 and Trp211 are the most conserved residues directly involved in the binding to the substrate, while Glu177 and Arg180 are involved in the catalytic mechanism responsible of the N-glycosidase activity of the protein. Site-direct mutagenesis studies showed that the mutation of amino acids important for the catalytic activity causes a substantial reduction in activity. Frankel and co-workers found that a positive charge at position Arg180 in RTA is essential for the solubility and the

enzymatic activity (Frankel *et al.*, 1990); the conversion of Glu177 to Gln reduces enzyme activity of about 200-fold (Ready *et al.*, 1991). In the case of saporin-6, Tyr72 (Tyr80 in ricin) mutation is crucial for the catalytic activity of the protein with respect to Tyr120 (Tyr123 in ricin) mutation; the mutants of Glu176 (Glu177 in ricin) and Arg179 (Arg180 in ricin) are 20-fold and 200-fold less active than the wild-type, respectively (Bagga *et al.*, 2003). Interestingly, mutation of Trp208 in saporin (Trp211 in ricin) do not affect its *in vitro* enzymatic activity and cytotoxicity (Bagga *et al.*, 2003), but the same amino acid is important for the structural integrity of PAP (Rajamohan *et al.*, 2000). The target adenine is inserted inside the catalytic cleft, where the architecture of both invariant tyrosine rings is appropriate for sandwiching the aromatic ring of the adenine (Mozingo and Robertus, 1992). The structure of the catalytic site cleft remains constant among RIPs, with the exception of the orientation of some side-chains and the number of hydrogen bonds and water molecules that can be vary. Tyr80 is the most variable residue in the active site, whose side-chain can assume a range of positions (Husain *et al.*, 1994). Thanks to its flexibility, Tyr80 seems to work as a moving door allowing the substrate to enter and assume the best favorable orientation in the active site (Vater *et al.*, 1995; de Virgilio *et al.*, 2010). The adenine-binding site can also hold guanine (in PAP and trichosanthin) or pteric acid (in ricin and PAP) (Yan *et al.*, 1997; Kurinov *et al.*, 1999; Gu and Xia, 2000). This suggests that the enzymatic activity is not directed only toward adenine, but also toward other purine derivatives. Other residues are highly conserved in the type 1 and the A-chains of type 2 RIPs and are mainly involved in the stabilization of the catalytic conformation (Katzin *et al.*, 1991; Hao *et al.*, 2001). Not conserved amino acids in the active site can participate in the binding to the substrate, indicating that different RIPs can bind the adenine target in different ways. A group of highly conserved amino acids has been identified outside of the active site, creating a sort of internal structure that probably gives a support to the RIP catalysis. (Di Maro *et al.*, 2014).

As for the A-chains, the three-dimensional structure of the B-chains of type 2 RIPs is very similar. Nevertheless, there are remarkable differences in amino acids residues of galactose binding sites. This explains the different binding specificity. The 1 $\alpha$  subdomain presents a lower affinity for lactose than 2 $\gamma$  subdomain (Hatakeyama *et al.*, 1986). Moreover, 2 $\gamma$  subdomain can bind the N-acetylgalactosamine (GalNAc), while this binding cannot occur in 1 $\alpha$  subdomain, due to steric hindrance (Rutenber and Robertus, 1991). The main differences in the primary sequence are observed in the

galactose binding residues, especially in Tyr248 in 2 $\gamma$  subdomain. The presence of a positive charge in this domain causes a loss of functionality because the hydrophobic interaction between the pyranose ring of galactose and the aromatic ring of Tyr is lost (Van Damme *et al.*, 2000). X-ray crystallography of ebulin 1 (a non-toxic type 2 RIP) revealed changes in crucial amino acids within the 2 $\gamma$  sugar binding site, which cause a reduction of the affinity for the galactoside residues of cell membrane surface, thus reducing the cytotoxicity of the protein (Ferrerias *et al.*, 2010). This suggests that the carbohydrate-binding properties play an important role in the cytotoxicity of type 2 RIPs. Other highly conserved residues located in the core of the two domains are not involved in the sugar-binding, but they have an important structural function in preserving the symmetry of the domains (Feng *et al.*, 2010).

#### **1.1.4 Interaction of RIPs with cells: mechanism of entry**

Differences in cytotoxicity between type 1 and type 2 RIPs are related to the different interactions of these proteins with cells, which appear to depend on the protein structure. The presence of a lectin B-chain allows type 2 RIPs to interact with galactose-containing glycoproteins and glycolipids on the cell surface, promoting their cell entry (Stirpe, 2004). An alternative mechanism involves the interaction between mannose cell receptors and carbohydrate side chains that are present in the toxin.

Most of the knowledge on cell entry mechanism of type 2 RIPs comes from studies on ricin. Ricin and possibly other type 2 RIPs can reach the endosomal compartment through clathrin-dependent or clathrin-independent mechanisms (Sandvig and van Deurs, 1996). The RIP can bind to receptors located in specialized depressions of cell membrane, giving rise to clathrin-coated vesicles (Giansanti *et al.*, 2010). However, experimental evidence showed that clathrin-dependent endocytosis mechanism is not crucial for toxin cell entry and that ricin mostly acts by RIP-receptor recognition (Puri *et al.*, 2012). Once inside the cell, the RIP could be recycled to cell surface or transported to lysosomes for degradation or translocate to the Golgi apparatus. The different destination might cause different cytotoxicity. The majority of RIPs translocate to the Golgi apparatus and follow retrograde transport to the endoplasmic-reticulum (ER), then enter the cytosol interacting with the ER-associated degradation pathway (ERAD) machinery (Sandvig *et al.*, 2005). Since translocation through the ER membranes causes the unfolding of the protein with loss of activity, it seems that RIPs are able to escape degradation, because they contain a low number of lysines, which

make them resistant to proteolysis (Johannes *et al.*, 2008). In ER lumen the disulfide bond that links the two chains of the RIP is reduced (Mayerhofer *et al.*, 2009). In the case of ricin, only the 5% translocate to the Golgi apparatus (van Deurs *et al.*, 1988) and this represents the portion of toxin responsible of cell intoxication. The non-degraded form of the toxin is excreted by cells and is available for further entry into other cells (Battelli *et al.*, 2004; Hartley and Lord, 2004).

The reduced toxicity of non-toxic type 2 RIPs depends in part on their inefficient ability to translocate within cells. For example, ebulin 1 showed low affinity to membrane galactosyl residues (Pascal *et al.*, 2001; Ferreras *et al.*, 2011). However, the low cytotoxicity of this type of RIPs is also linked to their intracellular destination. As ricin, nigrin b can enter the cell, but it is more rapidly and extensively degraded and excreted from the cell (Battelli *et al.*, 1997). Although volkensin is excreted by cells faster than ricin, it shows higher toxicity. This could be due to the low content of lysines which make it resistant to proteolysis. The most toxic type 2 RIPs stenodactylin and lanceolin have the same intracellular routing of ricin, but their high cytotoxicity seems to be related to their high affinity to receptors, greater uptake and lower proteolysis, which allows the re-uptake of non-degraded RIPs (Battelli *et al.*, 2010). The low cytotoxicity of type 1 RIPs is explained by the absence of the lectin chain, which reduces entry to the cells (Barbieri *et al.*, 1993). The endocytic mechanism of type 1 RIPs is still unclear and different hypotheses have been proposed. They can be internalized similarly to type 2 RIPs, after binding to either the galactosyl residues or the mannose receptor on the cell membrane (Cavallaro *et al.*, 1995). A further hypothesis suggests the cell entry by passive “fluid phase” endocytosis (pinocytosis), which allows the internalization of the toxin without receptor binding (Madan and Ghosh, 1992). This means that the toxicity is lower than type 2 RIPs, but high in cells in which the pinocytosis is a common process, such as macrophages and trophoblast. Saporin follows a Golgi-independent pathway to the cytosol (Vago *et al.*, 2005) and recently, it has been observed its nuclear localization (Bolognesi *et al.*, 2012). Instead, PAP presents retro-translocation mechanism from the ER to the cytosol, similar to type 2 RIPs (Parikh *et al.*, 2005). This observation suggests that type 1 RIPs may also be able to follow the cellular route for misfolded proteins without being degraded by the proteasome. This evidence indicate that the intracellular routing of type 1 RIPs shows diversity within the group or depending on the cell type.

## 1.2 Biological activities of RIPs

### 1.2.1 RNA N- glycosylase activity

RIPs have the common ability to induce an irreversible inactivation of ribosomes, causing the arrest of protein synthesis. This enzymatic RNA N-glycosidase activity, defined ribotoxic activity, is caused by the internalization and activation of the A-chain and for a long time it has been considered as the only enzymatic process caused by RIPs (Endo *et al.*, 1987). To date, it has been discovered that RIPs have a number of different enzymatic activities, most of which can be simply a reflection of their activity on the rRNA, whereas other mechanisms are completely new (Girbes *et al.*, 2004). RIPs are officially classified as rRNA N-glycosylases (EC 3.2.2.22). They recognize a specific and universally conserved region of 14 nucleotides on 28S rRNA, splitting the N-C glycosidic bond between a specific adenine and its ribose in the sequence GAGA on the rRNA. In the case of rat liver ribosomes, this site is A4324 and is positioned within a single-stranded loop called sarcin/ricin, located in the VII domain of the ribosome (Endo *et al.*, 1987) (figure 1.2). This region is the site of interaction of the ribosome with elongation factors. After adenine removal, the apurinic site does not allow the GTPase-dependent binding of elongation factor-1 (EF-1) and elongation factor-2 (EF-2) to the 60S subunit of the ribosome, thus blocking the translation (Stirpe *et al.*, 2006). Sarcin/ricin loop is highly conserved across species, being found in 28S rRNA of rat and *Xenopus*, in 26S rRNA of yeast and in 23S rRNA of *E. coli*. All RIPs exhibit RNA N-glycosylase activity on ribosomes with differences in the specificity for the substrate. N-terminal end of these toxins seems to determine the substrate specificity. In general, type 2 RIPs seem to be more active on animal ribosomes, whereas type 1 RIPs have a wider specificity. For example, the type 1 RIP PAP can remove adenine on ribosomes of plants, yeasts, bacteria and animals. Instead, other RIPs, such as ricin, are very active on ribosomes of animals and yeasts, but their activity is very low or absent on plants and *E. coli* ribosomes (Barbieri *et al.*, 1993).

The activity on and the specificity for the substrate is not only determined by the structural diversity of RIPs, both by the ribosomal proteins, that can facilitate or not the RIP access to the GAGA loop. Several experimental evidence show that ribosomes have different sensitivity to the toxins, such as L9 and L10 ribosomal proteins of rat liver, that are the main binding target of ricin (Vater *et al.*, 1995), while L3 ribosomal protein

of yeast is the binding target of PAP (Hudak *et al.*, 1999). L3 ribosomal protein is highly conserved and this would explain the wide spectrum of specificity of PAP to ribosomes of different organisms.

Although native ribosomes are the favorite substrate, RIPs can also act on naked rRNA (deproteinized) at higher concentrations than those needed to act on intact ribosomes (Endo *et al.*, 1991). It is interesting to note that some RIPs can deadenilate naked rRNA derived from ribosomes on which they normally do not show specificity. For example, ricin A-chain does not act on intact *E. coli* ribosomes, but it is able to deadenilate its naked 23S RNA.

Usually a single adenine is removed from ribosomes, but some RIPs, such as saporin, PAP and trichosanthin, are capable of mediating multiple depurination (Barbieri *et al.*, 1994).

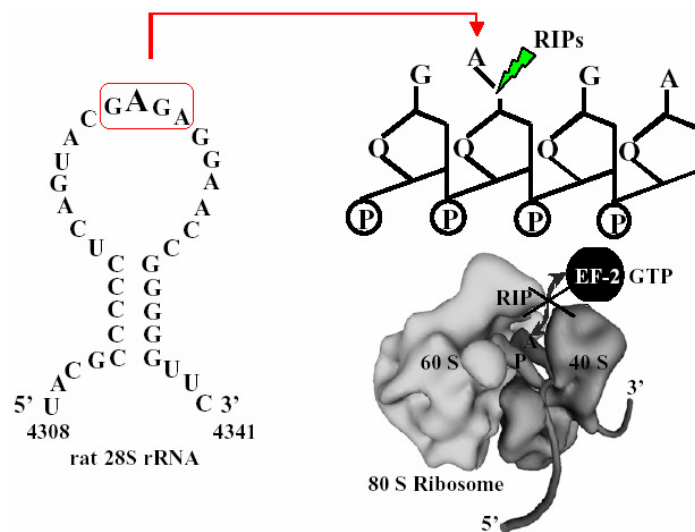


**Fig. 1.2.** Enzymatic mechanism of RIPs.

### 1.2.2 Polynucleotide:adenosine glycosylase activity (PNAG)

Through the development of fluorescence-based HPLC-methods (Zamboni *et al.*, 1989), RIPs were shown to act on other nucleotide substrates, such as herring sperm DNA, tRNA, mRNA and viral RNA (Girbés *et al.*, 2004). Based on the observation that RIPs can deadenylate a range of polynucleotides, the term polynucleotide:adenosine glycosidases (PNAG) was proposed (Barbieri *et al.*, 2001). RIPs show significant differences in PNAG activity, probably due to structural changes and to the type of substrate, as well as to experimental conditions. PNAG activity of all toxic type 2 RIPs

is significantly lower than type 1 RIPs; the reduction of the interchain disulfide bridge does not improve PNAG activity (Barbieri *et al.*, 1997).

Recently, it has been observed that RIPs are able to remove adenine from ADP-ribose chain of the activatedpoly (ADP-ribose) polymerase, which is involved in the DNA repair mechanism (Barbieri *et al.*, 2003). The damage of the polymerase can have a role in the inhibition of DNA repair, which seems to be independent from inhibition of protein synthesis (Sestili *et al.*, 2005). Ricin and PAP also exhibit a guanosine glycosidase activity and can remove guanine residues from both prokaryotic and eukaryotic rRNA (Endo *et al.*, 1987; Rajamohan *et al.*, 1999).

### **1.2.3 Effects on laboratory animals and humans**

The toxicity of RIPs have been investigated in numerous studies both *in vitro* and *in vivo*. Type 2 RIPs are more toxic than type 1 RIPs, thanks to the presence of the B-chain, which promotes the binding to cells and the subsequent internalization.

There is no evidence about the effect of type 1 RIPs in humans. However, trichosanthin showed to induce abortion (Lu and Jin, 1989) with fever, headache and joint pain, that disappear after 48 hours; it also causes skin rashes, muscle pain and neurological problems in HIV-infected patients (Byers *et al.*, 1994; Kahn *et al.*, 1990).

The toxicity of toxic type 2 RIPs and the symptoms produced after ricin poisoning have been known for a long time (Balint, 1974). Low doses of ricin produce digestive tract convulsions, whereas higher doses cause gastrointestinal symptoms, with subsequent hemorrhaging in the stomach and intestine, and degenerative diseases of the heart, liver and kidney, with consequent death. The inhalation of small particles induce severe respiratory symptoms (Balint, 1974).

The effects of RIPs have been mainly studied in rats, in which the onset of severe damages to the liver, kidney and spleen were observed. The precocity and severity of lesions induced by toxic type 2 RIPs is dose-dependent: high doses kill rats in a very short time, even when parenchymal organs have not yet fatal injuries. Ricin, modeccin and volkensin cause severe injuries in liver with consequent necrosis; ricin is the first to damn non-parenchymal cells (Stirpe, 2004), probably because of the cell macrophage activity, which allows to easily identify the toxin. These toxins were found to induce the production of tumor necrosis factor (TNF) and interleukins by human mononuclear cells (Licastro *et al.*, 1993; Hajto *et al.*, 1990; Yamasaki *et al.*, 2004). This could explain the

toxicity observed in animals poisoned with these toxins. Abrin causes necrosis of acinar pancreatic cells (Barbieri *et al.*, 1979). Apoptotic changes were observed in the intestine and lymphoid tissues of the rat poisoned with abrin and ricin (Griffiths *et al.*, 1987). No severe lesions were observed in rats poisoned with viscumin or volkensin (Stirpe, 2004). Always in mice, high doses of nigrin b cause intestinal problems (Girbes *et al.*, 2003). Type 1 RIPs administered to mice at high doses were shown to induce damages in the liver, kidney and spleen, and also necrosis (Battelli *et al.*, 1990).

RIPs are strongly immunogenic. In particular, they show high cross reactivity with RIPs belonging to the same family (Strocchi *et al.*, 1992), but they can cross react also with sera against RIPs of different families, as shown by lanceonin with the anti- PAP R and anti-momordin I sera (Stirpe *et al.*, 2007). The onset of an immune reaction against RIPs was also observed in laboratory personnel working with them (Szalai *et al.*, 2005). These toxins are also present in edible plants, including species that are eaten raw, and their allergenic properties might be the cause of allergies induced by some vegetables (Barbieri *et al.*, 2006; Stirpe *et al.*, 2006).

#### **1.2.4 Retrograde axonal transport**

Some toxic RIPs, including ricin, abrin and viscumin can be retrogradely transported along axons of the peripheral nerves to the cell body, where they inactivate ribosomes, resulting in neuronal death (Wiley and Kline, 2000). This process is called "suicide transport" and several studies have been done for the use of these toxins in the functional anatomy of neurons and to prospect a powerful new experimental strategy for the treatment of neurobiological problems (Harper *et al.*, 1980; Yamamoto *et al.*, 1985; Wiley and Oeltman, 1986; Paul and Devor, 1987). Adenia RIPs, including modeccin, volkensin (Harrison *et al.*, 1990), stenodactylin and lanceolin (Monti *et al.*, 2007) can be retrogradely transported not only along the peripheral nerves, but also along the central nervous system. These properties make Adenia RIPs a useful tool for the study of the functional anatomy of the central nervous system. In addition, lanceolin and stenodactylin displayed neurotoxicity in cells of the cerebellum granules, astrocytes and microglia (Monti *et al.*, 2007). The latter appeared to be the most sensitive to the action of the two toxins, probably due to their efficient internalization and the damage caused by a prolonged inhibition of protein synthesis (Battelli, 2004). The retrograde axonal transport can be used both to induce the degeneration or death of specific neurons and in

immunolesioning experiments, which consist in the use of immunoconjugates made of monoclonal antibodies and RIPs. The most interesting results were obtained with saporin-S6 (type 1 RIP) conjugated to the antibody OX7, specific for rat Thy 1, that is an antigen expressed on the neurons of the central nervous system (Wiley and Kline, 2000). This immunotoxin has been used with great success for the study of nerve connections.

The specific localization in the system central nervous of these toxins, both natural and inserted into artificial hybrid, depends on the vector, that in the case of natural molecules is represented by the B-chain of the RIPs. Therefore, this can prospect a use of the B-chain as a carrier for drugs and growth factors at specific sites difficult to reach.

### **1.2.5 RIPs and cell death mechanisms**

It was initially thought that RIPs cytotoxicity was correlated to protein synthesis inhibition resulting from ribosomal damage, thus causing necrosis in the intoxicated cells. However, subsequent studies demonstrated that RIPs were able to induce apoptosis. In 1987, Griffiths and collaborators were the first to observe the ability of ricin and abrin to induce apoptosis after intramuscular injection into rats (Griffiths *et al.*, 1987) and subsequently, apoptotic events were evidenced in ricin treatment of bovine pulmonary endothelial (Hughes *et al.*, 1996) and human macrophage U937 cells (Kochi and Collier, 1993). Several other RIPs demonstrated to induce apoptosis, such as viscumin (Bussing *et al.*, 1996), saporin (Bergamaschi *et al.*, 1996; Bolognesi *et al.*, 1996), pokeweed anti-viral protein from seeds (PAP-S), momordin (Bolognesi *et al.*, 1996) trichosantin (Zhang *et al.*, 2001; Li *et al.*, 2007), volkensin (Bussing *et al.*, 1998). The ability of type 1 and type 2 RIPs to induce cell death by apoptosis was extensively demonstrated both *in vitro* and *in vivo* models (Rao *et al.*, 2005; Zhang *et al.*, 2012; Fang *et al.*, 2012). Cells exposed to RIP-intoxication undergo apoptosis via different mechanisms, including the loss of mitochondrial transmembrane electrical potential gradient ( $\Delta\psi_m$ ), caspase activation and regulation of apoptotic proteins (Kim *et al.*, 2004; Narayan *et al.*, 2005). However, many questions have remained opened about the mechanism of RIP-induced apoptosis and the relationship between RIP N-glycosidase activity and the apoptotic events. Some reports indicate that protein synthesis inhibition is necessary for triggering apoptosis, but there is evidence that programmed cell death

occurred independent of protein synthesis inhibition. As result, three different hypotheses have been formulated concerning the rRNA N-glycosidase activity of RIPs: (i) indispensable, (ii) necessary but not sufficient or (iii) not relevant for the induction of apoptosis (Das *et al.*, 2012).

Kochi and Collier proposed that apoptotic events became visible only when protein synthesis is inhibited by about 90% (Kochi and Collier, 1993). On the contrary, rhabdomyosarcoma cells exposed to  $\alpha$ -sarcin showed apoptotic characteristics even at concentration below its IC<sub>50</sub>, whereas in the presence of the protein synthesis inhibitor cycloheximide any apoptotic events was induced, even at concentrations that abolished protein synthesis (Olmo *et al.*, 2001). Moreover, in addition of the pan caspase inhibitor Z-VAD-fmk, protein synthesis was not inhibited.

Many temporal/dose and mutagenesis studies evidenced the independence of the two events. For example, in ricin-treated cells morphological changes and the loss of mitochondrial membrane potential were observed before translation was completely inhibited (Soler-Rodríguez *et al.*, 1993). Mutant saporin lacking the inhibition activity of protein synthesis was reported to induce apoptotic cell death through mitochondrial cascade in U937 cells. (Sikriwal *et al.*, 2008). Horrix and co-workers demonstrated that low doses of ricin, volkensin and riproximin were able to induce the apoptotic pathway through activation of unfolded protein response (UPR) genes independently of protein synthesis inhibition (Horrix *et al.*, 2011).

In addition to the inhibition of translation, alternative mechanisms were proposed to explain how RIPs induce apoptosis.

By damaging rRNA, RIPs are capable of activating the ribotoxic stress response through activation of mitogen-activated protein kinases (MAPKs) leading to apoptosis. The first evidence was in 1997 when ricin,  $\alpha$ -sarcin and anisomycin showed the ability to induce the activation of SAPK/ JNK and p38 MAPK in response to specific signaling from damaged 28S rRNA and not simple related to protein synthesis inhibition (Iordanov *et al.*, 1997). How cells detect damaged 28S and trigger signalling through the ribotoxic stress response is still unclear. Mutant shiga toxin 1 lacking RNA N-glycosidase activity, prevented phosphorylation of p38 MAPK and consequently apoptosis in intestinal epithelial cells (HCT). On the contrary, the inhibition of p38 MAPK and JNK activation in HCT cells were able to prevent cell death. Ricin even showed to trigger a similar ribotoxic stress response in the macrophage cell line RAW 264.7 (Smith *et al.*, 2003). Blocking of p38 MAPK resulted in the inhibition of TNF- $\alpha$

release, culminating in apoptosis. This behavior was seen even with modeccin (Higuchi *et al.*, 2003).

Another mechanism proposed to RIP-induced apoptosis is the endoplasmic reticulum (ER) stress and the consequent unfolded protein response (UPR). ER is the intracellular organelle responsible for the correct folding and maturation of newly synthesized secretor and transmembrane proteins. Perturbations in the normal functions of the ER, a process named “ER-stress”, trigger UPR, which acts by arresting protein translation and transcription of genes to restore ER function. If ER dysfunction is severe or prolonged, UPR activates apoptotic signaling cascade. The activator of UPR is the chaperone BiP/Grp78. The presence of an overwhelming load of misfolded proteins induced Grp78 dissociation from its conformational binding state of the transmembrane receptor PERK, IRE1 and ATF6, allowing them to become active. The activated PERK phosphorylates the eIF2 $\alpha$  (eukaryotic translation initiation factor 2 $\alpha$ ), inhibiting translation with consequent growth arrest and promoting the transcription of activating transcription factor 4 (ATF4). Activated ATF6 translocates to the Golgi to activate UPR and ERAD genes, including the transcription factor XBP-1 (X-box binding protein 1), whose mRNA is alternatively spliced by IRE-1 and the resulted product upregulates UPR “stress genes” by directly binding to stress element promoters in the nucleus (Yadav *et al.*, 2014). Human adenocarcinoma cell lines MDA-MB-231 and HCT116 treated with type 2 RIPs were shown to activate genes connected with the UPR. The overexpression of these genes was regulated in a dose dependent manner after RIP treatment and suggested that RIPs induced ER stress, with subsequent apoptosis (Horrix *et al.*, 2011). Also shiga toxin 1 was able to induce activation of the ER stress sensors IRE1, PERK and ATF6 in human monocytic cells, culminating in apoptosis (Lee *et al.*, 2008).

Another mechanism proposed to induce apoptosis is by increasing of the reactive oxygen species (ROS) and by interaction with anti-oxidant proteins. Trichosanthin was shown to induce ROS production in human choriocarcinoma cells (JAR cells) after its interaction with a membrane-bound receptor. Intracellular calcium levels were shown to increase in parallel with ROS levels, suggesting that ROS production in trichosanthin-treated cells might be a consequence of calcium signaling (Zhang *et al.*, 2001). U937 cells treated with mistletoe lectin II (MLII) displayed an increased levels of hydrogen peroxide, which activated the intracellular stress signaling and JNK/SAPK pathways, culminating in apoptosis; in the same study the treatment with a ROS scavenger was

successful in rescue the cells from apoptosis (Kim *et al.*, 2003). Abrin was shown to induce an increase in ROS levels in U937 cells (Bhaskar *et al.*, 2008); the treatment with the ROS scavengers N-Acetyl-l-cysteine (NAC) and Trolox gave a significant protection in abrin-treated Jurkat cells (Saxena *et al.*, 2014). The treatment with ROS scavengers in neuroblastoma cells (NB100) treated with stenodactylin showed strong protective effects, saving the cells from death and allowing the survival of 75–100% of cell population (Polito *et al.*, 2016a).

Abrin was also found to directly interact with antioxidant protein-1 (AOP-1), which is located in the mitochondria protecting them from the action of ROS. The antioxidant activity inhibition of AOP-1 induced by abrin determined the increase of intracellular ROS, with a consequent release of cytochrome c from the mitochondria to the cytosol and activation of caspase-9 and caspase-3 (Shih *et al.*, 2001).

Apoptosis induced by the binding of the B-chain to cell receptors represents a further mechanism proposed for RIPs intoxication. In ricin-treated U937 cells the B-chain induced DNA fragmentation and morphological changes that are typical of apoptosis at a concentration that did not inhibit protein synthesis (Hasewaga *et al.*, 2000). *Sambucus nigra* agglutinins II (SNAII), which consist only of the carbohydrate-binding B-chains, produced caspase-dependent apoptosis in sensitive midgut CF-203 cells at low concentration (Shahidi-Noghabi *et al.*, 2010).

An alternative apoptotic pathway induced by RIPs could be connected to their DNase activity. Several RIPs, such as ricin, cinnamomin, gelonin, saporin-6 and dianthin 30 were shown to introduce specific cleavages into supercoiled DNA (Ling *et al.*, 1994; Roncuzzi and Gasperi-Campani, 1996; Brigotti *et al.*, 2002). Studies on saporin mutant showed that this toxin possessed both RNA glycosidase and genomic DNA fragmentation activity (Bagga *et al.*, 2003). The evidenced nuclear localization of saporin-6 in HeLa cells suggested that one cell death mechanism induced by the toxin could be DNA damage (Bolognesi *et al.*, 2012).

It was also observed that the induction of apoptotic cell death might be caused by RIPs even when they are constituents of immunotoxins (Bolognesi *et al.*, 1996; Polito *et al.*, 2009a).

In addition to apoptosis, the involvement of alternative cell death pathways elicited by RIPs were described. Both caspase-dependent and independent cell death mechanisms have been described for several RIPs. Interestingly, a same toxin can cause more than one death mechanism. For example, in Jurkat cells treated with abrin caspase-dependent

apoptosis was evidenced (Narayanan *et al.*, 2005). Instead, in human B cell line (U266B1) treated with the same toxin, an increase of ROS levels and lysosomal membrane permeabilization were found, whereas apoptosis and caspase activation were not observed. The authors hypothesized the involvement of caspase-independent programmed necrosis (Bora *et al.*, 2010). In human Hodgkin's lymphoma cell line (L540) treated with saporin and ricin, Polito and co-workers proposed a mechanism of cell death that is partially independent of both caspase activation and necrosis (Polito *et al.*, 2009a). The same group demonstrated that stanodactylin can induce multiple cell death pathways, which involve mainly apoptosis, but also necroptosis and the production of free radicals (Polito *et al.*, 2016a).

Finally, these data confirmed that RIPs clearly inhibit protein synthesis. Despite several studies have been conducted in order to elucidate the mechanism through which RIPs trigger apoptosis, many questions remain still unclear.

### **1.2.6 Antiviral activity**

Type 1 and some type 2 RIPs have been shown to possess antiviral activity against plants, fungal and animal viruses. The discovery of the antiviral properties of RIPs dates back to 1925, when Duggar and Armstrong demonstrated that leaf extract of *Phytolacca Americana* gave antiviral protection to tobacco plant (Duggar and Armstrong, 1925). After 50 years, the antiviral factor was extracted and called PAP (Pokeweed Antiviral Protein) (Irvin, 1983). Subsequently, many RIPs were shown to possess antiviral activity against plant viruses (Lodge *et al.*, 1993), fungi (Vivanco *et al.*, 1999), bacteria and animal viruses (Zhou *et al.*, 2000). The exact mechanism of RIP antiviral activity is still not completely understood.

Initially it was thought that RIPs interacted with plant ribosomes of the infected cells, inactivating them with consequent death of the cells and block of viral replication (Fernández-Puentes and Carrasco, 1980). Afterwards, thanks to recombinant techniques, mutated RIPs showed that the ribosome inactivation is not directly involved in antiviral activities and it was suggested that the mechanism of action of RIP consists in the direct deadenylation of viral nucleic acid (Barbieri *et al.*, 1997, Stirpe *et al.*, 2006). For example, PAP mutants expressed in transgenic tobacco plants, show protection against potato virus X (Tumer *et al.*, 1997) and fungal pathogen (Zoubenko *et al.*, 1997); other PAP mutants are able to depurinate HIV-1 RNA (Uckun *et al.*, 2003). PAP also show to

inhibit the production of human T-cell leukemia virus 1 (HTLV-1) (Mansouri *et al.*, 2009). In agriculture, the role of plant defense displayed by RIPs allowed to create transgenic plants resistant to infection by microorganisms. For example, the expression of PAP or trichosanthin protects the plant of tobacco from viral infections, though causing an altered phenotype (Lodge *et al.*, 1993). The separation of the antiviral function from enzymatic activity has been possible by creating mutants able to protect the plant, leaving the phenotype unaltered (Tumer *et al.*, 1997). Thanks to anti-fungal properties of RIPs, even transgenic tobacco plants resistant to infections by fungi have been created with success (Tumer *et al.*, 1999). Many other plants have been transfected with RIP genes, mainly with PAP, trichosanthin, dianthin and barley RIP (Dowd *et al.*, 2003; Rosenblum, 2004). RIPs have been shown to inhibit also animal viruses, for example blocking the viral replication of influenza virus (Tomlinson *et al.*, 1974), poliovirus, herpes simplex virus (Foà-Tomasi *et al.*, 1982) and HIV virus (Zarling *et al.*, 1990).

### **1.3 Toxic and non-toxic type 2 RIPs**

#### **1.3.1 Type 2 toxic RIPs from *Adenia***

*Adenia* genus belonging to Passifloraceae family includes about 100 species that are restricted to the tropics and subtropics, with centers of diversity mostly in Africa, in particular in Madagascar, and in Asia. The genus is characterized by conspicuous leaf glands present in the majority of species, from which the genus derives its name (Hearn, 2006). *Adenia* genus include trees, bushes, grasses, vines and lianas and it is adapted to several habitats, from the desert of Namibia coasts to the rainforest of South Asia. The elder plants have been used since ancient times, especially in traditional African medicine (Akendengue *et al.*, 2005). Many *Adenia* plants are known to contain potent poisons. For example, *Adenia lobata* is used in Nigeria to treat respiratory disorders, syphilis, gonorrhoea and nose cancer (Gill, 1992; Osuagwu and Ibeabuche, 2010), whereas in Ghana it is used for the treatment of diabetes mellitus (Mshana *et al.*, 2000). *Adenia cissampeloides* is used in Zimbabwe for the prevention of malaria (Talkmore *et al.*, 2015) and for the treatment of many diseases, such as gastro-intestinal and liver disorders, anemia, venereal diseases, parasitic infections, pain, depression and madness (Schmelzer and Gurib-Fakim, 2008). Moreover, some *Adenia* species were found to

contain several bioactive constituents. *A. lobata* contains several phytochemicals compounds with therapeutic benefits such as alkaloids, steroidal glycosides, saponins, flavonoids and tannins (Agoreyo *et al.*, 2012). In addition, it also shows anti-hyperglycaemic and antioxidant activity. The presence of phytochemical constituents similar to those of *A. lobata* is probably responsible of *in vitro* anti-plasmodic properties of *A. cissampeloides* (Talkmore *et al.*, 2015).

Some of the highly toxic type 2 RIPs were identified in *Adenia* species: modeccin from the roots of *A. digitata* (Barbieri *et al.*, 1980) and volkensin from the roots of *A. volkensii* (Barbieri *et al.*, 1984) were the first to be extracted; more recently *A. goetzii* lectin, lanceolin and stenodactylin were purified from the caudices of *A. goetzii*, *A. lanceolata* and *Adenia stenodactyla* (Stirpe *et al.*, 2007) (table 1.3). Type 2 RIPs extracted from *Adenia* genus are the most potent plant toxins known, able to irreversibly inhibit protein synthesis and to induce death in cells and in animals at very low doses. In particular, stenodactylin is considered the most potent plant toxin known for its toxicity both in cell cultures and in experimental animals. The peculiarity of *Adenia* toxins is the ability to be transported in a retrograde manner not only along peripheral nerves, such as ricin and abrin, but also within the central nervous system. (Wiley and Stirpe, 1988; Monti *et al.*, 2007). This property could have different medical and biotechnological applications in the field of neuroscience to selectively lesion specific neurons, i.e. in behaviour studies.

*Adenia* RIPs show an intracellular pathway very similar to that of ricin (see section 1.1.4). Their high cytotoxicity has been explained by their high affinity binding to the cell and efficient endocytosis, intracellular routing, partial resistance to proteolysis, and high accumulation into the cell especially in the case of stenodactylin. Lanceolin and stenodactylin have a higher uptake than that of volkensin (Battelli *et al.*, 2010). In addition, after binding to the cell membrane, they do not require the endosomal acidification to enter the cell, but the routing through the Golgi is essential for them. However, modeccin can reach the cytosol either by endosome acidification or by the involvement of nigericin (Ghosh and Wu, 1988).

**Table 1.3.** RIPs and lectins purified from *Adenia* species. (A) IC<sub>50</sub> values for the single A-chain, obtained under reducing conditions (Schrot *et al.*, 2015).

Proteins	Species	Tissues	IC <sub>50</sub>
<b>Type 2 RIPs</b>			
Modeccin = Modeccin 4B	<i>A. digitata</i>	roots	4 µg/mL; 66 ng/mL (A)
Modeccin 6B		roots	0.31 µg/mL
<i>Adenia goetzei</i> lectin	<i>A. goetzei</i>	caudex	55.1 µg/mL; 0.7 µg/mL (A)
Lanceolin	<i>A. lanceolata</i>	caudex	5.2 µg/mL; 1.1 µg/mL (A)
Stenodactylin	<i>A. stenodactyla</i>	caudex	5.6 µg/mL; 0.5 µg/mL
Volkensin	<i>A. volkensis</i>	roots	5 µg/mL; 0.37 nM (A)
<b>Type 2 RIPs candidate</b>			
<i>Adenia ellenbeckii</i> lectin	<i>A. ellenbeckii</i>	caudex	10.1 µg/mL; 1.2 µg/mL (A)
<i>Adenia glauca</i> lectin	<i>A. glauca</i>	caudex	>10 µg/mL; >5 µg/mL (A)
<i>Adenia keramanthus</i> lectin	<i>A. keramanthus</i>	caudex	10.0 µg/mL; 1.1 µg/mL (A)
<i>Adenia spinosa</i> lectin	<i>A. spinosa</i>	caudex	4.7 µg/mL; 0.8 µg/mL (A)
<i>Adenia venenata</i> lectin	<i>A. venenata</i>	caudex	2.4 µg/mL; 0.4 µg/mL (A)
<b>Lectins</b>			
<i>Adenia fruticosa</i> lectin	<i>A. fruticosa</i>	caudex	>100 µg/mL
<i>Adenia racemosa</i> lectin	<i>A. racemosa</i>	caudex	>400 µg/mL

### 1.3.2 Non-toxic type 2 RIPs from *Sambucus*

*Sambucus* genus, belonging to Adoxaceae family, includes shrubs and small trees spread in Europe, Asia, America and Africa (Tejero *et al.*, 2015). The elder plants have been used since ancient times, in particular by Romans for medicinal purposes. *S. nigra* berries have been widely used over the centuries in Europe for the treatment of a wide range of common problems, such as toothache, for ear and eye problems, wounds, skin burns, colics, dysentery, arthritis, rheumatism, fever, epilepsy, and other diseases. (Tejero *et al.*, 2015; Polito *et al.*, 2016b). The remains of seeds and charcoal of *S. ebulus*, *S. nigra* and *S. racemosa*, dating back to the Neolithic and Chalcolithic (Copper Age), have been found in archaeological excavations. It is possible that population of northern Italy (Mariotti-Lippi *et al.*, 2010) and southern France (Martin *et al.*, 2008) used the wild elderberry as a complement to cereals.

*Sambucus* genus consists of about 20 species from which several RIPs were extracted, both type 1 and type 2, and lectins, which can be produced simultaneously in different tissues or in the same tissue of the same plant (table 1.4). The amount of protein expressed in a specific tissue can vary with the development of the plant and during the seasons. For example, ebulin 1, extracted from the leaves of *S. ebulus*, is present in

young plants in higher level than those of SELId lectin; with the development of the plant, the level decrease and disappear during senescence, whereas lectin level increase (Rojo *et al.*, 2003). Nigrin b, extracted from the bark of *S. nigra*, is highly expressed in spring and summer (Ferrerias *et al.*, 2010).

Sambucus RIPs, both type 1 and type 2, are able to depurinate rRNA and to inhibit protein synthesis in a cell-free system constituting of a rabbit reticulocytes lisate with  $IC_{50}$  in the order of nM (Girbes *et al.*, 1993a, b). Type 2 RIPs from Sambucus showed a low cytotoxicity, comparable to that of type 1 RIPs, even though they are endowed with lectin activity and are able to strongly inhibit protein synthesis in cell-free systems. For example, the  $IC_{50}$  values in HeLa cells treated with ebulin 1 and nigrin b were 64.3 and 27.6 nM, respectively, with respect to 0.67 pM observed with ricin (Citores *et al.*, 1996). Toxicity of Sambucus RIPs was also tested in mice, showing a  $LD_{50}$  of 2 and 12 mg/kg for ebulin 1 and nigrin b, respectively, with respect to 0.003 mg/kg observed with ricin (Girbes *et al.*, 1993b).

The low toxicity of non-toxic type 2 RIPs could be due to an inefficient translocation through the plasma membrane or to different intracellular modifications that do not allow them to reach the ribosomes. The interaction of nigrin b and the highly toxic type 2 RIP volkensin with HeLa cells was compared, both showing a similar binding affinity, but lower than that of ricin. This result suggested that the low cytotoxicity of nigrin b might depend on a different intracellular pathway with respect to toxic type 2 RIPs. After internalization into the endosomes, nigrin b is rapidly degraded into the lysosomes and then exocytosed. All nigrin b excreted is totally inactive, whereas a percentage of toxic type 2 RIPs remain active after exocytosis and can be recycled (Battelli *et al.*, 2004). Nigrin b was found to bind different glycoproteins on the plasma membrane and utilize a different intracellular routing than ricin. Moreover, inhibition of protein synthesis by nigrin b seems to be a consequence of the spontaneous translocation of the RIP from the endosome to the cytosol, which occurs when the concentration of the toxin is high, so that it can reach the ribosomes (Ferrerias *et al.*, 2011).

**Table 1.4.** RIPs and lectins purified from *Sambucus* species.(Ferrerias *et al.*, 2011).

<b>Proteins</b>	<b>Species</b>	<b>Tissues</b>
<b>Type 1 RIPs</b>		
Ebulitins $\alpha$ , $\beta$ , $\gamma$	<i>S. ebulus</i>	Leaves
Nigritins f1, f2	<i>S. nigra</i>	Fruits
<b>Heterodimerictype 2 RIPs</b>		
Ebulin l	<i>S. ebulus</i>	Leaves
Ebulin f	<i>S. ebulus</i>	Fruits
Ebulin r1, r2	<i>S. ebulus</i>	Rhizome
Nigrin b, basic nigrin b, SNA I', SNLRPs	<i>S. nigra</i>	Bark
Nigrin l1, l2	<i>S. nigra</i>	Leaves
Nigrin f	<i>S. nigra</i>	Fruits
Nigrin s	<i>S. nigra</i>	Seeds
Sieboldin b	<i>S. sieboldiana</i>	Bark
Basic racemosin b	<i>S. racemosa</i>	Bark
<b>Tetramerictype 2 RIPs</b>		
SEA	<i>S. ebulus</i>	Rhizome
SNA I	<i>S. nigra</i>	Bark
SNAIf	<i>S. nigra</i>	Fruits
SNAflu-I	<i>S. nigra</i>	Flowers
SSA	<i>S. sieboldiana</i>	Bark
SRA	<i>S. racemosa</i>	Bark
<b>Monomericlectins</b>		
SELlm	<i>S. ebulus</i>	Leaves
SEA II	<i>S. ebulus</i>	Rhizome
SNA II	<i>S. nigra</i>	Bark
SNAIm and SNAIVl	<i>S. nigra</i>	Leaves
SNA IV	<i>S. nigra</i>	Fruits
SNA III	<i>S. nigra</i>	Seeds
SSA-b-3 and SSA-b-4	<i>S. sieboldiana</i>	Bark
SRAbm	<i>S. racemosa</i>	Bark
<b>Monomericlectins</b>		
SELld	<i>S. ebulus</i>	Leaves
SELfd	<i>S. ebulus</i>	Fruits
SNAld	<i>S. nigra</i>	Leaves

Studies on the amino acid sequences and a comparison with toxic type 2 RIPs revealed that ebulin l share a homology with ricin A-and B chains of 34% and 48%, respectively (Pascal *et al.*, 2001). X-ray diffraction analysis showed that ebulin l have an overall folding similar to ricin, but different galactose binding properties. In ricin, both 1 $\alpha$  and 2 $\gamma$  subdomains bind galactose and lactose; instead, in ebulin l only 1 $\alpha$  subdomain bind both galactose and lactose in a similar way to ricin, whereas 2 $\gamma$  site is able to bind only

the galactose, but differently from ricin. The orientation and the positioning of galactose within the binding cleft are different and this probably causes steric interference. This could be responsible of the weaker interaction with cells, thus of the low cytotoxicity of ebulin 1 (Ferrerias *et al.*, 2010).

Thanks to their high enzymatic activity and less non-specific toxicity, the non-toxic type 2 RIPs ebulin 1 and nigrin b have been used in preclinical studies in order to reduce the toxic side effects, which are characteristic of the RIP-based therapy. In particular, two immunotoxins have been constructed: the first one directed towards the transferrin receptor, which is highly expressed in some cell lines and in many human tumors (Citores *et al.*, 2002); the second one specific for the endothelial receptor CD105 (endoglin), which is strongly expressed during neoangiogenesis and in vessels of tumor tissues (Benítez *et al.*, 2005; Muñoz *et al.*, 2007). These immunotoxins showed high cytotoxicity with IC<sub>50</sub> value in the picomolar range.

Moreover, mice treated with an intravenous injection of a lethal dose of nigrin b (16 mg/kg), showed intestinal lesions and the disappearance of the intestinal villi and crypts. Sub-lethal doses (5 mg/kg) of the toxin induced the complete recovery of the normal functions nine days after the injection. In particular, apoptotic changes were observed in highly proliferating stem cells of the intestinal crypts (Gayoso *et al.*, 2005). Recently, these apoptotic changes were also observed in mice treated with ebulin 1 (Jiménez *et al.*, 2013).

## **1.4 RIP employment in experimental and clinical medicine**

### **1.4.1 Immunotoxins**

In the medical field, RIPs have been studied for their antitumor activity. Since 1970, several studies evidenced that the toxicity of RIPs, especially ricin, was higher toward cancer cells compared to healthy cells (Lin *et al.*, 1970; Fodstad *et al.*, 1977). This effect is probably due to the higher permeability of the membrane of neoplastic cells compared to that of normal cells, determined by changes in the lipid and protein composition of the tumor cell. Although possessing an efficient cell killing mechanism, they lack selectivity toward cell targets necessary for the therapeutic use. Most of the interest in RIPs in the biomedical field is the possibility of directing them in a selective manner against undesired or harmful cells. This was achieved by linking them to

carriers to obtain conjugates, which specifically recognize antigens or receptors that are expressed on the membrane surface of the targeted cells. These conjugates are defined immunotoxins (ITs) and can be useful to treat cancer and also immunological disorders (Madhumathi and Verma, 2012). The carriers used for conjugation include hormones, growth factors, cytokines, interleukins, antigens and vitamin-binding proteins, but monoclonal and polyclonal antibodies seem to be the most powerful (Bolognesi and Polito, 2004). ITs can be obtained by chemically conjugation of the toxin to an antibody or antibody fragment. It is necessary that the two moieties be conjugated via covalent bond stable in the extracellular environment, in order to allow IT to exert its action. However, this bond has to be reversible, so that it can easily be broken once IT is internalized into the cell. The most used chemical bond for this purpose is the disulfide bridge between cysteine residues, which may be already present in the toxin or chemically inserted. The resulting product is stable but heterogeneous and often not suitable for clinical practice. New generation ITs are synthesized using recombinant DNA techniques, in which the gene encoding an antibody fragment is fused with the gene encoding a modified toxin. The production of these ITs could be achieved using different expression hosts, such as bacteria (Wang *et al.*, 1997), yeasts (Lombardi *et al.*, 2010) and algae (Mayfield, 2013), resulting in the production of a single-chain fusion protein. After binding of the antibody moiety to the target cell surface, IT is internalized through the endocytic compartment. In the endosome, the bond between antibody and toxin is reduced, allowing the toxin moiety to reach the cytosol and exert its enzymatic activity. Both type 1 and type 2 RIPs have been used for the construction of IT. Saporin, abrin and especially ricin are among the most used. Type 2 RIPs are highly toxic, but have the disadvantage of non-specific cell binding of the B-chain. Different strategies have been proposed, such as the use of: (i) modified or blocked B-chain; (ii) isolated and/or deglycosylated A chain; (iii) type 1 RIPs and (iiii) non-toxic type 2 RIPs (e.g., ebulin 1 and nigrin b) as toxic part of IT (Stirpe, 2004). Also many type 1 RIPs have been employed to construct ITs and in some cases type 1 RIP-containing ITs resulted more active than those containing RTA (Siena *et al.*, 1988; Bolognesi *et al.*, 1992). In fact, type 1 RIPs have the advantage of being less dangerous, more stable and easy to prepare with respect to type 2 RIPs. Saporin-S6 is the most utilized type 1 RIP for the construction of ITs (Polito *et al.*, 2011; Polito *et al.*, 2013). In particular, saporin-S6 containing ITs were largely used in neuroscience studies for selectively destroying neurons (Wiley, 2008; Bolognesi *et al.*, 2016).

The best results in IT-based therapy were obtained in haematological field, both in cancer therapy and against autoimmune immunological disorders.

### **1.4.2 Anti-tumor therapy**

To date, several immunotoxins containing type 1 or the A-chain of type 2 RIPs have shown encouraging results in numerous pre-clinical models (Fracasso *et al.*, 2010) and clinical trials (Polito *et al.*, 2011; Palanca-Wessels *et al.*, 2014), with the best results in the experimental treatment of hematological malignancies (Dosio *et al.*, 2014). The cell-killing efficiency of ITs mainly depends on the cell type, antigen availability, binding affinity and intracellular routing. RTA or blocked ricin were used in patients with B- and T-cell leukemia and lymphomas (Bolognesi and Polito, 2004), whereas ITs containing saporin conjugated to an anti-CD30 or anti-CD22 monoclonal antibody were used for the treatment of patients with Hodgkin's and non-Hodgkin's lymphoma, respectively (Polito *et al.*, 2011). Several clinical trials based on RIP-containing ITs are underway. Despite the encouraging results, several limitations have been reported; among them the poor penetration of the conjugates into solid tumors, side effects, such as vascular leak syndrome (VLS) and hepatotoxicity, and immunogenicity (Stirpe, 2004).

The poor penetration into solid tumors can be overcome by the employment of smaller conjugates, such as antibody fragments (scFv) or using ITs against the endothelial cells of tumor blood vessels, resulting in thrombosis and consequent ischemia of the tumor (Stirpe, 2004).

VLS is caused by an endothelial damage, which induce an increase of vascular permeability and it is characterized by weight gain, edema, hypoalbuminemia, hypotension and sometimes dyspnea (Pincus *et al.*, 2011). It has been proposed that VLS is due to short amino acid motifs of the toxin, which interact with integrins localized on endothelial cells, favoring the internalization of the toxin with consequent cell death (Baluna *et al.*, 2000). Modification or deletion of these sequences were shown to be effective in reducing toxin-induced VLS (Wang *et al.*, 2007; Weldon *et al.*, 2013). Instead, liver toxicity seems to be a multifactorial event and to depend on the type of toxin that is used (Battelli *et al.*, 1994).

One of the main problems in the clinic use of ITs is the onset of the immune response, which does not allow a repeated administration of the conjugate, except for

immunodeficient patients. The immunogenicity can be overcome by using ITs with partially or fully humanized antibodies (Hoogenboom *et al.*, 1992). Several immunosuppressive treatments were performed in order to reduce IT-associated immune response, even if with poor results (Alewine *et al.*, 2015). Moreover, a therapy with alternation of ITs containing different toxins could avoid the immune response against the toxin moiety.

Other strategies have been proposed in order to enhance the toxicity of ITs. The use of tenside-like compounds, such as saponins, in combination with ITs was found to enhance endosomal escape (Gilalbert-Oriol *et al.*, 2014). Moreover, the employment of photochemical internalization (PCI) technology was found to be very efficient. PCI is based on the activation by light of photosensitizers located in endocytic vesicles, causing a controlled membrane breakage with consequent release of molecules from the endocytic vesicles. As ITs enter cells by receptor-mediated endocytosis, PCI could allow the release of the toxin inside the tumor (Weyergang *et al.*, 2011).

### 1.4.3 Immune disorders

ITs have been used also for autoimmune diseases. The first IT used in clinical trials was the anti-CD5/RTA for the treatment of rheumatoid arthritis, systemic lupus erythematosus and insulin-dependent diabetes mellitus (Strand *et al.*, 1993; Stafford *et al.*, 1994; Skyler *et al.*, 1993). One approach was to conjugate the RIP with antigens responsible for the disease in order to directly interact with the immunocompetent cells. Tetanus toxoid conjugated to ricin was able to eliminate specific antibody-producing B-cell clones, leaving intact the remainder of the B-cell repertoire (Volkman *et al.*, 1982). RTA was also conjugate to human thyroglobulin for the treatment of patients with Hashimoto disease (Rennie *et al.*, 1983). Glennie and co-workers evaluated ITs consisting of monoclonal anti-idiotypic conjugated to saporin in the treatment of guinea pig B lymphocytic leukemia. The immunoglobulin-secreting leukemic cells were selectively eliminated (Glennie *et al.*, 1987). Two ITs were used for the treatment of AIDS, using the type 1 RIP PAP: one directed against the viral antigens expressed on the surface of infected cells and the second able to recognize antigens on CD4+ lymphocytes, in which the virus replicates (Pincus, 1996). Good results were obtained in specific suppression of immune response to acetylcholine receptor. ITs containing antibody against the nicotinic acetylcholine receptor and RIP were used for the

treatment of focal muscle spasm (Hott *et al.*, 1998) and strabismus by destroying oculomotor muscle (Christiansen *et al.*, 2002). Moreover, a fusion protein composed of a portion of the extracellular domain of the nicotinic acetylcholine receptor and the type 1 gelonin was used in the experimental treatment of myasthenia gravis. (Hossann *et al.*, 2006).

RIPs have been also used for the prevention and control of transplant rejection and graft-versus host disease (GVHD). Ricin-containing ITs against antigens on mature T lymphocytes have been evaluated both in vitro and in vivo studies (Vallera, 1982; Vallera, 1983). Even ATG-saporin-S6 (Polito *et al.*, 2009b) and CTLA-4-saporinS6 (Tazzari *et al.*, 2001) were used for this purpose.



*Chapter 2*

**Kirkiin: a new toxic type 2  
RIP from the caudex of  
*Adenia kirkii***



## AIM OF THE PROJECT

Type II RIPs are the most potent plant toxins known, able to irreversibly inhibit protein synthesis and to induce death in cells and in animals at very low doses. They were identified only in a few plant species, differently from type 1 RIPs that have been discovered in many plants belonging to different families, even phylogenetically unrelated. Until now, approximately 84 type 2 RIPs have been purified in a few *genera* (*Sambucus*, *Aralia*, *Polygonatum*, *Cucurbita*, *Momordica*, *Hura*, *Ricinus*, *Abrus*, *Adenia*, *Iris*, *Cinnamomum*, *Ximenia*, *Adenia*, *Erantis*, *Phoradendron* and *Viscum*). In particular, those extracted from plants belonging to the *Adenia* *genus* are among the most powerful plant toxins identified. In addition to modeccin and volkensin, extracted from the roots of *Adenia (Modecca) digitata* and *Adenia volkensisii*, respectively (Barbieri *et al.*, 1993), that are known from many years, other two potent toxins from the caudices of *Adenia lanceolata* (lanceolin) and *Adenia stenodactyla* (stenodactylin) were more recently described (Stirpe *et al.*, 2007). The high cytotoxicity of *Adenia* RIPs is probably due to their high affinity cell binding, efficient endocytosis and intracellular routing, resistance to proteolysis, and, regarding stenodactylin, high accumulation into the cell (Battelli *et al.*, 2010).

*Adenia* toxins are the only type 2 RIPs retrogradely transported along peripheral nerves and in the central nervous system (Wiley & Kline IV, 2000; Pelosi *et al.*, 2005; Monti *et al.*, 2007). This property has different medical and biotechnological applications in the field of neurophysiology and for the experimental treatment of pain. Moreover, because of their high cytotoxicity, these proteins could be used for pharmacological purpose, both native, for local-regional treatments, and as components of immunotoxins, for systemic treatments. These properties prompted us to evaluate whether other species belonging to *Adenia* *genus*, contain lectins or RIPs structurally similar to others already purified from the same *genus*, and possibly endowed of peculiar biological properties.

In this study, the presence of galactose-binding lectins was investigated in the caudex of four plants belonging to *Adenia* *genus* (*Passifloraceae* family), namely: *A. epigea*, *A. monodelpha*, *A. lindenii* and *A. kirkii*. All plants contain lectins that are able to agglutinate human erythrocytes in a range between 4-8 µg/ml. The lectins from *A. lindenii* and *A. kirkii* had the highest cytotoxicity. In particular, that from *A. kirkii*, named kirkiin, showed strong ability to inhibit cell protein synthesis, with a cytotoxicity comparable to that of stenodactylin. This prompted us to further deepen

the study of this protein, with particular regard to its biochemical, enzymatic and cytotoxic properties, and to its three-dimensional structure.

The name *Adenia kirkii* was given by Heinrich Gustav Adolf Engler in 1891 to a member of Passifloraceae family, spread in Kenya, eastern Tanzania and Zanzibar. The word “aden” derives from the greek and means gland, as these plants have typical glandular-shaped leaves, and “kirkii” derives from Thomas Kirk (1828-1898) a famous botanical of New Zealand (Egglı and Newton, 2013). The plant has green flowers, narrow and lobed leaves and a caudex as reserve organ, situated at the base of the plant; it can reach a height of 3 meters and a caudex up to 30 cm in diameter (figure 1).



**Fig. 1.** *Adenia kirkii*.

In order to clarify the pathogenetic mechanisms of kirkiin intoxication, inhibition of protein synthesis and loss of cell viability were evaluated. As many studies showed that RIPs induce apoptosis in several cell systems (Bolognesi *et al.*, 1996), the involvement of apoptotic mechanism was clarified. The study was focused especially on cells of nervous origin for their known high sensitivity to RIPs and for the possible use of kirkiin in neurophysiological studies. In addition, structural and enzymatic characterization of the new toxin was performed in collaboration with Prof. Ferreras at the University of Valladolid. The amino acid sequence of kirkiin was determined and a comparison with the sequences of other type 2 RIPs (toxic and non-toxic) was

performed, in order to provide useful information about the amino acids that are directly or indirectly involved in kirkiin toxicity. A three-dimensional structure was also predicted. Knowledge about the amino acid sequence associated with the structure analysis of the RIP is essential in understanding the protein function and to correlate structural differences among RIPs to their different cytotoxic mechanisms.

## RESULTS AND DISCUSSION

### 2.1 Partial purification and characterization of *Adenia* lectins

Caudices of *A. epigea*, *A. lindenii*, *A. monodelpha* and *A. kirkii* were processed as described in section 4.2.1. The extracts were subjected to chromatography on an acid treated Sepharose CL-6B column, and the lectins were eluted with 0.2 M galactose. On gel electrophoresis (figure 2.1) the unreduced proteins from *A. epigea* and *A. lindenii* gave one main band with apparent molecular weight (Mw) of 30 kDa approximately. The lectins from *A. monodelpha* gave two main bands with Mw 32 kDa and 34 kDa and one band with Mw >66 kDa approximately. Under non-reducing conditions the electrophoretic pattern did not change. The unreduced lectins from *A. kirkii* gave two main bands with apparent Mw 32 kDa and 60 kDa, approximately. After reduction, *A. kirkii* showed three bands with Mw 28 kDa, 31 kDa and 35 kDa approximately.

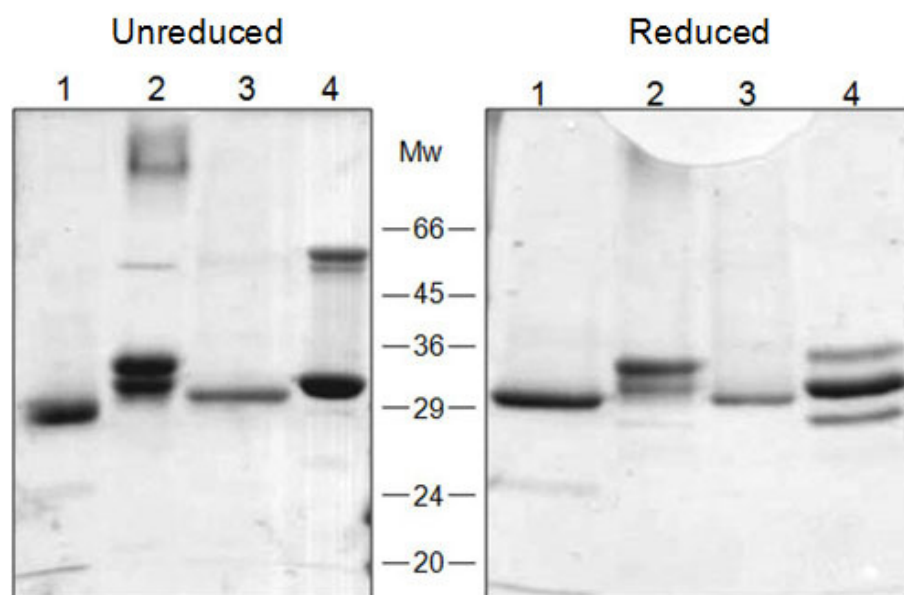


**Fig. 2.1.** SDS-PAGE of *Adenia* lectins. The molecular weights are expressed in kDa. The electrophoresis was carried out on 20% homogeneous gel of polyacrylamide (staining with Coomassie Blue). Lectins from *A. epigea* (lane 1), *A. monodelpha* (lane 2), *A. lindenii* (lane 3) and *A. kirkii* (lane 4) were analysed under unreduced (left) and reduced (right) conditions.

The purified proteins from all plants were assayed for the inhibition of protein synthesis by a rabbit reticulocyte lysate (table 2.1). The *A. kirkii* lectins showed the highest translational inhibiting activity, with IC<sub>50</sub> values of 7.44 and 3.78 µg/ml for the unreduced and reduced protein, respectively. The lectin from *A. lindenii* exhibited IC<sub>50</sub> values of about 37 µg/ml, whereas the lectins from *A. monodelpha* and *A. epigea* showed a weak inhibition activity. All the lectins had agglutinating activity for human erythrocytes (table 2.1). The presence of agglutination was indicated by an uniform coating of the bottom of the well by erythrocytes, while the absence of agglutination was indicated by a red button of erythrocyte sedimentation on the bottom of the microtiter plate surrounded by a concentric clear zone. The minimum lectin concentration causing agglutination ranged from 4.02 to 8.12 µg/ml.

Therefore, the lectins from *A. lindenii* and *A. kirkii* showed the highest toxicity. In particular, those from *A. kirkii* showed strong ability to inhibit cell protein synthesis, with a toxicity comparable to stenodactylin, the most potent cytotoxic type 2 RIP. This prompted us to deepen the study of the toxins from *A. kirkii*.

**Table 2.1.** Biological activities of proteins purified by affinity chromatography.

Adenia species	Inhibitory activity on protein synthesis (cell-free)		Haemagglutinating activity
	Rabbit reticulocyte lysate IC <sub>50</sub> (µg/ml)		
	Unreduced protein	Reduced protein	Minimum concentration causing agglutination (µg/ml)
<i>A. monodelpha</i>	>100	60.7	5.06
<i>A. kirkii</i>	7.44	3.78	4.02
<i>A. epigea</i>	>100	>100	4.59
<i>A. lindenii</i>	37.1	37.6	8.12

### 2.1.1 Purification of *A. kirkii* lectins

As described above, *A. kirkii* showed the presence of two lectins with different molecular weight, which strongly inhibited protein synthesis by a rabbit reticulocyte lysate system. As a consequence, a further purification procedure was undertaken in order to allow their separation. A peak of protein material was eluted by Sepharose CL-6B; about 108 mg of total proteins with RIP activity were obtained from 100 g of fresh tissue. The yield was 13,1% (table 2.2).

**Table 2.2.** Purification summary table.

Preparation from caudex	Protein (mg/ml)	Total protein (mg)	Total protein (%)	IC <sub>50</sub> (μg/ml) <sup>a</sup>	Specific activity (U/mg) <sup>b</sup>	Total activity (U) <sup>c</sup>	Yield (%)
Crude extract	3,46	1730	100	55	18,2	31454,5	100
CL-6B eluate	2,84	107,9	6,2	9,2	108,7	4130,4	13,1
S-100 peak 1	1,43	24,2	1,4	11,1	90,1	2184,0	6,9
S-100 peak 2	1,49	62,4	3,6	≥50	-	-	-

<sup>a</sup> Concentration of protein that inhibits the 50% of protein synthesis in unreduced conditions, measured by linear regression.

<sup>b</sup> Units of IC<sub>50</sub> in 1 mg of protein.

<sup>c</sup> Specific activity multiplied the total mg of proteins.

Subsequently, a chromatography step by gel filtration on Sephacryl S-100 was performed in order to separate the two lectins. The eluate from CL-6B (about 38 ml) was concentrated to 2 ml on YM-10 membrane under nitrogen pressure and then loaded into the column. Chromatography allowed the complete separation of the two lectins. As shown in figure 2.2, CL-6B peak was resolved into two peaks, the first one corresponding to the high molecular weight lectin and the second one to the low molecular weight lectin, with a yield of approximately 14 mg and 36 mg per gram of tissue, respectively (for more details see table 2.2).

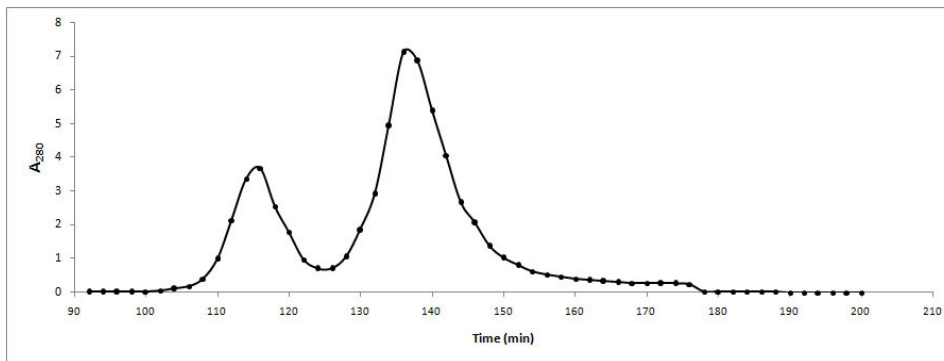


**Fig. 2.2.** Chromatography by gel filtration on Sephacryl S-100 of CL-6B eluate. Proteins were separated on the basis of the different size and eluted in PBS.

The fractions corresponding to each peak were collected and analyzed by SDS-PAGE on a 8-25% gradient gel in order to verify their purity (figure 2.3). Fractions corresponding to the high molecular weight lectin (lane 1) and fractions corresponding to the low molecular weight lectin (lane 4) were used for further analyses.

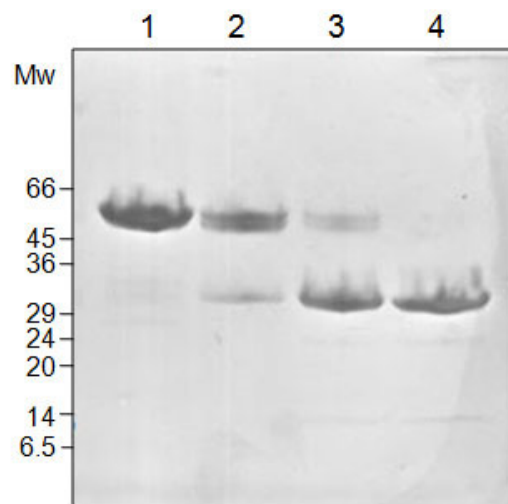


**Fig. 2.3.** SDS-PAGE of S-100 fractions under non-reducing conditions. Lane 1 corresponds to the first peak; lane 2 corresponds to the tail of the first peak; lane 3 corresponds to the beginning of the second peak and lane 4 corresponds to the second peak. The electrophoresis was carried out on a 8-25% gradient polyacrylamide gel (staining with Coomassie Blue). Molecular weights of the standard are expressed in kDa.

Electrophoretic analysis by SDS-PAGE on a 4-15% gradient gel was performed under reducing and non-reducing conditions. High molecular weight lectin revealed the presence of a single band with mobility corresponding to 58 kDa under non-reducing conditions (figure 2.4, lane 4). After reduction with 2-mercaptoethanol, two bands of about 27 kDa and 35 kDa were obtained (figure 2.4, lane 2). Based on the data reported in the literature, the A-chain of type 2 RIPs weights about 20-30 kDa, whereas B-chain

about 30-35 kDa (Stirpe, 2004). Therefore, we can assume that the two bands of approximately 27 and 35 kDa represent the A-chain and the-B chain of a type 2 RIP, respectively. The low molecular weight lectin showed only one band of about 32 kDa both in reducing and non-reducing conditions, compatible with a single-chain lectin (figure 2.4, lane 1 and lane 3, respectively).

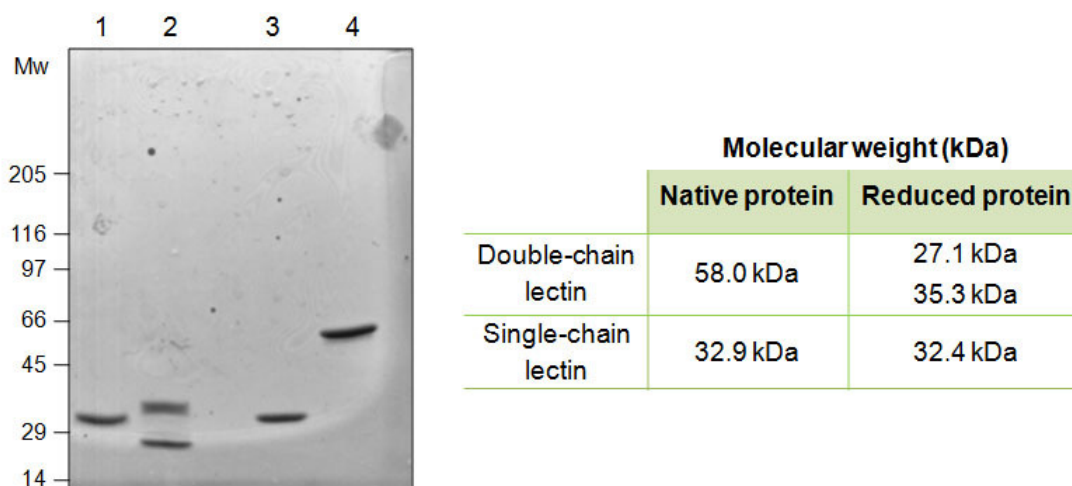


**Fig. 2.4.** SDS-PAGE of lectins under reducing and non-reducing conditions. Lane 1 and 2 correspond to the reduced low molecular weight and high molecular weight lectins, respectively. Lanes 3 and 4 correspond to the unreduced low molecular weight and high molecular weight lectins, respectively. The electrophoresis was carried out on a 4-15% gradient polyacrylamide gel (staining with Coomassie Blue). Molecular weights of the standard are expressed in kDa.

## 2.1.2 Enzymatic properties

### 2.1.2.1 Effects on protein synthesis

The effect of the purified lectins on mammalian ribosomes was evaluated *in vitro* in a cell-free system consisting of a lysate of rabbit reticulocytes, by assaying their inhibitory activity on protein synthesis through determination of the incorporation of L-[4,5-<sup>3</sup>H]-leucine (figure 2.5). The two proteins were assayed both in native form and in reducing conditions, thus eliminating the possible steric hindrance given by B-chain.

Double-chain lectin showed a strong inhibition of protein synthesis, displaying IC<sub>50</sub> values (concentration inhibiting 50% of protein synthesis) of 11.1 µg/ml in the native status and of 1 µg/ml under reducing conditions. These results were comparable to those obtained for other *Adenia* RIPs already studied, that showed IC<sub>50</sub> values in the range of

0.4-1.2  $\mu\text{g/ml}$  under reducing conditions and of 2.4-7.5  $\mu\text{g/ml}$  under non-reducing conditions (Pelosi *et al.*, 2005) (table 2.3). Therefore, these data suggested that the double-chain lectin purified from *A. kirki* is a toxic lectin with RIP activity and the name of kirkiin was given to it. Instead, single-chain lectin revealed a very low inhibition activity with  $\text{IC}_{50}$  value greater than or equal to the maximum dose used (50  $\mu\text{g/ml}$ ). As the single-chain lectin did not inhibit protein synthesis at the tested doses, we chose to continue the research only with the type 2 toxin kirkiin.

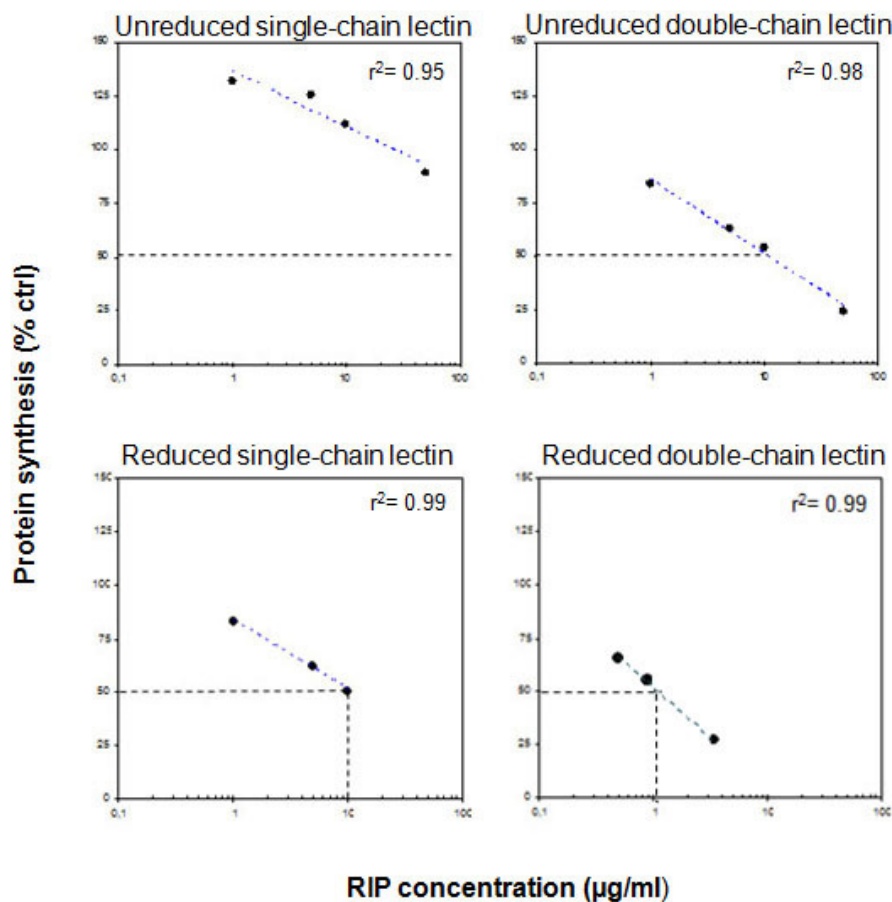


**Fig. 2.5.** Inhibition of protein synthesis assay on a lysate of rabbit reticulocytes. Protein synthesis was determined by measuring the radioactivity incorporated by proteins.  $\text{IC}_{50}$  was calculated by interpolation on the regression line. The results are the means of two independent experiments, each performed in duplicate.

**Table 2.3.** Comparison of IC<sub>50</sub> values between purified lectins and different RIPs from *Adenia* genus both in reducing and non-reducing conditions. Data of lanceolin and stenodactylin are from Pelosi *et al.*, 2005.

	IC <sub>50</sub> (µg/ml)			
	single-chain lectin	double-chain lectin	lanceolin	stenodactylin
<b>reduced</b>	> 50	1.01	1.1	0.5
<b>unreduced</b>	≥ 50	11.1	5.2	5.6

### 2.1.2.2 rRNA N-glycosylase activity

N-glycosylase activity of kirkiin was performed by RNA depurination assay of eukaryotic ribosomes, using a rabbit reticulocyte lysate as substrate. This activity was compared to that of the type 2 RIP ricin. RIPs recognize a specific and universally conserved region of 28S rRNA, splitting the glycosidic bond between an adenine and its ribose on the RNA. This site is A4324 in rat liver ribosomes and it is positioned within a single-stranded loop called sarcin/ricin loop (SRL). When adenine is removed, the treatment of the apurinic site with aniline acetate at pH 4.5 releases a 449-nucleotide fragment (Endo's fragment). This fragment, which is released from 3' end of 28S rRNA, is characteristic of the enzymatic action of RIPs (Endo *et al.*, 1987) and can be detected by denaturing gel electrophoresis (5% polyacrylamide-7M urea). Kirkiin displayed the ability to remove the adenine on rabbit reticulocyte ribosomes, as evidenced by the appearance of a fragment similar to that formed by ricin. No RNA fragment was observed in control samples and in samples treated in absence of aniline. This result confirms that the ability of inhibition of protein synthesis of kirkiin is related to the N-glycosylase activity on eukaryotic ribosomes (figure 2.6).

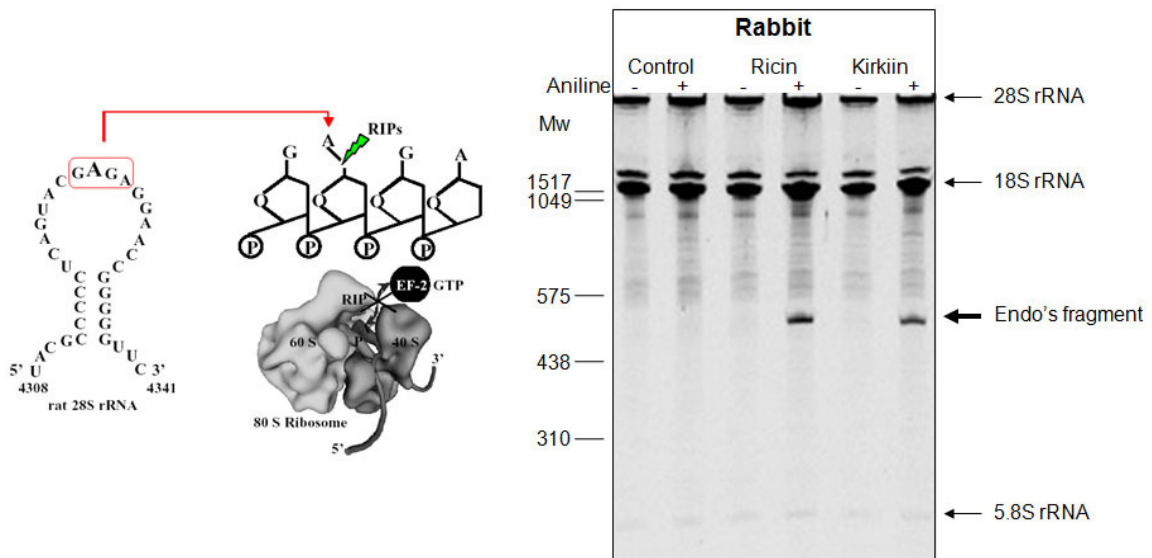


**Fig. 2.6.** rRNA N-glycosylase activity of kirkiin and ricin on rabbit reticulocyte ribosomes. Each lane contained 3  $\mu$ g of RNA. The arrows indicate the RNA fragments released after aniline acetate treatment at pH 4.5 (+). Numbers indicate the size of the standards (M) in nucleotides. On the left, Sarcin Ricin Loop of the large rRNA from rat is represented.

As the rRNA N-glycosylase activity might play a role in plant defence, for example against fungi, the effect of kirkiin was assayed on ribosomes from *Saccharomyces cerevisiae*, which might be homologous to ribosomes from putative plant pathogens. Similarly to what described above, the toxin was incubated with an S-30 lysate of yeast ribosomes and the apurinic rRNA was treated with aniline acetate. As shown in figure 2.7, kirkiin and ricin displayed rRNA N-glycosylase activity on yeast ribosomes, as indicated by the release of the diagnostic fragment (Endo and Tsurugi, 1988) upon treatment with aniline acetate. The released fragments displayed sizes of 360 nucleotides, in accordance with that expected for the SRL deglycosylation (368 nucleotides for yeast) (Iglesias *et al.*, 2015). Therefore, this result indicates that kirkiin is able to exert its action also on unicellular eukaryotes, inactivating their ribosomes.

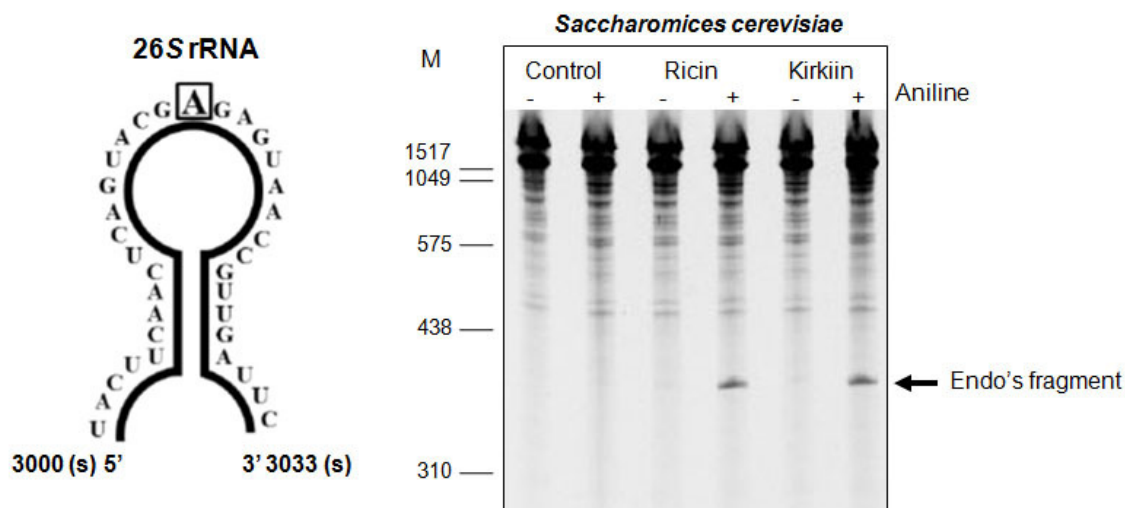


**Fig. 2.7.** rRNA N-glycosylase activity of kirkiin and ricin on yeast ribosomes. Each lane contained 3  $\mu$ g of RNA. The arrow indicates the Endo's fragment released after aniline acetate treatment at pH 4.5 (+). Numbers indicate the size of the standards (M) in nucleotides. On the left, Sarcin Ricin Loop of the large rRNA from *S. cerevisiae* is represented

### 2.1.2.3 Polynucleotide:adenosine glycosylase activity

Because of their different abilities to depurinate nucleic acids, the name of polynucleotide:adenosine glycosylase (PNAG) has been alternatively proposed for RIPs. RIPs have been shown a very variable activity on different types of nucleic acids. In fact, the PNAG activity of all toxic type 2 RIPs is significantly lower than type 1 RIPs (Barbieri *et al.*, 1997). PNAG activity of kirkiin was assayed on DNA of salmon sperm (ssDNA) and viral RNA of the tobacco mosaic virus (TMV) and it was compared with the activity of ricin. After incubation of the toxin with ssDNA, the amount of released adenine was determined by measuring the absorbance at 260 nm of the supernatant obtained by centrifugation of the samples. Both in reduced and unreduced conditions, no significant activity was detected on ssDNA substrate with respect to ricin, although the latter has a PNAG activity substantially lower than type 1 RIPs. According to what already observed with toxic type 2 RIPs (except for ricin) (Barbieri *et al.*, 2004), kirkiin did not increase the activity on ssDNA, even after the reduction of the interchain disulphide bridge (figure 2.8).

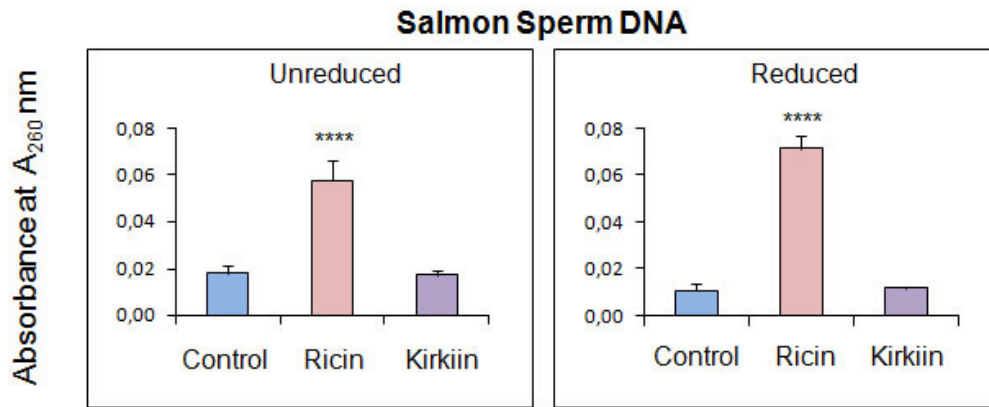


**Fig. 2.8.** Polynucleotide:adenosine glycosylase activity of kirkiin and ricin on salmon sperm DNA (ssDNA). The amount of released adenine was determined by measuring the absorbance at 260 nm of the supernatant obtained by centrifugation of the samples. The results are the means of two independent experiments, each performed in duplicate.  $p < 0.0001$ , test Anova/Bonferroni.

Many RIPs are potent inhibitors of animal and/or plant viruses, although the mode of action for the antiviral activity is not still clear. The discovery of a depurinating activity of RIPs on viral RNA allowed hypothesizing a possible use of RIPs as antiviral agents. Therefore, PNAG activity of kirkiin was assayed on RNA of TMV by denaturing gel electrophoresis (5% polyacrylamide-7M urea) of the apurinic RNA after treatment with aniline acetate. A marginal depurination of RNA was observed with kirkiin with respect to control and it resulted slightly less than that shown by ricin (figure 2.9a). Similarly to what was done for the ssDNA, the amount of released adenine was determined by measuring the absorbance at 260 nm of the supernatant obtained by centrifugation of the samples. The slight adenine release induced by kirkiin on TMV RNA confirmed the data obtained by electrophoresis; however, the difference observed was not significant (figure 2.9b).

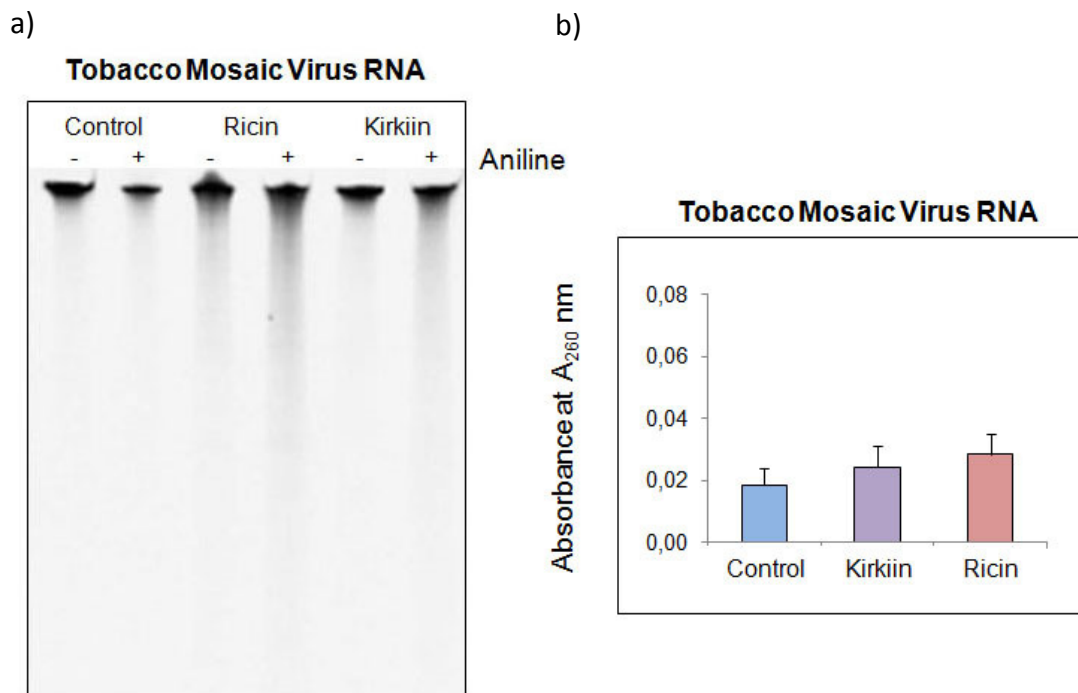


**Fig. 2.9.** Polynucleotide:adenosine glycosylase activity of kirkiin and ricin on RNA of TMV. a) Denaturing gel electrophoresis (5% polyacrylamide-7M urea) of the apurinic RNA after treatment with aniline acetate at pH 4.5 (+). Each lane contained 1  $\mu$ g of RNA. b) Amount of released adenine determined by measuring the absorbance at 260 nm of the supernatant obtained by centrifugation of the samples. The results are the means of two independent experiments, each performed in duplicate. No significant differences were observed (confidence interval 95%, test Anova/Bonferroni).

#### 2.1.2.4 Endonuclease activity on supercoiled plasmid DNA

It was reported that some RIPs showed endonuclease activity on plasmid DNA, promoting the conversion of supercoiled DNA in the relaxed or linear form (Aceto *et al.*, 2005). This ability can be important in order to understand the possible biological roles of RIPs, for example in plant defence against pathogenic micro-organisms or viruses.

The endonuclease activity of kirkiin was evaluated on the pCR 2.1 plasmid and it was compared with ricin. The reaction consists in the incubation of the toxin with the plasmid and subsequent analysis of DNA on agarose gel. Both kirkiin and ricin promoted a slight conversion of supercoiled DNA into a relaxed form with a magnesium-dependent activity (figure 2.10). Therefore, kirkiin showed a weak endonuclease activity, much lower than that displayed by single-chain RIPs (Iglesias *et al.*, 2015), and acted by cutting only one of the two helices of the plasmid DNA.

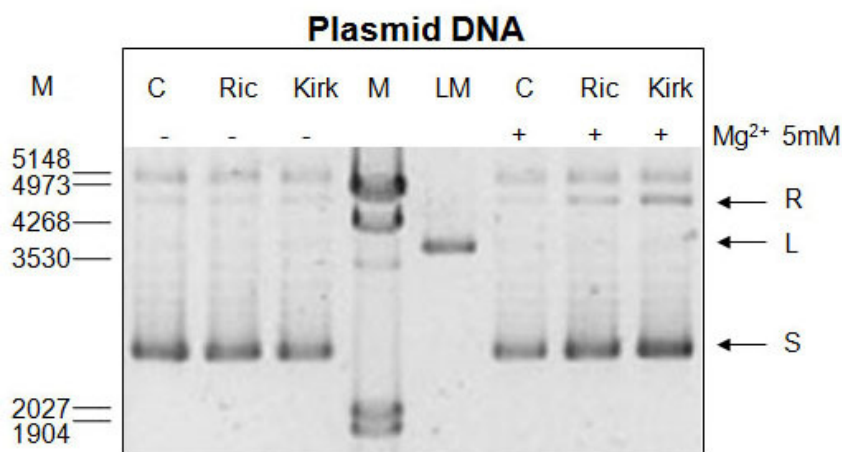


**Fig 2.10.** Endonuclease activity of kirkiin (Kirk) and ricin (Ric) on supercoiled plasmid DNA (pCR 2.1) with respect to control (C). Each lane contained 100 ng of plasmid DNA. The arrows indicate the supercoiled (S), the linear (L) and the relaxed (R) forms of the plasmid. Numbers indicate the size of the standards (M) in nucleotides and (LM) represents the linear form of the plasmid used as standard.

Summarizing, the results obtained confirmed that kirkiin has the enzymatic characteristics of a type 2 RIP such as ricin, showing an evident N-glycosylase activity on mammalian and yeast ribosomes, but a weak activity on other nucleotide substrates.

### 2.1.3 Isoelectric focusing

Isoelectric focusing assay was performed to measure the isoelectric point (pI) of the new toxin by electrophoresis on pH gradient gel created by an ampholyne solution. Kirkiin showed four bands at pI values of 5.5, 5.6, 5.7 and 6. These PI values are similar to those found for lanceolin (range between 5.4-5.7), whereas they are slightly more basic than those of stenodactylin (range between 4.8-5) (Stirpe *et al.*, 2007) and more acidic than those of volkensin (range between 7-7.2) (Barbieri *et al.*, 1993) (figure 2.11). The four bands probably indicate various isoforms of the protein, characterized by a different degree of glycosylation, which may determine different isoelectric points.

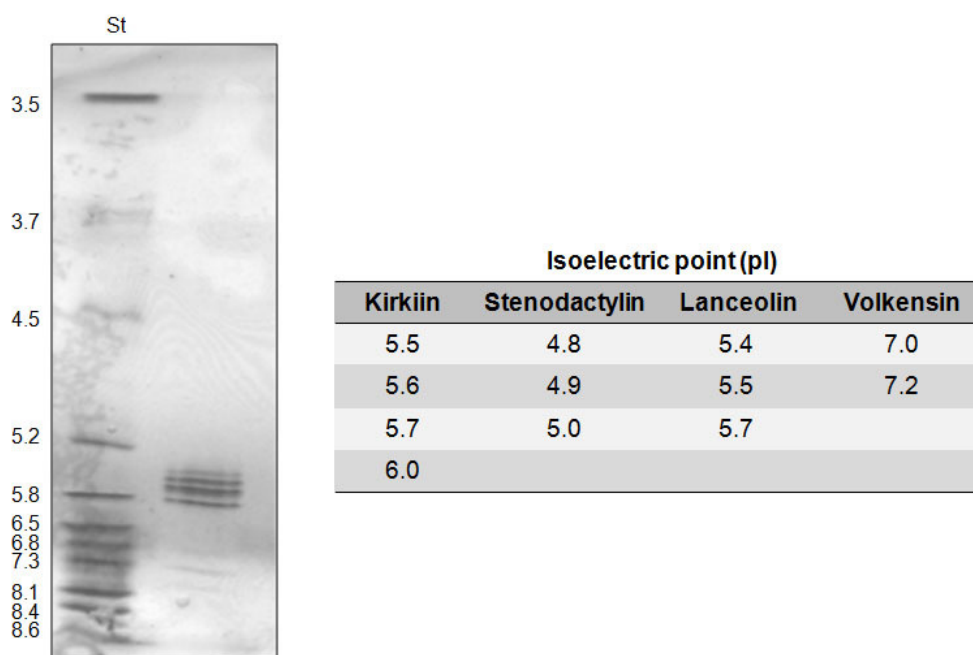


**Fig. 2.11.** Isoelectric focusing. Isoelectric point of kirkiin compared with the ampholyne gradient (St). Densitometric analysis of the bands was reported in the table on the right and compared with data of other *Adenia* RIPs (Barbieri *et al.*, 1993 and Stirpe *et al.*, 2007).

#### 2.1.4 Immunological properties

As RIPs are highly immunogenic, an enzyme immunoassay was performed to evaluate the cross-reactivity between kirkiin and some sera containing antibodies against various double-chain and single-chain RIPs. The analysis of cross-reactivity may be of great interest in order to identify toxins useful for prolonged therapeutic treatment with immunotoxins. In fact, by varying the type of toxin it is possible to reduce the immune response and prolong the use of RIPs in the therapies, preserving their therapeutic efficacy.

The immunological properties of kirkiin were tested with sera against different type 2 toxins: ricin and other three RIPs of *Adenia* species, volkensin, stenodactylin and lanceolin. The new RIP highly cross-reacted with sera against *Adenia* toxins. This strong interaction is not surprising, since all these toxins have been purified from plants belonging to the same family and seem to have a high homology in amino acid sequence. Moreover, no cross-reaction was evidenced with the serum against ricin (figure 2.12).

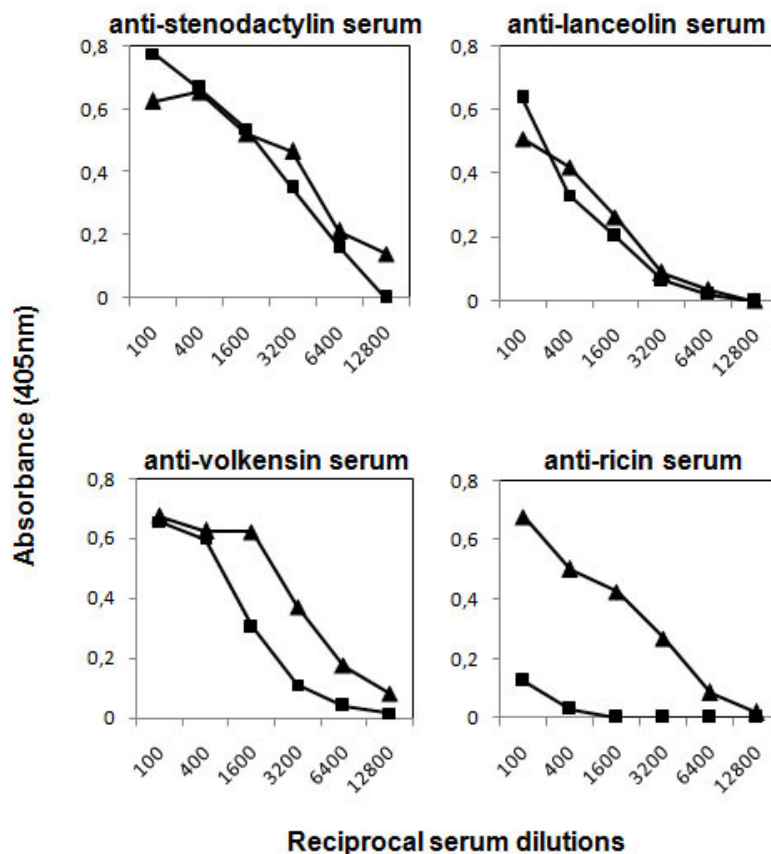


**Fig. 2.12.** Enzyme-linked immunosorbent assay (ELISA) with anti-type 2 RIPs sera. The values of absorbance at 405 nm are expressed in function of the reciprocal of the antibody dilution. Values of the type 2 RIPs with the respective anti-sera are reported in (▲), while those related to kirkiin are represented in (■). The results are the means of at least three independent experiments.

The new RIP was also tested with antisera against some type 1 RIPs: PAP, saporin and momordin. Kirkiin showed partial cross-reactivity with anti-PAP and anti-momordin sera, while did not react with the serum against saporin S6 (figure 2.13). No cross-reaction with anti-ricin and anti-saporin sera represents a good advantage, as these two toxins are the RIPs most used as components of immunoconjugates (Gilabert-Oriol *et al.*, 2014). This can prospect the use of a kirkiin containing-immunotoxin in prolonged therapeutic treatments in substitution of immunotoxins containing ricin and saporin.

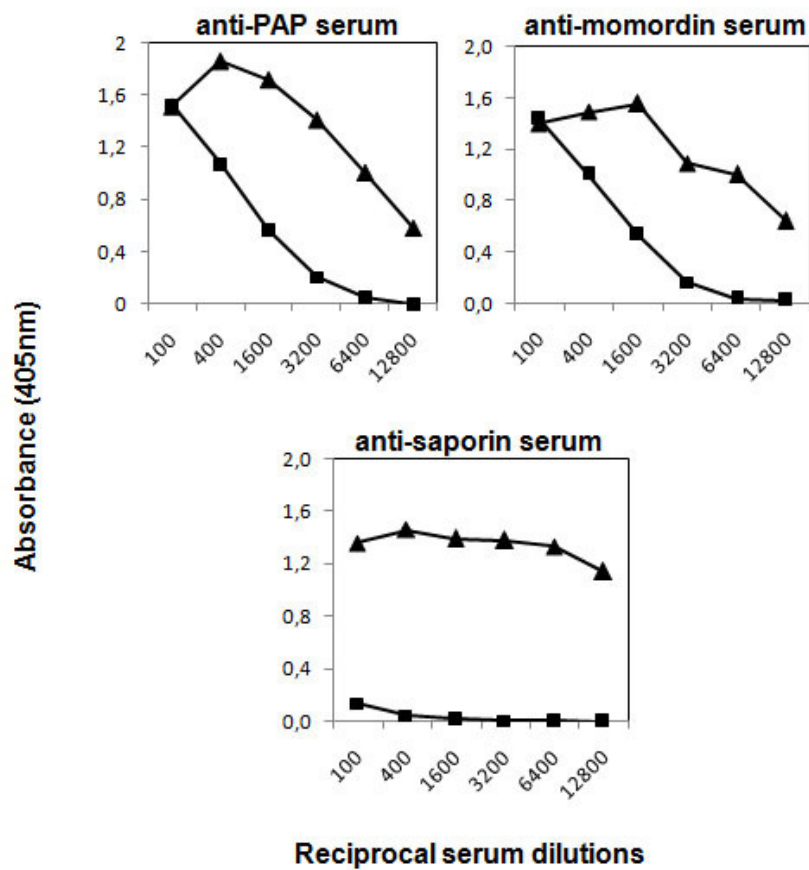


**Fig. 2.13.** ELISA assay with anti-type 1 RIPs sera. The values of absorbance at 405 nm are expressed in function of the reciprocal of the antibody dilution. Values of the type 1 RIPs with the respective anti-sera are reported in (▲), while those related to kirkiin are represented in (■). The results are the means of at least three independent experiments.

## 2.2 Cytotoxic effects in cell cultures

### 2.2.1 Inhibition of protein synthesis

Kirkiin cytotoxicity was evaluated by its ability to inhibit protein synthesis in two human cell lines: HeLa (derived from uterine cervix carcinoma) and NB100 (derived from a neuroblastoma). Cells were treated with scalar concentrations of RIP from  $10^{-15}$ M to  $10^{-11}$ M for 72 hours and protein synthesis was assessed by incorporation of  $^3\text{H}$ -leucine into the new synthesized proteins. Kirkiin resulted extremely effective on the tested cell lines with  $\text{IC}_{50}$  values extremely low, ranging from  $10^{-14}$ M to  $10^{-13}$ M. HeLa cells were slightly more sensitive than NB100 cells, with an  $\text{IC}_{50}$  value of  $7.58 \times 10^{-14}$ M against  $1.26 \times 10^{-13}$ M in NB100. For both lines, kirkiin was able to inhibit protein synthesis of more than 95% at the concentration of  $10^{-12}$ M (figure 2.14).

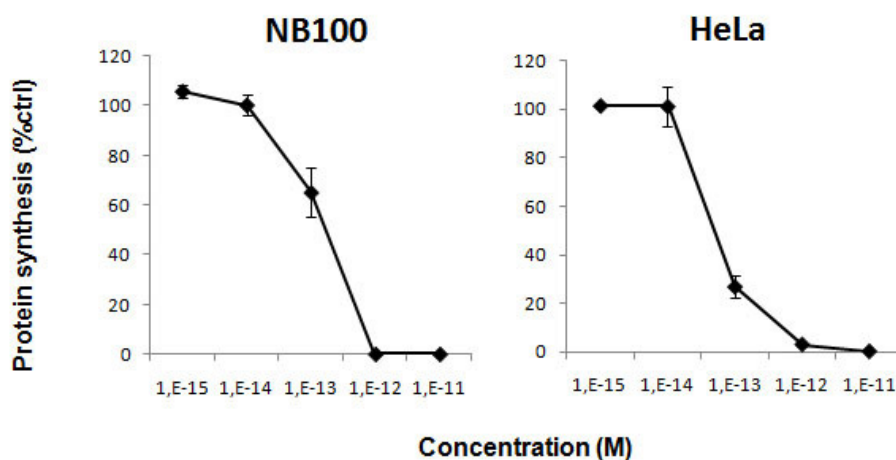


**Fig. 2.14.** Inhibition of protein synthesis in HeLa and NB100 cells treated with scalar concentrations of kirkiin. Cells ( $2 \times 10^3$ /well) were incubated for 72 hours with the RIP. After further 4 hours of incubation in the presence of  $[4,5-^3\text{H}]$ -leucine, the radioactivity incorporated into the new synthesized proteins was measured. Protein synthesis is represented in abscissa and it is expressed as percentage of control values. The results are the means of two independent experiments, each performed in duplicate.

$\text{IC}_{50}$  values of other *Adenia* RIPs obtained on the same cell lines are reported in table 2.4. Kirkiin showed an  $\text{IC}_{50}$  on NB100 cell line comparable to the other RIPs (Stirpe *et al.*, 2007), whereas the  $\text{IC}_{50}$  value obtained on HeLa cells was comparable to that of

stenodactylin ( $1.9 \times 10^{-14}\text{M}$ ), but much lower than those of lanceolin ( $1.5 \times 10^{-12}\text{M}$ ) and volkensin ( $1.1 \times 10^{-12}\text{M}$ ) (Battelli *et al.*, 2010).

**Table 2.4.** Comparison of  $\text{IC}_{50}$  values of kirkiin and other toxic type 2 RIPs from *Adenia* on NB100 and HeLa cells. The values of stenodactylin, lanceolin and volkensin were taken from Stirpe *et al.*, 2007 and Battelli *et al.*, 2010.

	$\text{IC}_{50}$ (M)	
	NB100	HeLa
<b>Kirkiin</b>	$1.3 \times 10^{-13}$	$7.6 \times 10^{-14}$
<b>Stenodactylin</b>	$3.3 \times 10^{-13}$	$1.9 \times 10^{-14}$
<b>Lanceolin</b>	$6.9 \times 10^{-13}$	$1.5 \times 10^{-12}$
<b>Volkensin</b>	$4 \times 10^{-13}$	$1.1 \times 10^{-12}$

### 2.2.2 Cell viability assay

To better understand the cytotoxic mechanism induced by kirkiin, cell viability experiments were performed by assessing the reduction in metabolic activity, as a result of the treatment of the two cell lines with scalar concentrations of the RIP (from  $10^{-15}\text{M}$  to  $10^{-11}\text{M}$ ) for 72 hours. In order to verify the correlation between the two events, cell viability and inhibition of protein synthesis were performed in parallel. As shown in figure 2.15, protein synthesis and cell viability proceeded in parallel at long incubation time (72 hours), as commonly found with other type 2 RIPs (Wang *et al.*, 2006). At  $10^{-11}\text{M}$  concentration, the RIP was able to reduce cell viability and to inhibit protein synthesis of more than 95% in NB100 cells. Regarding HeLa cells treated with kirkiin, protein synthesis and cell viability curves revealed a steeper trend and the RIP induced death in almost all of the cells (approximately 96%) at a concentration one order of magnitude lower ( $10^{-12}\text{M}$ ), compared to NB100 cells.

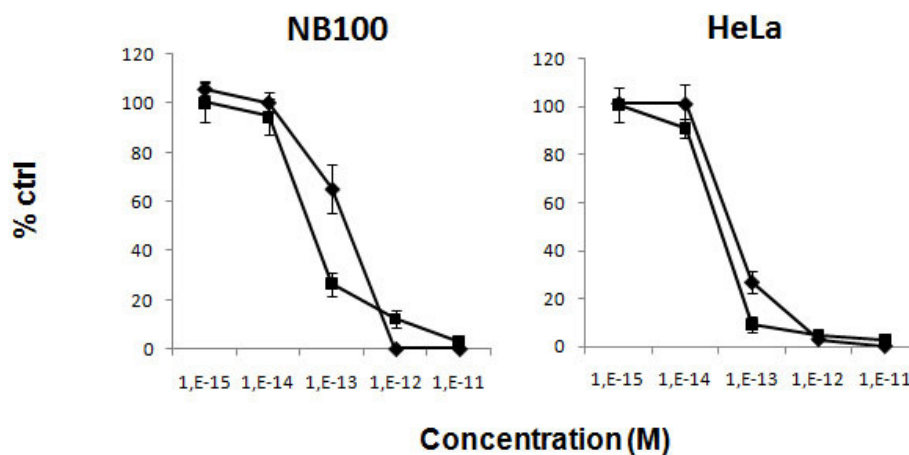


**Fig. 2.15.** Comparison of protein synthesis (◆) and cell viability (■) in HeLa and NB100 cells treated with kirkiin for 72 hours. Both parameters are expressed as percentage of controls. The results are the means of three independent experiments, each performed in triplicate.

The concentrations that reduce the cell viability of 50% ( $EC_{50}$ , effective concentration fifty) were calculated by linear regression from the cytotoxicity curves. The  $EC_{50}$  values were  $4.5 \times 10^{-14}M$  for NB100 and  $5.3 \times 10^{-14}M$  for HeLa cells. As for  $IC_{50}$ , even  $EC_{50}$  of kirkiin obtained on NB100 cells was comparable to that of stenodactylin ( $9.9 \times 10^{-14}M$ ), but lower than that of lanceolin ( $6.3 \times 10^{-13}M$ ). Even for HeLa cells was observed a similar behavior to that observed for the inhibition of protein synthesis, as kirkiin and stenodactylin resulted much more toxic than lanceolin and volkensin (table 2.5).

**Table 2.5.** Comparison of  $EC_{50}$  values of kirkiin and other toxic type 2 RIPs from *Adenia* on NB100 and HeLa cells. The values of stenodactylin, lanceolin and volkensin were taken from Stirpe *et al.*, 2007 and Battelli *et al.*, 2010. NA: Not Available

	$EC_{50}$ (M)	
	NB100	HeLa
<b>Kirkiin</b>	$4.5 \times 10^{-14}$	$5.3 \times 10^{-14}$
<b>Stenodactylin</b>	$9.9 \times 10^{-14}$	$5.4 \times 10^{-14}$
<b>Lanceolin</b>	$6.3 \times 10^{-13}$	$3.7 \times 10^{-12}$
<b>Volkensin</b>	NA	$3.7 \times 10^{-12}$

### 2.2.3 Time-response experiments on NB100 cell line

Toxins from *Adenia* plants are the only type 2 RIPs retrogradely transported along the axon, both in peripheral nerves and in the central nervous system (Wiley and Stirpe, 1988; Monti *et al.*, 2007). Therefore, they are used to study the anatomy and physiology of the central nervous system (Wiley, 1992). For this reason, subsequent studies were focused on NB100 cell line of neuroblastic origin.

In order to evaluate the minimum time required to obtain a complete loss of cell viability, time-course experiments were conducted on NB100 cells exposed to kirkiin at a concentration of  $10^{-11}$ M, which represented the first concentration of RIP able to reduce cell viability and to inhibit protein synthesis of more than 95% compared to controls after 72 hours. The time curve showed a significant reduction of the metabolic activity starting from 8 hours (about 90%), that gradually decreased over time until reaching a viability of about 40% at 24 hours and about 6% at 48 hours. By linear regression analysis,  $ET_{50}$  (effective time 50) of 20.4 hours was calculated, which represents the time necessary to reduce the cell viability of 50% (figure 2.16).

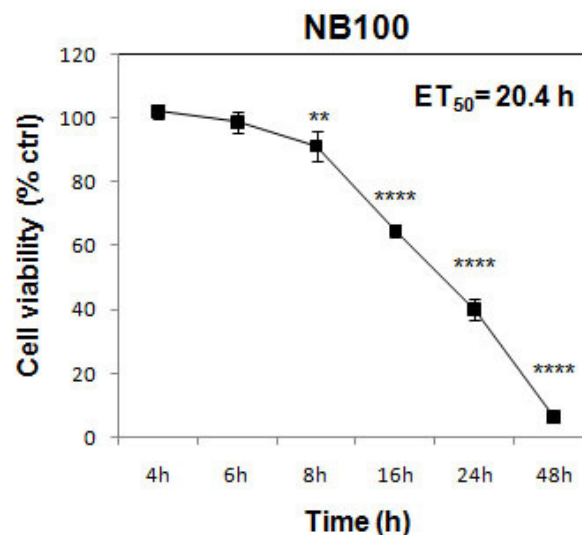


**Fig. 2.16.** Time-response curve. Viability of NB100 cells ( $2 \times 10^3$  cells/well) treated with kirkiin ( $10^{-11}$ M) after the indicated times. Viability was evaluated using a colorimetric assay based on MTS reduction. The results are the means of three independent experiments, each performed in triplicate, and are represented as percentage of control values obtained from cultures grown in the absence of RIP. \*\* $p < 0.01$ ; \*\*\*\* $p \leq 0.0001$ , Anova/ Bonferroni.

## 2.3. Assessment of apoptosis

### 2.3.1. Microscopic analysis

Many RIPs, both type 1 and type 2, are able to induce apoptosis in the intoxicated cells (Polito *et al.*, 2009a). The presence of cellular morphological changes in NB100 cells treated with kirkiin at the concentration of  $10^{-11}$ M was examined using phase-contrast microscopy. After 16 hours of treatment, morphological characteristics of apoptosis were visible, which became more evident at 48 hours, such as cell shrinkage, loss of contact with adjacent cells, formation of cytoplasmic protrusions and apoptotic bodies (figure 2.17).

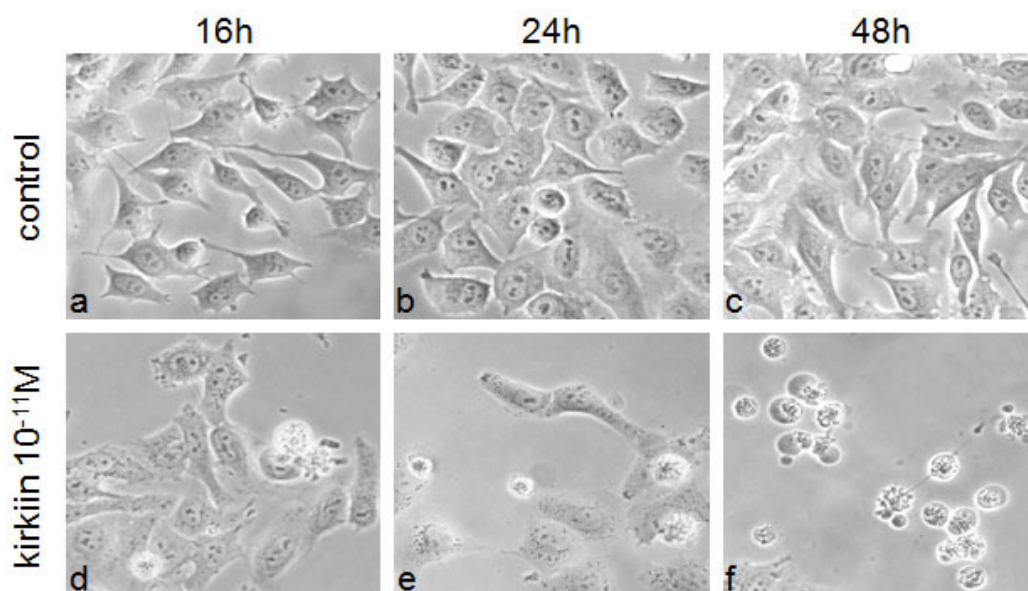


**Fig.2.17.** NB100 cells morphology by phase-contrast microscopy: untreated (a, b, c) and treated with kirkiin at  $10^{-11}$ M (d, e, f) for 16, 24 and 48 hours, respectively (400× magnification).

Apoptosis was monitored by fluorescence microscopy using DAPI and JC-1 staining. The staining of NB100 cell nuclei with DAPI showed that kirkiin intoxication induced a reduction of cell density and an increase of pyknotic nuclei (figure 2.18).

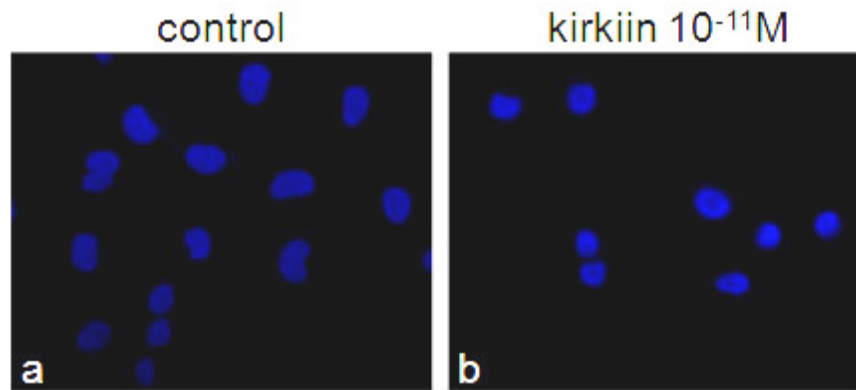


**Fig. 2.18.** NB100 cells morphology by fluorescence microscopy after DAPI staining: untreated (a) and treated with kirkiin at  $10^{-11}$ M for 24 hours (600 $\times$  magnification).

A typical feature of programmed cell death is the disruption of active mitochondria, which consists of changes in the membrane potential and alterations of the mitochondria redox state. Alterations of the mitochondrial membrane potential ( $\Delta\psi_m$ ) were detected through fluorescence in cells exposed to kirkiin ( $10^{-11}$ M) for 24 and 48 hours, after staining with JC-1, a lipophilic, cationic dye that can selectively enter the mitochondria and reversibly change color from green to red as the membrane potential increases. In healthy cells with high  $\Delta\psi_m$ , JC-1 forms J-aggregates yielding red fluorescence. In apoptotic or unhealthy cells with low  $\Delta\psi_m$ , JC-1 remains in the monomeric form with green fluorescence.

Untreated cells showed a strong red fluorescence due to the characteristic J-aggregates in the mitochondria, indicating intact  $\Delta\psi_m$ . In cells treated with kirkiin, JC-1 remained in the monomeric form, yielding green fluorescence and indicating dissipation of the  $\Delta\psi_m$ , which is more evident at 48 hours. These results confirm that cells undergo apoptosis programmed cell death after kirkiin intoxication and that mitochondria are involved (figure 2.19).

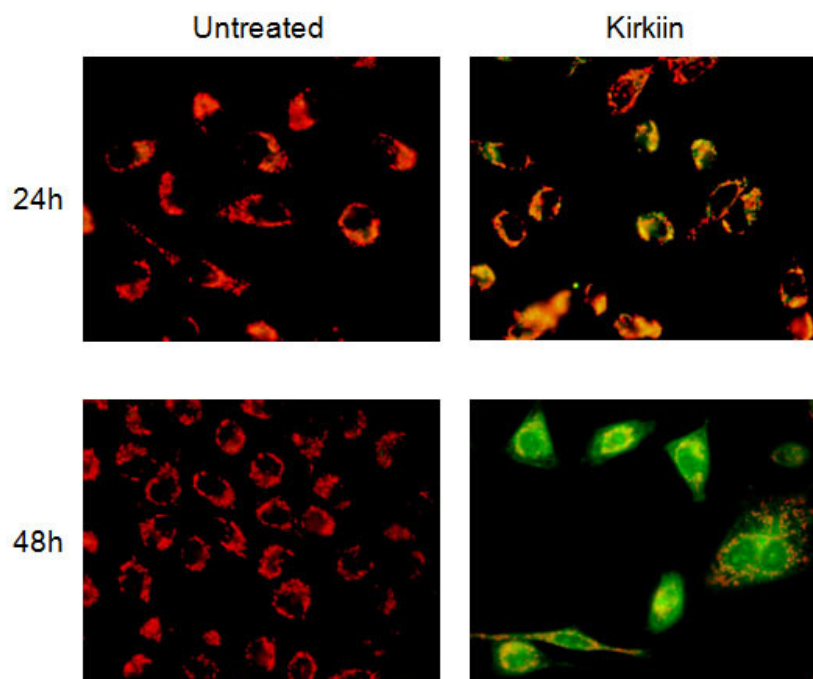


**Fig. 2.19.** Mitochondrial transmembrane potential in NB100 cells treated with kirkiin ( $10^{-11}$ M) for 24 and 48 hours, stained with JC-1 and then analyzed with fluorescence microscopy (600 $\times$  magnification).

### 2.3.2 Cytofluorimetric analysis

Apoptosis was also monitored by double staining with Annexin V-EGFP/Propidium iodide (PI) through flow cytofluorimetric analysis of NB100 cells, in order to quantify the percentage of apoptotic cells and evaluate the involvement of necrosis. PI-positive cells are in the upper left quadrant, while cells in late apoptosis and early apoptosis are in the upper and lower right quadrants, respectively. After 24 hours of intoxication with the RIP, a small percentage of treated cells were in late stage apoptosis (8.3%); this percentage increased over time to about 36% at 48 hours (figure 2.20). The positivity to Annexin V/PI in flow cytofluorimetric analysis confirmed the involvement of apoptosis and the absence of necrosis after kirkiin treatment of NB100 cells.

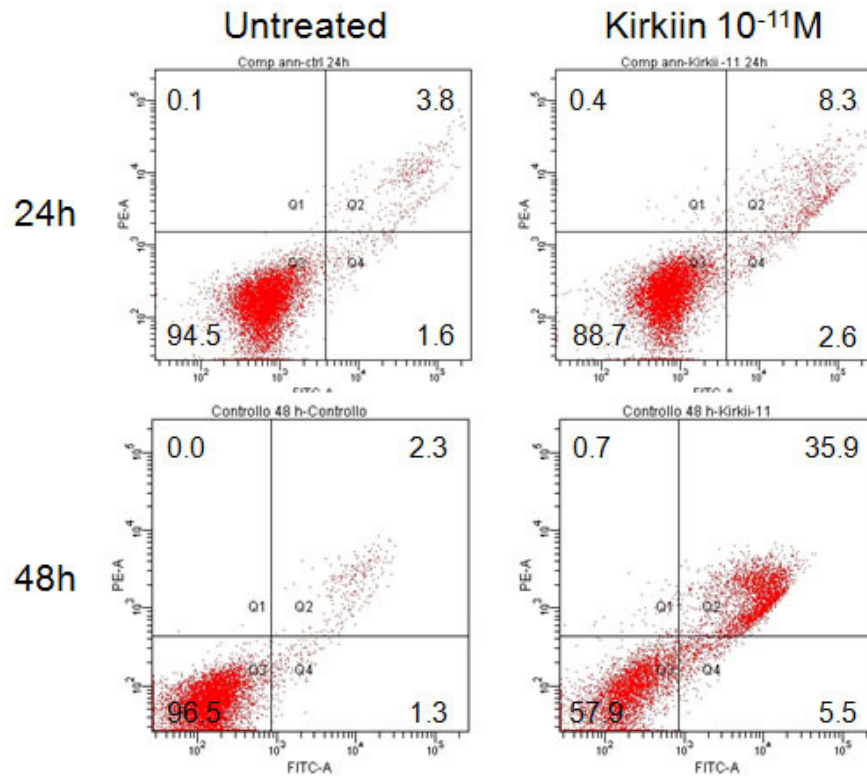


**Fig. 2.20.** Evaluation of apoptosis by Annexin V-EGFP/PI staining, followed by flow cytometry analysis. Representative plots of Annexin V (FITC channel)/PI (PE channel) staining of NB100 cells untreated or treated with kirkiin ( $10^{-11}$  M).

### 2.3.3 Caspase 3/7 activation

To assess the involvement of caspase-dependent apoptosis, caspase 3/7 activation was measured in NB100 cells exposed to kirkiin  $10^{-11}$ M, in a time range from 4 to 48 hours. A strong time-dependent activation of caspase 3/7 was observed, which became significant with respect to control after 6 hours of treatment (143,5%) and highly significant after 8 hours (160%). The level of caspase activity grew exponentially over time, reaching a plateau after 48 hours (1093%). Instead, the reduction of viability became significant starting from 8 hours of treatment (91% of viability) (figure 2.21). The high activation level of effector caspases confirmed that the cells underwent the caspase-dependent apoptosis of the same magnitude compared with other toxic type 2 RIPs and at very low doses ( $10^{-11}$ M) (Polito *et al.*, 2016a).

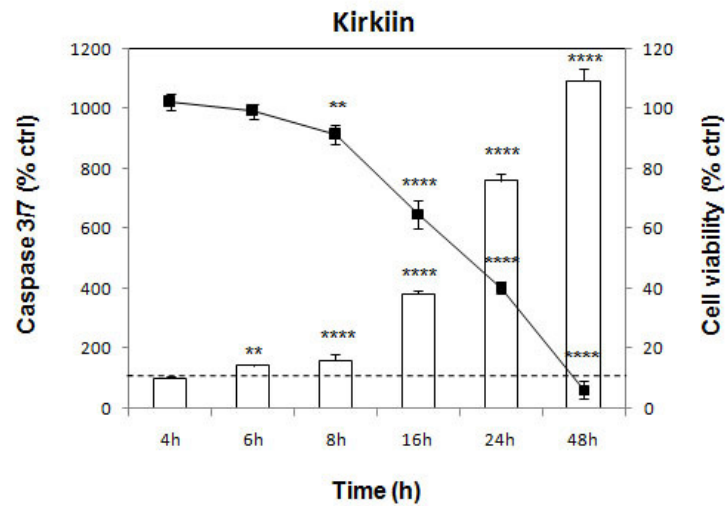


**Fig. 2.21.** Caspase 3/7 activation (columns) in NB100 cells ( $2 \times 10^3$  cells/well) treated with kirkiin ( $10^{-11}$  M), compared with cell viability (■). Caspase activity was expressed as percentage of control values obtained from cultures grown in the absence of RIP. The results are the means of three independent experiments, each performed in triplicate.  $p < 0.01$ , \*\*\*\* $p < 0.0001$ , Anova/Bonferroni test.

Summarizing, kirkiin-treated cells exhibited the morphological features characteristic of apoptosis and stimulated the apoptotic pathway as demonstrated by the strong activation of the effector caspase 3/7 and the positivity to Annexin V/PI in flow cytometric analysis.

## 2.4 Kirkiin amino acid sequence

### 2.4.1 Isolation and cloning of the kirkiin gene

#### 2.4.1.1 Selection of the oligonucleotides for PCR amplification

The nucleotide sequence of kirkiin was partially determined from DNA extracted from the caudex of *A. kirkii*, by PCR with gene-specific primers designed on the basis of the sequences available for other Adenia RIPs (stenodactylin, modeccin, lanceolin A1, lanceolin A2 and volkensin), as described in section 4.2.11. As a result of the high sequence homology among RIPs derived from plants of Adenia and on the basis of the information available in GenBank on volkensin amino acid sequence (CAD61022), five oligonucleotides were designed for PCR amplification of the kirkiin gene: three primers for kirkiin A-chain amplification, two based on the N-terminal end (A1 and the degenerated A2) and one on the B-chain N-terminal (B1 reverse); and two primers for kirkiin B-chain amplification (B1 and B5 reverse) in the N-terminal and C-terminal ends, respectively (figure 2.22). The sequences of the primers are reported in section 4.2.11. The primer A1, designed in proximity of N-terminal end of the A-chain did not produce amplification, did not allowing the determination of the N-terminal end of the protein (about 10 amino acids on the basis of Adenia sequences alignment). As a consequence, kirkiin amino acid sequence was determined by using the A2 primer.

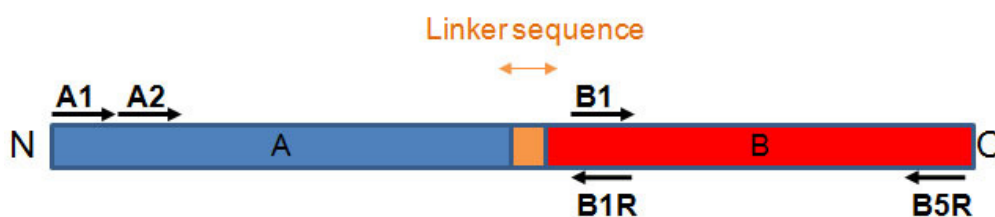


**Fig. 2.22.** Schematic representation of kirkiin gene precursor. Black arrows represent the primers designed for PCR amplification of the kirkiin gene. The sequences of the primers are reported in section 4.2.11. (A) is the sequence encoding A-chain; (B) is the sequence encoding B-chain; (N) and (C) are the N-terminal and C-terminal ends of the kirkiin gene, respectively.

### 2.4.1.2 Molecular cloning and sequencing of genomic DNA fragments encoding kirkiin

Total DNA was extracted from the caudex of *A. kirki* through DNeasy Minikit (Qiagen) according to the manufacturer's instruction. From approximately 100 mg of frozen tissue, 1.2  $\mu$ g of total DNA were obtained. Genomic DNA was used as template for PCR amplification in order to determine the amino acid sequence of kirkiin (section 4.2.12). Two pairs of primers allowed to amplify two genomic DNA fragments corresponding to: the A-chain with part of the B-chain (A2 and B1R primers) and the entire sequence of kirkiin (A2 and B5R primers). The primers designed for B-chain generated an artifact of amplification (B1 and B5R primers). The amplified fragments were analyzed by agarose gel electrophoresis, showing the expected size of about 0.8 kb for the A-chain with part of the B-chain (figure 2.23 A, lane 1) and about 1.6 kb for the entire sequence (figure 2.23 B, lane 1).

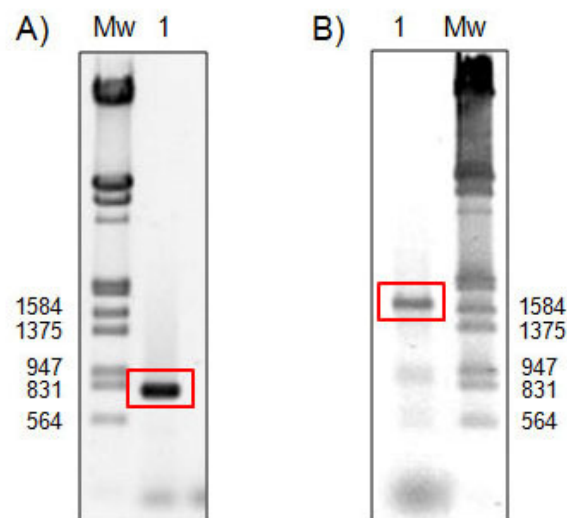


**Fig. 2.23.** Amplification of kirkiin A-chain with part of the B-chain (A, lane 1), and the entire sequence (B, lane 1). Mw:  $\lambda$  Hind III/EcoRI double digest DNA marker. The red squares indicate the amplification products.

The two purified amplicons were cloned into the vector pCR®II used for the transformation of highly competent cells InVαF'. The antibiotic-resistance conferred by the plasmid vector, allowed the growth of transformed bacterial cells only. The recombinant white colonies (*lacZ*-negative; see section 4.2.13) were analyzed by PCR, using the universal primers "M13" and "M13 reverse". The population of transformants positive for the presence of the fragments corresponding to the A-chain with part of the B-chain and the entire protein was 8/8 and 4/30, respectively.

The transformed white colonies were picked up for plasmid purification and restriction analysis with *EcoR*I enzyme. The agarose gel analysis reported in figure 2.24 showed that plasmids corresponding to the A-chain with part of the B-chain (gel A), contained fragments of the expected size after plasmid digestion (about 0.8 kb), whereas the plasmids corresponding to the entire sequence (gel B) revealed the presence of two bands of about 0.9 kb and 0.7 kb after digestion. This result was probably due to the presence of a restriction point for *EcoR*I inside the kirkiin sequence.

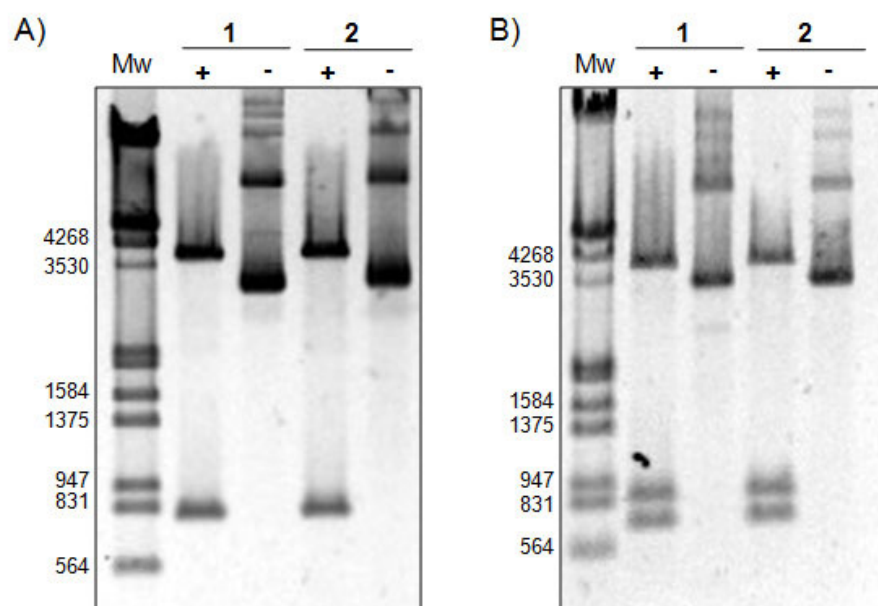


**Fig. 2.24.** Restriction analysis of the purified plasmids digested with *EcoR*I enzyme (+) and non-digested (-). The agarose gel A shows the digestion of two plasmids containing the A-chain with part of the B-chain (lanes 1 and 2); the agarose gel B shows the digestion of two plasmids containing the entire sequence (lanes 1 and 2). Mw:  $\lambda$  Hind III/*EcoR*I double digest DNA marker.

To exclude that the amplification had generated a non specific band, a further PCR amplification of the purified plasmids corresponding to the entire sequence was performed with the specific primers (A2 and B5R). A fragment of the expected size (about 1.6 kb) was obtained (figure 2.25).

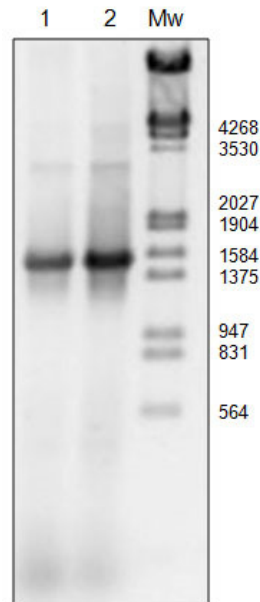


**Fig. 2.25.** PCR amplification of the purified plasmids corresponding to the entire sequence with the specific primers (A2 and B5R). Both lanes showed the amplification of a fragment of about 1.6 kb. Mw:  $\lambda$  Hind III/EcoRI double digest DNA marker.

The purified plasmids were sequenced by CENIT Support system of Villamayor (Salamanca, Spain). The information obtained on the sequence were analyzed using the algorithms available on <http://expasy.org>. The genomic DNA sequences obtained for the A-chain with a part of the B-chain and for the entire sequence (were aligned and reported in figure 2.28).

#### 2.4.1.3 Molecular cloning and sequencing of a cDNA encoding kirkiin A-chain

Total RNA was extracted from the caudex of *A. kirki* through RNeasy Minikit (Qiagen) according to the manufacturer's instruction. From approximately 100 mg of tissue, about 2.7  $\mu$ g of total RNA were obtained. Reverse transcription was performed with 1  $\mu$ g of total RNA using the primer ATP-J1, as explained in section 4.2.10. The obtained cDNA was used as template for PCR amplification with the same primers used for the sequencing of the genomic DNA (see section 4.2.12). A pair of primers allowed to amplify a cDNA fragment corresponding to the A-chain with part of the B-chain (A2

and B1R). As seen for genomic DNA, the primers designed for B-chain generated an artifact of amplification. The amplified fragment was analyzed by agarose gel electrophoresis, showing the expected size of about 0.8 kb (figure 2.26).

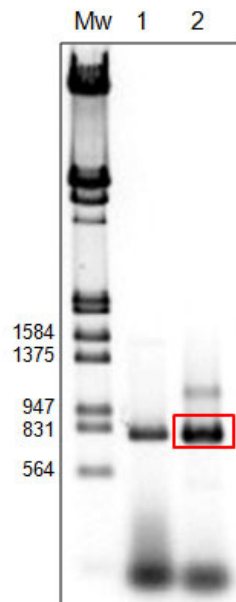


**Fig. 2.26.** Amplification of kirkiin cDNA corresponding to A-chain with part of the B-chain (lane 2). Mw:  $\lambda$  Hind III/EcoRI double digest DNA marker. The red square indicates the amplification product.

As before, after ligation of the fragments into pCR®II vector and transformation of *E.coli* InVaF' cells, plasmids were purified and analyzed by restriction digest with EcoR1 enzyme. The agarose analysis was reported in figure 2.27. The purified plasmids were sequenced by CENIT Support system of Villamayor (Salamanca, Spain).

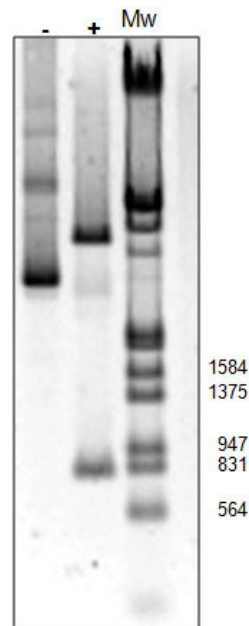


**Fig. 2.27.** Restriction analysis of the purified plasmid digested with EcoRI enzyme (+) and non-digested (-). The agarose gel shows the digestion of a plasmid containing the A-chain with part of the B-chain. Mw:  $\lambda$  Hind III/EcoRI double digest DNA marker.

Below, the cDNA sequence encoding kirkiin A-chain with part of the B-chain was represented in alignment with the genomic DNA sequences obtained for the A-chain with part of the B-chain and for the entire sequence (of which only positions from 1 to 794 are represented) (figure 2.28). The sequences differ in two nucleotides (positions 351 and 504, represented in box in the figure); however, they are included in codons which encode the same amino acids (CAC/CAT encoding His and GTC/GTT encoding Val in positions 351 and 504, respectively). These differences can be due to the presence of gene isoforms or simply to errors introduced by Taq Polymerase during the amplification.

```

A genomic      GCCACGGTAGAGAGGTACACTCAGTTTATAATGCTCTTAAGGAACGAACTGGCGGGTGAT 60
A cDNA         GCCACGGTAGAGAGGTACACTCAGTTTATAATGCTCTTAAGGAACGAACTGGCGGGTGAT 60
AB genomic     GCCACGGTAGAGAGGTACACTCAGTTTATAATGCTCTTAAGGAACGAACTGGCGGGTGAT 60
*****

A genomic      GTTTCCTCCACAGGGAATACGCAGGCTGAGGAATCCGGCTGATATTCAGCCTTCACAGCGT 120
A cDNA         GTTTCCTCCACAGGGAATACGCAGGCTGAGGAATCCGGCTGATATTCAGCCTTCACAGCGT 120
AB genomic     GTTTCCTCCACAGGGAATACGCAGGCTGAGGAATCCGGCTGATATTCAGCCTTCACAGCGT 120
*****

A genomic      TTTATTCTTATACAACCTCAACGGCTTCGTAGGCTCCGTCACCTTGATAATGGACGTCAGC 180
A cDNA         TTTATTCTTATACAACCTCAACGGCTTCGTAGGCTCCGTCACCTTGATAATGGACGTCAGC 180
AB genomic     TTTATTCTTATACAACCTCAACGGCTTCGTAGGCTCCGTCACCTTGATAATGGACGTCAGC 180
*****

A genomic      AATGCGTATCTATTGGGTATGAGAGCCGCAACTTTGTGTATCACTTCAACGATGTCTCT 240
A cDNA         AATGCGTATCTATTGGGTATGAGAGCCGCAACTTTGTGTATCACTTCAACGATGTCTCT 240
AB genomic     AATGCGTATCTATTGGGTATGAGAGCCGCAACTTTGTGTATCACTTCAACGATGTCTCT 240
*****

A genomic      ACCTCTTCGATCGCCGATGTTTCCAGACGTACAACGTCAACAGTTGCCATTGGAAGGC 300
A cDNA         ACCTCTTCGATCGCCGATGTTTCCAGACGTACAACGTCAACAGTTGCCATTGGAAGGC 300
AB genomic     ACCTCTTCGATCGCCGATGTTTCCAGACGTACAACGTCAACAGTTGCCATTGGAAGGC 300
*****

A genomic      GGCTATCCCAGCATGCGACACTATGCGCCGGAGAGAGATCAAATGACCATGGATTTCATC 360
A cDNA         GGCTATCCCAGCATGCGACACTATGCGCCGGAGAGAGATCAAATGACCATGGATTTCATC 360
AB genomic     GGCTATCCCAGCATGCGACACTATGCGCCGGAGAGAGATCAAATGACCACGGATTTCATC 360
*****

A genomic      GAACTGGCATAACGCTGTTGATACGCTCTACTATAGTAGTCAAGGCTACGAACAGATCGCG 420
A cDNA         GAACTGGCATAACGCTGTTGATACGCTCTACTATAGTAGTCAAGGCTACGAACAGATCGCG 420
AB genomic     GAACTGGCATAACGCTGTTGATACGCTCTACTATAGTAGTCAAGGCTACGAACAGATCGCG 420
*****

A genomic      CGTTCACCTCGTCTGCTCTGCGCCGGGATGGTTGCAGAAGCCGCCGGTTCGGCTACATCGAG 480
A cDNA         CGTTCACCTCGTCTGCTCTGCGCCGGGATGGTTGCAGAAGCCGCCGGTTCGGCTACATCGAG 480
AB genomic     CGTTCACCTCGTCTGCTCTGCGCCGGGATGGTTGCAGAAGCCGCCGGTTCGGCTACATCGAG 480
*****

A genomic      GGGCTGGTGCGTCAAAGCAITGTCGGGCCAGGAGACTACGGAACTTTCAGACCCGGATGCG 540
A cDNA         GGGCTGGTGCGTCAAAGCAITGTCGGGCCAGGAGACTACGGAACTTTCAGACCCGGATGCG 540
AB genomic     GGGCTGGTGCGTCAAAGCAITGCCGGGCCAGGAGACTACGGAACTTTCAGACCCGGATGCG 540
*****

A genomic      TTGATGTACTCAGTCGTGACAGCGTGGCAGACTCTTTCAGAAAGAATCCAGGGATCCTTC 600
A cDNA         TTGATGTACTCAGTCGTGACAGCGTGGCAGACTCTTTCAGAAAGAATCCAGGGATCCTTC 600
AB genomic     TTGATGTACTCAGTCGTGACAGCGTGGCAGACTCTTTCAGAAAGAATCCAGGGATCCTTC 600
*****

A genomic      GACGGAGCTTCCAGCCAGTTCAGCTGGGGTATGCCAGCGATCCCTTTTATTGGGACAAC 660
A cDNA         GACGGAGCTTCCAGCCAGTTCAGCTGGGGTATGCCAGCGATCCCTTTTATTGGGACAAC 660
AB genomic     GACGGAGCTTCCAGCCAGTTCAGCTGGGGTATGCCAGCGATCCCTTTTATTGGGACAAC 660
*****

A genomic      GTCGCACAGGCCATCACCAGGCTGTCATCATGCTATTCGCCTGCGCTAAAACCTCCAAG 720
A cDNA         GTCGCACAGGCCATCACCAGGCTGTCATCATGCTATTCGCCTGCGCTAAAACCTCCAAG 720
AB genomic     GTCGCACAGGCCATCACCAGGCTGTCATCATGCTATTCGCCTGCGCTAAAACCTCCAAG 720
*****

A genomic      CAATCCGATCCCCCATGGTGATAAGGTCCTTTGTGGATAGGAACGATCCTGTCTGCCCT 780
A cDNA         CAATCCGATCCCCCAT----- 737
AB genomic     CAATCCGATCCCCCATGGTGATAAGGTCCTTTGTGGATAGGAACGATCCTGTCTGCCCT 780
*****

A genomic      TCCGGGGAGACGACT----- 797
A cDNA         -----
AB genomic     TCCGGGGAGACGACT---continuing--- 794

```

**Fig. 2.28.** Alignment between the cDNA sequence encoding kirkiin A-chain (A cDNA) and DNA sequences encoding the A-chain with part of the B-chain (A genomic) and the entire sequence (AB genomic), of which only positions from 1 to 794 are represented. Identical residues (\*). The sequences differ in two nucleotides (positions 351 and 504, represented in box in the figure).

### 2.4.2. Sequence analysis

The full-length kirkiin gene, missing the N-terminal portion, showed an ORF of 1539 bp, encoding a protein of 513 amino acids. The gene contains 721 bp encoding the A-chain (240 amino acids with a theoretical Mw of 28324.21 Da) and 774 bp encoding the B-chain (258 amino acids with a theoretical Mw of 28506.13 Da), separated by a sequence linker of 45 bp (15 amino acids between amino acids 241 and 255). The C-terminal end of the A-chain and the linker sequence was estimated on the basis of the homology with the volkensin gene (figure 2.29). The restriction sites analysis through the program Webcutter 2.0 confirmed the presence of a restriction point for EcoR1 in kirkiin B-chain (position 844, g/aattc).

In order to identify the structurally conserved regions, multiple sequence alignments were performed between kirkiin and several toxic and non-toxic type 2 RIPs, using the program Clustal Omega. Kirkiin amino acid sequence shows a high percentage of identity with RIPs purified from plants of the same genus (96% with stenodactylin and 87% with volkensin), whereas a lower identity ranging from 36% to 41% is evidenced with other type 2 RIPs, amongst which the highest identity is shown with ricin (41.4%). A higher degree of identity can be observed among B-chains (ranging from 42% to 48%, except for *Adenia* RIPs) with respect to A-chains (table 2.6). This data are in agreement with those previous reported in the literature for other type 2 RIPs (Barbieri *et al.*, 1993). The high sequence homology supported the hypothesis that RIP B-chain is a product of a gene duplication event (Di Maro *et al.*, 2014).

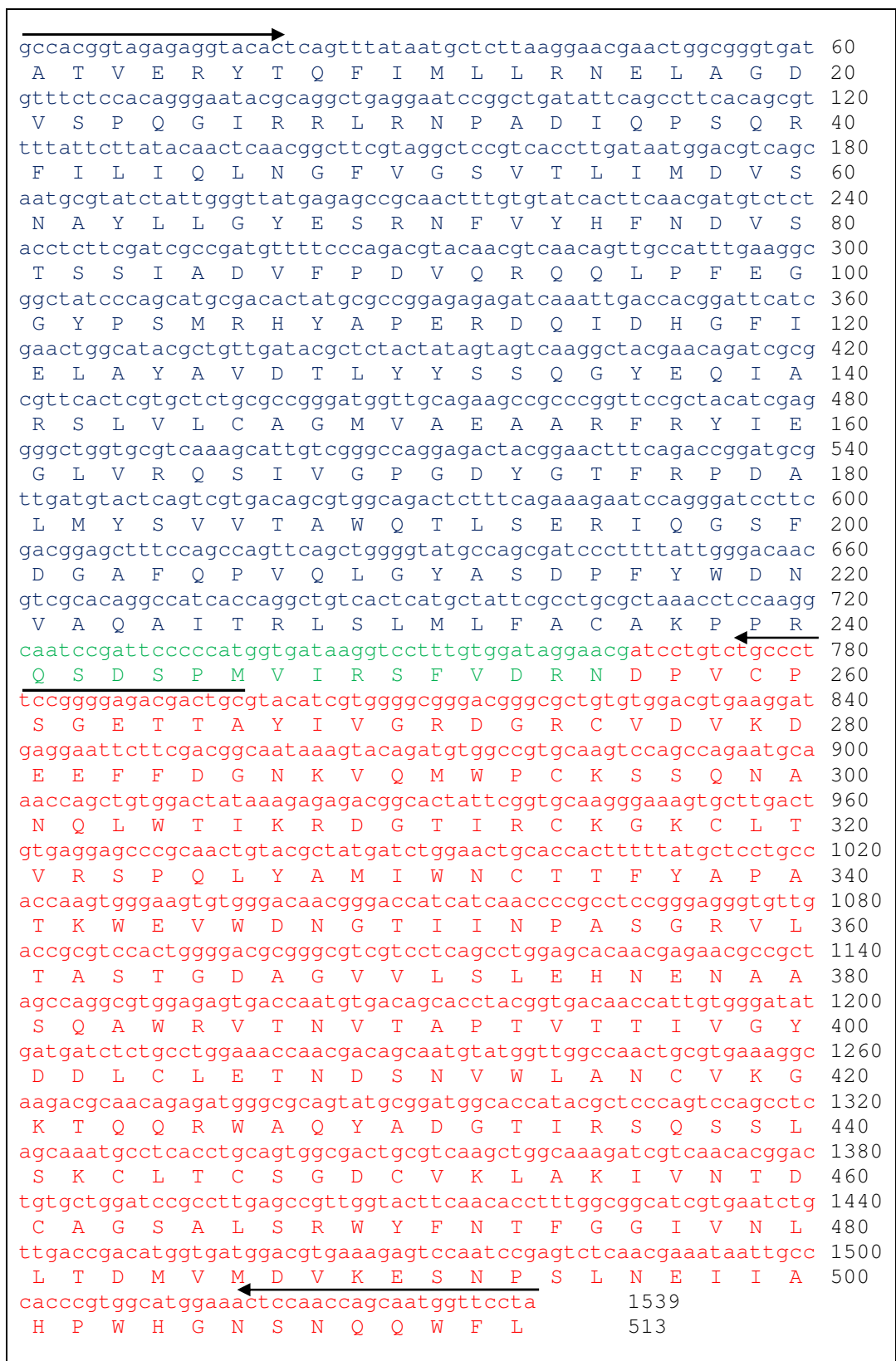


**Fig. 2.29.** Full length sequence and derived amino acid sequence of the kirkiin gene. The A chain is represented in blue, the B chain in red and the sequence of the linker peptide in green. Black arrows indicate the position of the primers used for PCR amplification.

**Table 2.6.** Identity of A-chains, B-chains and complete sequences among kirkiin and nine type 2 RIPs.

	Identity (%) (kirkiin) A-chain	Identity (%) (kirkiin) B-chain	Identity (%) (kirkiin) Complete
<b>Stenodactylin</b>	97.6	95.4	96.3
<b>Volkensin</b>	84.4	89.2	87
<b>Ricin</b>	35.1	48.4	41.4
<b>Abrin</b>	32.4	46.9	40.6
<b>Cinnamomin</b>	37.8	42.7	39.7
<b>Ebulin I</b>	32.9	47.4	39.4
<b>Viscumin</b>	31.4	46.5	39
<b>Nigrin b</b>	32.9	45.8	38.3
<b>Riproximn</b>	30.4	42.2	36.5

Given the availability of kirkiin amino acid sequence, it was possible to predict the three-dimensional structure with a computational model. The program I-TASSER (Treading Assembly Refinement) was used, which builds the 3D structure of the protein of interest by implementing several threading programs and comparing the predicted models with those present in databank. The missing N-terminal end of kirkiin was replaced with that of volkensin, in order to avoid introducing errors during the folding of the protein.

On the basis of the sequence homology (41.4%) and of the crystallographic analysis available in databank, ricin (PDB entry code 2aai) was used as a reference model in order to obtain useful information on amino acids directly or indirectly involved in the toxic activity and to identify any structural differences that may affect the function of the protein. The alignment with ricin was imported in “Discovery Studio 3.5 suite” program for manual processing, introducing appropriate gaps in the sequence and maintaining the alignment of the conserved regions (figure 2.30). This analysis highlighted that the overall folding of ricin is conserved in kirkiin, apart from few discrepancies due to some deletions and insertions in loop regions (figure 2.31). The A-chain consists of three domains: the first domain includes the N-terminal end and is composed of six  $\beta$ -sheets and two  $\alpha$ -helices; the second domain is the most conserved among the A-chains of type 2 RIPs and is formed by five  $\alpha$ -helices; the third domain

consists of two  $\alpha$ -helices, two antiparallel  $\beta$ -sheets and an unstructured coil region in the C-terminal. Similarly to other type 2 RIPs, kirkiin B-chain is made of two similar globular domains, exclusively formed by  $\beta$ -sheets in a trefoil structure (three  $\beta$ -sheets, one-loop and one  $\beta$ -sheet). Each domain consists of three main sub-domains ( $1\alpha$ ,  $1\beta$  and  $1\gamma$  for the domain 1;  $2\alpha$ ,  $2\beta$  and  $2\gamma$  for the domain 2), which are homologous to the corresponding sub-domains of ricin B-chain (figure 2.32). Only two of these sub-domains,  $1\alpha$  and  $2\gamma$ , bind galactose. Two further subdomains are represented,  $1\lambda$  and  $2\lambda$ , responsible for the bind to the A-chain and for the interconnection between the two B-chain domains, respectively (figure 2.30).

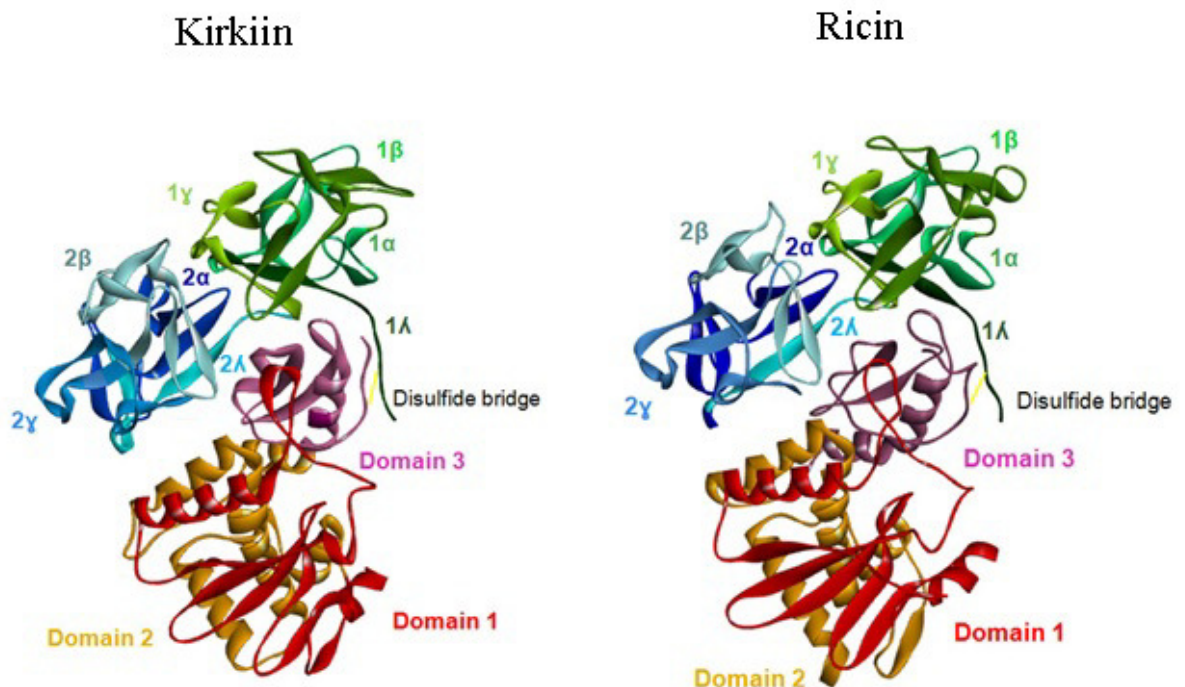


**Fig. 2.30.** Kirkiin 3D model predicted by I-TASSER protein structure prediction program and crystallographic analysis of ricin (PDB entry code 2aai).

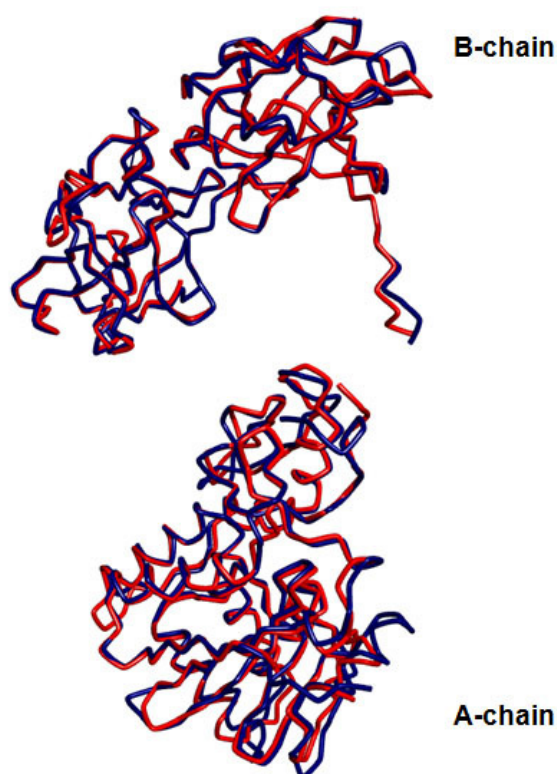


**Fig. 2.31.** Ricin and kirkiin structure folding by alignment imported in Discovery Studio program. RMSD 1.75 Å.

1 $\alpha$	17	NGLCVDV	RDRFHNGNAI	QLWPC	KSNTDANQ	IWT	TLKRDNT	IRS	59
1 $\alpha'$	17	DGRCVDV	KDEEFFDGNKV	QMWPC	KSSQNANQ	IWT	IKRDGT	IRC	59
2 $\alpha$	148	YGLCLOAN	-----	SGQVWIEDC	-SSEKAEQQ	WALYADGS	IRP	183	
2 $\alpha'$	146	DDL	CLETN	-----	DSNVWLANC	-VKGKTQQR	WAQYADGT	IRS	181
1 $\beta$	60	NGKCLT	TYGYS--	PGVYVMI	YDCNTAAT	DATRW	QIWDNGT	IIN	100
1 $\beta'$	60	KGKCLT	V--RS--	PQLYAMI	WNCTTFY	APATKWE	VWDNGT	IIN	98
2 $\beta$	187	RDNCLT	SDSNI--	RETVVK	ILSC-GP	ASSGQR	WMFKNDG	TILN	226
2 $\beta'$	192	SGDCVK	LA-----	KIVNTD	CAGSALS	HWYFNT	FFGGI	VN	224
1 $\gamma$	103	SSLVLA	AATSGN--	SGTTLT	--VQTN	IYAVSQ	WLPTN	-----	135
1 $\gamma'$	101	SGRVLT	AATSGD--	AGVVLS	--LEHN	ENAASQ	AWRVTN	-----	133
2 $\gamma$	229	SGLVLD	VVRASD---	PSLKQI	ILYPLH	GDPNQ	IWLPLF	-----	262
2 $\gamma'$	227	TDMVMD	VKESN---	PSLNEI	IAHPWH	GNSNQ	QWFL	-----	258

**Fig. 2.32.** Alignment of the amino acid sequence stretches of the homologous subdomains of ricin B-chain (1 $\alpha$ , 2 $\alpha$ , 1 $\beta$ , 2 $\beta$ , 1 $\gamma$ , 2 $\gamma$ ) with the corresponding stretches of kirkiin B-chain (1 $\alpha'$ , 2 $\alpha'$ , 1 $\beta'$ , 2 $\beta'$ , 1 $\gamma'$ , 2 $\gamma'$ ). Identical residues are boxed and conserved hydrophobic residues are indicated by asterisks (\*). The cysteine residues participating in forming disulfide bridges in the  $\alpha$  and  $\beta$  subdomains are represented in yellow. The position of Cys206 in the subdomain 2 $\beta'$  of kirkiin is shifted by two positions when  $\alpha$  and  $\beta$  subdomains are aligned. The amino acids involved in the carbohydrate-binding sites are highlighted in green.

As previously reported in table 2.6, kirkiin A-chain showed a sequence homology with volkensin and ricin A-chains of 84.4% and 35.1%, respectively. It includes two cysteine residues, Cys157 and Cys246, the latter located at the C-terminal (figure 2.33). Kirkiin B-chain, instead, showed a higher sequence homology with volkensin and ricin B-chains, with identity values of 89.2% and 48.4%, respectively. The B-chain has twelve cysteine residues, three more than those present in ricin. It is known for other type 2 RIPs that the C-terminal cysteine of the A-chain forms an interchain disulfide bridge with the cysteine at the N-terminal of the B-chain and that the two domains of the B chain are each organized around two disulfide bridges. On the basis of the sequence alignments with other type 2 RIPs and of the three-dimensional structure, it seems that this scheme is also present in kirkiin. As regards the three more cysteines sited on the B-chain, on the basis of the 3D model, the Cys59 seems to be isolated in the domain 1, while the other two (Cys191 and Cys195) are located in a loop in the domain 2, close enough to form a disulfide bridge. Therefore, it might be interesting to investigate the role of these cysteine residues of kirkiin B-chain and if their reduction can affect the biological property of the molecule.

Two possible glycosylation sites were detected by the program NetNGlyc1.0 in the B-chain at the position Asn93-Gly94-Thr95 and Asn133-Val134-Thr135. The presence of carbohydrates could explain the difference in the molecular weight of the B chain calculated on the basis of the amino acid sequence (28.5 kDa) and that observed by electrophoretic mobility (35 kDa) (figure 2.33).

A-chain

```

Ricin      I F P K Q Y P I I N F T T A G A T V Q S Y T N F I R A V R G R L T T G A D V R H E I P V L P N R V G L P I N Q R F I L V E L S N H A E L S V 70
Kirkiin    ----V F P K V P F D V P K A T V E R Y T Q F I M L L R N E L A G D V S - P Q G I R R L R N P A D I Q P S Q R F I L I Q L N G F V - G S V 64
Volkensin  ----V F P K V P F D V P K A T V E S Y T R F I R V L R D E L A G G V S - P Q G I R R L R N P A E I Q P S Q G F I L I Q L T G Y V - G S V 64
          : * : * .   * * * : * * * *   : * . . . : . . . : *   * *   . :   . * * * * : * . . . . * *

Ricin      T L A L D V T N A Y V V G Y R A G N S A Y F F H P D N Q E D A E A I T H L F T D V Q N R Y T F A F G G N Y D R L E Q L A G N L R E N I E L G 140
Kirkiin    T L I M D V S N A Y L L G Y E S R N F V Y H F N D V --- S T S S I A D V F P D V Q R - Q Q L P F E G G Y P S M R H Y A P - E R D Q I D H G 129
Volkensin  T L I M D V R N A Y L L G Y L S H N V L Y H F N D V --- S A S S I A S V F P D A Q R - R Q L P F G G G Y P S M R N Y A P - E R D Q I D H G 129
          ** : * * * * * : * *   * * :   . . . * : * * * .   : * * * *   . . . *   * * * : *

Ricin      N G P L E E A I S A L Y Y S T G G T Q L P T L A R S F I I C I Q M I S E A A R F Q Y I E G E M R T R I R Y N --- R R S A P D P S V I T L 207
Kirkiin    F I E L A Y A V D T L Y Y S S Q G Y E --- Q I A R S L V L C A G M V A E A A R F R Y I E G L V R Q S I V G P G D Y G T F R P D A I M Y S V 196
Volkensin  I V E L A Y A V D R L Y S Q - N N N --- Q I A L G L V I C A G M V A E A S R F R Y I E G L V R Q S I V G P G D Y R T F R P D A I M Y S I 195
          *   * : * * * . . .   : *   . . . *   : * * * * * : * * * * * : *   *   * *   * *   * *   * *   * *   * *   * *

Ricin      E N S W G R L S T A I Q E S N Q G A F A S P I Q L Q R R N G S K F S V Y D V S I L I P I I A I M V Y R C A P P P S S Q F 267
Kirkiin    V T A W Q T L S E R I Q G S F D G A F Q P - V Q L G Y A - S D P F Y W D N V A Q A I T R L S I M L F A C A K P P R --- 251
Volkensin  V T Q W Q T L S E R I Q G S F N G A F Q P - V Q L G Y A - S D P F Y W D N V A Q A I T R L S I M L F V C S Q P P R --- 250
          . *   * *   * * * . . . * *   . . . *   : * : *   *   : * * * * * : * * * * *

```

B-chain

```

Ricin      A D V C M D P E P I V R I V G R N G L C V D V R D G R F H N G N A I Q L F P C K S N T D A N Q L W T L K R D N T I R S N G K C L T T Y G Y S 70
Kirkiin    D P V C P S G E T T A Y I V G R D G R C V D V K D E E F D G N K V Q M W P C K S Q N A N Q L W T I K R D G T I R C K G K C L T V -- R S 68
Volkensin  D P V C P S G E T T A F I V G R D G R C V D V K V E E F D G N K V Q M W P C K S Q N A N Q L W T I K R D G T I R C Q G K C L T V -- R S 68
          * *   . *   .   * * * * * * * * * *   . * . . . *   : * * * * * * * * * * * * * * * * * * * * * * * * * * * * * *

Ricin      P G V Y V M I Y D C N T A A T D A T R W Q I W D N G T I I N P R S S L V L A A T S G N S G T T L T V Q T N I Y A V S Q G W L P T N N T Q P F 140
Kirkiin    P Q L Y A M I W N C T T F Y A P A T K W E V W D N G T I I N P A S G R V L T A S T G D A G V V L S L E H N E N A A S Q A W R V I N V T A P T 138
Volkensin  P Q L Y A M I W D C T T F Y A P A T K W E V W D N G T I I N P A S G R V L T A P T G E A G V T L N L Q F N E Y A A S Q A W R V I N V T V P T 138
          * : * . * * * * * * * * * * * * * * * * * * * * * * * * * * * * * * * * * * * * * * * * * * * * * * * * * * * * * * * * * * * *

Ricin      V T T I V G L Y G L C L Q A N S G Q V W I E D C S S E K A E Q Q W A L Y A D G S I R P Q Q N R D N C L T S D S N I R E T V V K I L S C G P A 210
Kirkiin    V T T I V G Y D D L C L E T N D S N V W L A N C V K G K T Q Q R W A Q Y A D G T I R S Q S S L S K C L T C S G D C V K L A K I V N T D C A G 208
Volkensin  V T T I V G Y D D L C L E T N G N G V W L A N C V K G K A Q Q R W T L Y A D G T I R S Q S T L S K C L A C S G S C V K L A K I V N T D C A G 208
          * * * * * * * * * * * * * * * * * * * * * * * * * * * * * * * * * * * * * * * * * * * * * * * * * * * * * * * * * * * *

Ricin      S S G Q R W M F K N D G T I L N L Y S G L V L D V R A S D P S L K Q I I L Y P L H G D P N Q I W L P L F 262
Kirkiin    S A L S R W Y F N T F G G I V N L L T D M V M D V K E S N P S L N E I I A H P W H G N S N Q Q W F L -- 258
Volkensin  S A N S R W Y F D N Y G G I V N L R T G M V M D V K E S N P S L N E I I A H P W H G N S N Q Q W F L -- 258
          * : . * * * * . * * * * * . . . * * * * * * * * * * * * * * * * * * * * * * * * * * * * * * * * * * * * * * * * *

```

**Fig. 2.33.** Protein sequence alignment of kirkiin with ricin (acc.no P02879) and volkensin (acc.no CAD61022). The missing N-terminal end of kirkiin was replaced with that of volkensin (represented in red). Identical residues (\*), conserved substitutions (:), and semi-conserved substitutions (.) are reported. Cysteine residues are highlighted in yellow. The position of Cys206 in ricin B-chain is shifted by one position after the alignment. The amino acid residues formed the active site are highlighted in gray, whereas the amino acids involved in the carbohydrate-binding sites are highlighted in green. The positions of the intramolecular and intermolecular disulfide bonds of ricin are indicated by solid lines. The possible glycosylation sites are highlighted in light blue. Dashes denote gaps introduced to obtain maximal homology.

A study on amino acids conservation among various type 2 RIPs was carried out for both A- and B-chains. The analysis was performed using 41 amino acid sequences of A-chains of type 2 RIPs and 46 amino acid sequences of B-chains and lectins. The sequence alignments were performed using the Mega6 program with the default parameters manually modified aligning a number of amino acids characteristic of the sequences, such as those of the active site for the A-chains and the cysteines for the B-chains. The aligned sequences were graphically represented by sequence logos created with WebLogo 3 (figure 2.34). On the basis of the structure obtained for kirkiin, the conserved amino acids for each chain were represented with “Discovery Studio3.5 suite” program (figure 2.35 for A-chain and 2.36 for B-chain). In this representation, it was highlighted not only the conserved amino acids of the active site and of the galactose binding sites, but also the most conserved outside of these sites.

As regards the A-chain, most of the highly conserved amino acids among type 2 RIPs are also conserved in kirkiin. Alignment of amino acid sequences shows that the amino acids responsible for the enzymatic mechanism of the active site are conserved in all the A chains of type 2 RIPs and are also present in kirkiin: Tyr74, Tyr113 and Trp200 (Tyr100, Tyr144 and Trp241 in the sequence logo) are the amino acids responsible for the substrate binding to the active site, whereas Glu163 and Arg166 (Glu202 and Arg205 in the sequence logo) are the amino acids responsible for the N-glycosylase activity of the protein. In figure 2.37, the amino acids of the active site of kirkiin and ricin A-chains are represented in detail. These residues are located in equivalent positions in the three-dimensional structure of ricin and kirkiin, creating a kind of pocket among the three domains of the A chain, although the orientation of some of them in kirkiin can vary with respect to ricin. Another highly conserved amino acid located in the active site, Phe167 (206 in the sequence logo), is also present in kirkiin; its function is still unclear, but seems to be involved in stabilizing the conformation of the side chain of Arg166 (Di Maro *et al.*, 2014). Other amino acids in the active site that can interact with the adenine are not conserved. It is known that RIPs may use different ways to bind the substrate. Some residues located near the active site of ricin (Asn78, Arg134, Gln173, Ala178, Glu208 and Asn209) are probably involved in the stabilization of the active site and almost all are conserved among the A-chains of type 2 RIPs, with the exception of kirkiin. In the A chain of the latter, Asn78, Arg134 and Ala178 of ricin are conserved (Asn72, Arg123 and Ala164 in kirkiin, respectively), while Gln173, Glu208 and Asn209 are replaced in kirkiin by Gly159, Val197 and

Thr198, respectively. These substitutions are also present in stenodactylin and volkensin A-chains (Chambery *et al.*, 2004). In addition, Ser204 (245 in the sequence logo) located close to the active site and evolutionarily conserved among RIPs with the function of stabilizing the conformation of the side chain of Trp200 (Chambery *et al.*, 2007), is also conserved in kirkiin.

In figures 2.38 and 2.39, 1 $\alpha$  and 2 $\gamma$  galactose-binding sites of kirkiin and ricin B-chains are represented. The amino acid residues involved in the binding are located in equivalent positions in the three-dimensional structure of both proteins, although the orientation of some of them in kirkiin can vary with respect to ricin. All the amino acids involved in 1 $\alpha$  binding domain of ricin B-chain are conserved in kirkiin (Asp22, Gln35, Trp37, Asn46 and Gln47). All amino acids residues forming the 2 $\gamma$  sugar-binding site of ricin are conserved in the B-chain of kirkiin (Asp232, Ile244, Asn253 and Gln254), with the exception of the residue Tyr248 that is replaced by His246 in kirkiin. The same substitution was observed in volkensin (Chambery *et al.*, 2004), in R. communis agglutinin (Roberts *et al.*, 1985) and in PMRIPm of *P. multiflorum* (Van Damme *et al.*, 2000). Mutagenesis site-specific studies on ricin B-chain showed that the substitution of Tyr248 with His remarkably reduced the binding activity to the galactose (Lehar *et al.*, 1994). In fact, the introduction of a positive charge in the 2 $\gamma$  binding site prevents the hydrophobic interaction between the pyranose ring of galactose and the aromatic ring of tyrosine, reducing the function of the lectin domain. Moreover, in ebulin I the substitution of Tyr248 of ricin with the aromatic residue Phe is responsible of its reduced toxicity. The assumption that this substitution in 2 $\gamma$  domain would affect the binding activity of the protein, does not correlate with the results obtained for kirkiin. On the contrary, kirkiin is highly cytotoxic, although this change in 2 $\gamma$  domain.

The majority of highly conserved amino acids among RIP B-chains are also conserved in kirkiin, with the exception of Cys59, Arg103, Gln173 and Ser212. Only three amino acids localized in 1 $\alpha$  galactose binding site of kirkiin are highly conserved, Asp22 (27) Asn46 (55) and Gln 47 (56); while in 2 $\gamma$  domain all the amino acids are preserved except His246. As reported in the literature, other highly conserved amino acids, not involved in the sugar-binding, seem to be important in maintaining the symmetry of the domains (Di Maro *et al.*, 2014).

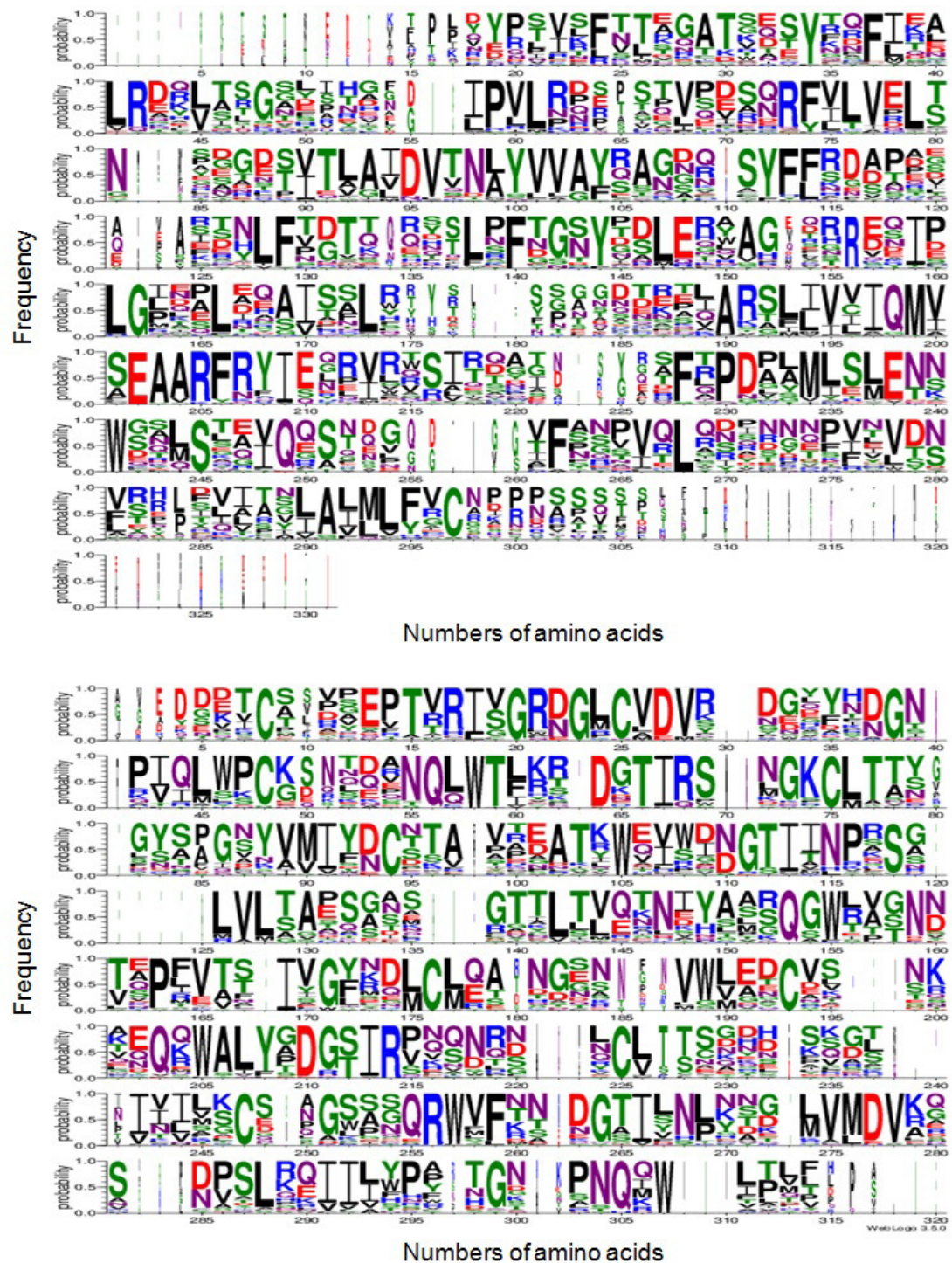


**Fig. 2.34.** Amino acids conservation among A-chains (up) and B-chains (down) of type 2 RIPs. The analysis was performed using 41 amino acid sequences of A-chains of type 2 RIPs and 46 amino acid sequences of B-chains and lectins, aligned with the Mega6 program. The height of the letters is proportional to the frequency of that amino acid in that position with respect to all the amino acids, while the width corresponds to the frequency of that amino acid including the gaps of the sequences. 40/53 highly conserved amino acids are conserved in kirkiin A-chain; 64/69 highly conserved amino acids are conserved in kirkiin B-chain.

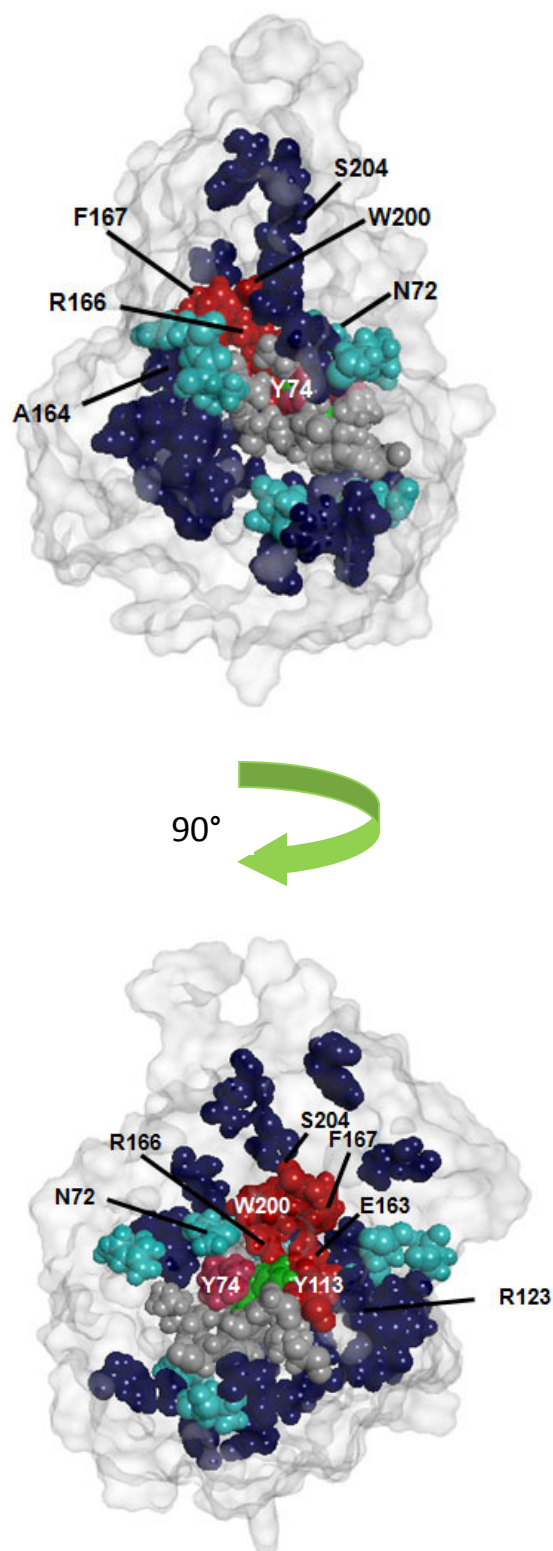


**Fig. 2.35.** 3D representation of kirkiin A-chain, in which the amino acids conserved among type 2 RIPs are represented. Adenin is represented in green. The amino acids conserved inside the active site are represented in dark red (>90%) and in light red (>80%); the amino acids conserved outside the active site are represented in dark blue (>90%) and in light blue (>80%); non-conserved amino acids are represented in grey.

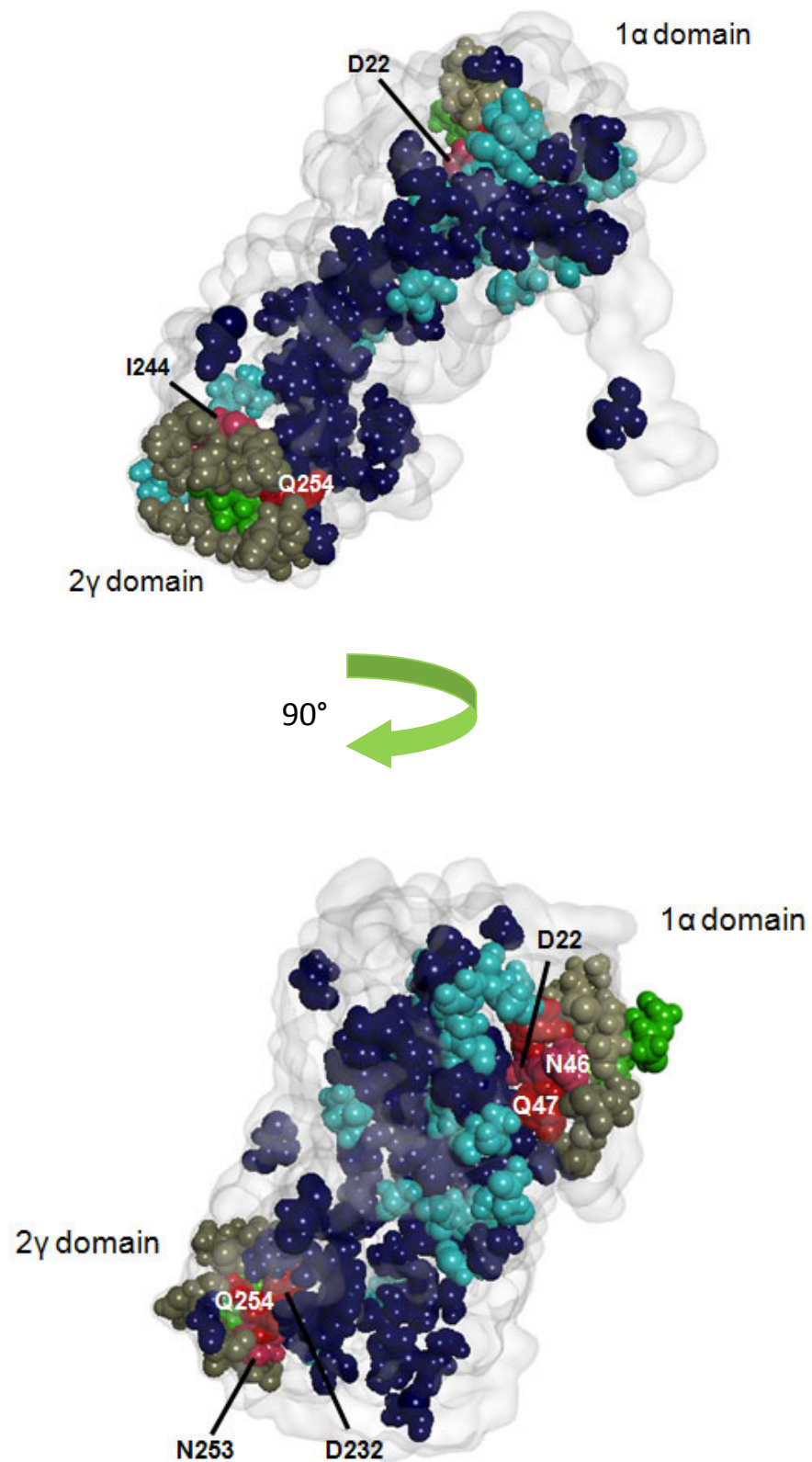


**Fig. 2.36.** 3D representation of kirkiin B-chain in which the amino acids conserved among type 2 RIPs are represented. The sugar is represented in green. The amino acids conserved inside the sugar-binding site are represented in dark red (>90%) and in light red (>80%); the amino acids conserved outside the sugar-binding site are represented in dark blue (>90%) and in light blue (>80%); non-conserved amino acids are represented in grey.

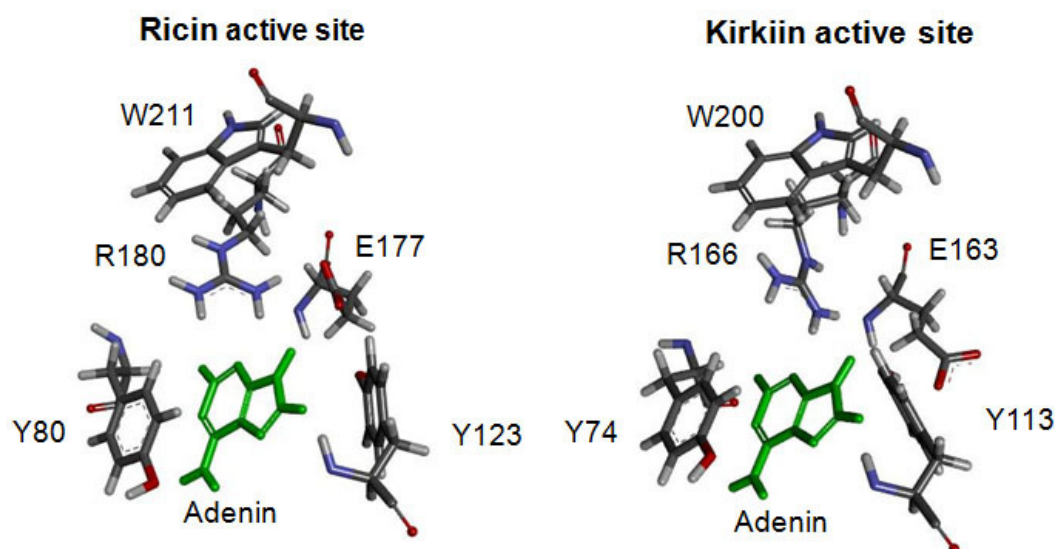


**Fig. 2.37.** 3D representation of the amino acids of the active site of kirkiin and ricin A-chains. Adenin is represented in green. Docking was predicted with COACH program.

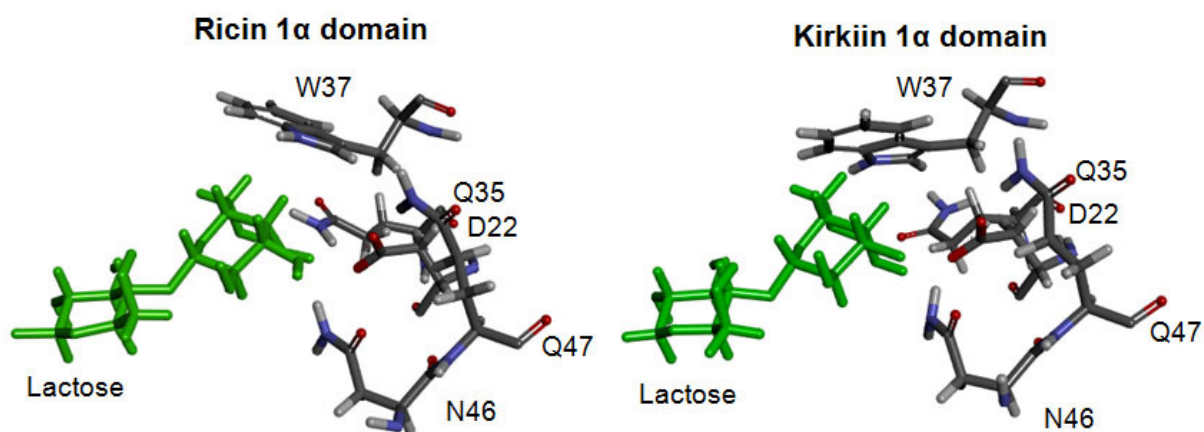


**Fig. 2.38.** 3D representation of the amino acids of 1 $\alpha$  domain of kirkiin and ricin B-chains. Lactose is represented in green. Docking was predicted with COACH program.

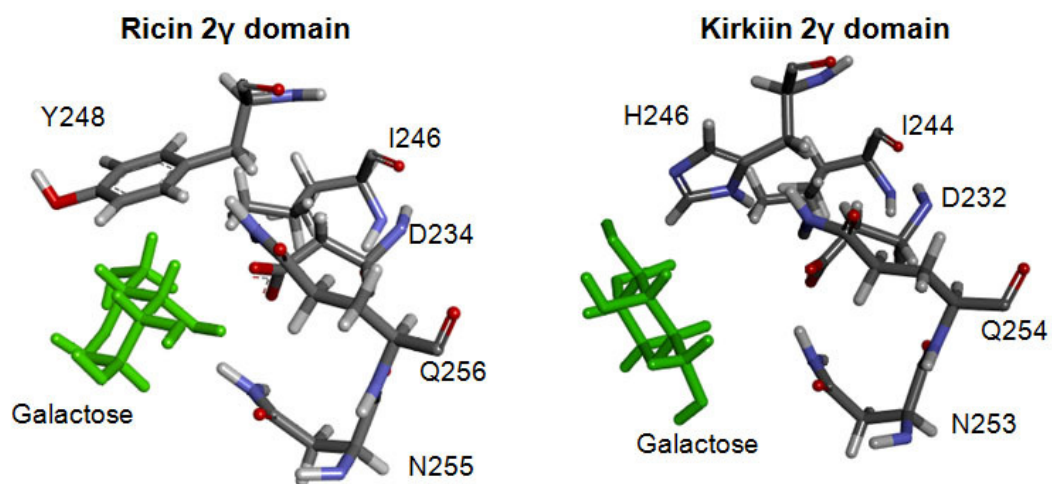


**Fig. 2.39** 3D representation of the amino acids of 1 $\alpha$  domain of kirkiin and ricin B-chains. Galactose is represented in green. Docking was predicted with PATCHDOCK program.

## CONCLUSION

This study demonstrates that *A. kirki* contains a high amount of two proteins that have the characteristics of galactose-specific lectins and agglutinate erythrocytes. In particular, one of these, called kirkiin, shows biochemical, enzymatic and cytotoxic characteristics of type 2 RIPs. Kirkiin shows N-glycosylase activity on mammalian and yeast ribosomes, but little or no activity on other nucleotide substrates (viral RNA, ssDNA). This toxin is able to completely inhibit protein synthesis both in a cell-free system and in cells and to induce cell death by apoptosis at very low doses in the tested cell lines.

The toxin is immunologically similar to other *Adenia* toxins, which is not surprising, in that they all came from plants belonging to the same Passifloraceae family and have many similarities in their amino acid sequences. Kirkiin partially cross-reacts with sera against type 1 RIPs momordin and PAP, while does not react with sera against ricin and saporin S6. This results represent a remarkable advantage in prospecting the use of an immunotoxin containing kirkiin in prolonged therapeutic treatments in substitution to immunotoxins containing ricin and saporin, which are two of the most used RIPs as toxic components of immunoconjugates.

The amino acid sequence analysis showed that kirkiin possesses all the characteristics of a protein with N-glycosylase enzymatic activity. Despite differences in the amino acid sequence with respect to other RIPs, the results of the modelling studies indicated that the three-dimensional structure of kirkiin preserves the overall folding of type 2 RIPs.

The hypothesis that the substitution of His246 in kirkiin 2 $\gamma$  domain can affect the binding, does not correlate with the results obtained by cytotoxicity. Another interesting aspect is that, despite the high degree of conservation of amino acid residues of both A- and B-chains, kirkiin shows a difference in terms of toxicity compared with other type 2 RIPs. Further studies on the conservation of polar and hydrophobic interactions both on the interface between the chains and on the domains near the active site will be useful, in order to fully understand the correlation between structure and function of the molecule and in general of all RIPs. Any differences could clarify the interaction with various nucleotide substrates and the different biological behavior of the toxin, not due to differences in the active site.

In conclusion, the high cytotoxicity of kirkiin and other toxins derived from plants of the *genus* *Adenia* represents an important opportunity for the present and future development of new drugs, both native, for limited local treatments, and conjugated to carrier molecules selective for tumor cells, for local or systemic treatments. Moreover, the assessment of the ability of these toxins to be transported in a retrograde manner in the central nervous system may have very interesting applications in neuroanatomy, neurophysiology and therapy.

*Chapter 3*

**Cell death pathways induced  
by non-toxic type 2 RIPs from  
Sambucus**



## AIM OF THE PROJECT

Sambucus RIPs, both type 1 and type 2, are able to strongly inhibit protein synthesis in a cell-free system consisting of a rabbit reticulocytes lisate, with  $IC_{50}$  in nM range (Girbes *et al.*, 1993a, b). Despite this, type 2 RIPs from Sambucus showed a low cytotoxicity, comparable to that of type 1 RIPs, even though they are endowed with lectin activity. Thanks to their high enzymatic activity and low non-specific toxicity, the two non-toxic type 2 RIPs ebulin 1, extracted from the leaves of *S. ebulus*, and nigrin b, extracted from the bark of *S. nigra* (figure 1), have been used to construct immunotoxins directed towards the transferrin receptor, highly expressed in some cell lines and in many human tumors (Citores *et al.*, 2002), and immunotoxins specific for the endothelial receptor CD105 (endoglin), strongly expressed during neo-angiogenesis and in vessels of tumor tissues (Benítez *et al.*, 2005; Muñoz *et al.*, 2007). These immunotoxins showed high cytotoxicity with  $IC_{50}$  values in the picomolar range. The use of ebulin 1 and nigrin b as component of immunotoxins could present some advantages with respect to toxic type 2 RIPs: less probability to develop VLS; less systemic toxic effects when toxins are released outside of the target cells, after breakage of the bond with the antibody; and more safety for the operator during the purification processes (Ferrerias *et al.*, 2011).

The understanding of cell death pathways implicated in RIP intoxication represents an important aspect both in preclinical and clinical studies, as in cancer therapy it is important to choose a toxin that does not induce necrosis, in order to reduce or avoid side effects.



**Fig. 1.** Leaves of *S. ebulus*(on the left) and bark of *S. nigra* (on the right).

Despite the potential and the therapeutic value of ebulin 1 and nigrin b have been well described, the pathogenic mechanism of their toxicity remains unsolved.

The study carried out in this thesis was focused on understanding the pathogenesis of the cellular intoxication induced by the non-toxic type 2 RIPs from *Sambucus* in a neuroblastoma-derived cell line, which is particularly sensitive to RIPs both single-chains and double-chains (Barbieri *et al.*, 1993). The obtained results were compared with those of the toxic type 2 RIPs ricin and stenodactylin and the type 1 RIP saporin. Knowledge about the cell death mechanisms implicated might allow a better pharmacological use of these toxins, with an increase in their therapeutic efficacy against target cells.

## RESULTS AND DISCUSSION

In a preliminary study, ebulin 1 and nigrin b showed a strong ability to inhibit protein synthesis *in vitro* in a cell-free system consisting of a lysate of rabbit reticulocytes. The IC<sub>50</sub> values resulted 8.7 ng/ml and 5.4 ng/ml for ebulin 1 and nigrin b, respectively. These data were comparable to those reported in the literature for other type 1 and type 2 RIPs (Ferrerias *et al.*, 2011). In table 3.1, IC<sub>50</sub> values of ebulin 1 and nigrin b were compared with those of ricin and stenodactylin, and the single-chain RIP saporin. The IC<sub>50</sub> values of the two RIPs from Sambucus are of the same order of magnitude of both ricin and saporin. The high IC<sub>50</sub> of stenodactylin (already described in the literature by Stirpe *et al.*, 2007) has been justified with the difficulty to reduce the interchain disulphide bridge of the molecule without inactivating the A-chain.

**Table 3.1:** Effect of type 1 and type 2 RIPs on protein synthesis in a cell-free system consisting of a lysate of rabbit reticulocytes.

IC <sub>50</sub> (ng/ml)				
Ebulin 1	Nigrin b	Stenodactylin	Ricin	Saporin
8.7	5.4	498*	6	1.8

\* probable incomplete reduction of the RIP

Despite of the high translational inhibition activity in the cell-free system, ebulin 1 and nigrin b showed a low cytotoxicity on NB100 cells, with EC<sub>50</sub> values quite similar for both toxins from Sambucus (10<sup>-8</sup>M), but 5-6 log higher than toxic type 2 RIPs and 3 log higher than saporin (table 3.2). These results reflect experimental evidence already described in the literature in other cellular models (Ferrerias *et al.*, 2011). The low toxicity of Sambucus RIPs could be traced back to a low binding affinity for the membrane receptors. Moreover, their lower toxicity compared to that of type 1 RIPs, probably suggests an inefficient translocation across the plasma membrane, an ineffective reduction of the disulphide bond between A- and B-chains, or an unfavorable intracellular routing, which would impact on their toxic effect (Battelli *et al.*, 1997; Rojo *et al.*, 1997).

**Table 3.2:** Comparison of EC<sub>50</sub> of type 2 RIPs (toxic and non-toxic) and the type 1 RIP saporin in NB100 cells, after 48 hours of incubation with RIPs.

EC <sub>50</sub> (M)				
Ebulin I	Nigrin b	Stenodactylin	Ricin	Saporin
2.0x10 <sup>-8</sup>	1.4x10 <sup>-8</sup>	2.5x10 <sup>-14</sup>	6.5x10 <sup>-13</sup>	1.8x10 <sup>-11</sup>

### 3.1. Cell viability assay

As non-toxic type 2 RIPs showed a low toxicity to NB100 cell line, subsequent studies were conducted using the two RIPs from *Sambucus* at a concentration of 10<sup>-7</sup>M, that was 10 times higher than the EC<sub>50</sub> value, in order to obtain a more marked cytotoxic effect and to better understand the pathways implicated in cell death. Time-course experiments were conducted in a range between 4 and 96 hours and the viability was assayed using a colorimetric method based on MTS reduction.

The viability curves corresponding to the two toxins showed a similar trend. Ebulin I and nigrin b significantly reduced cell viability after 8 hours ( $p < 0.01$ ), which gradually decline until reaching a viability of less than 60% at 24 hours and about 10% at 72 hours for both toxins. The cell viability is completely reduced to 0 after 96 hours (figure 3.1). The time necessary to reduce the viability of 50% (ET<sub>50</sub>) was calculated by linear regression interpolation. Ebulin I showed an ET<sub>50</sub> after 24.4 hours with an  $r^2$  of 0.978, while in nigrin b it was obtained after 26.3 hours with an  $r^2$  of 0.969.

These results suggested that ebulin I and nigrin b were both able to completely eliminate NB100 cells; however, they need more time than other RIPs to fully carry out their cytotoxic effect.

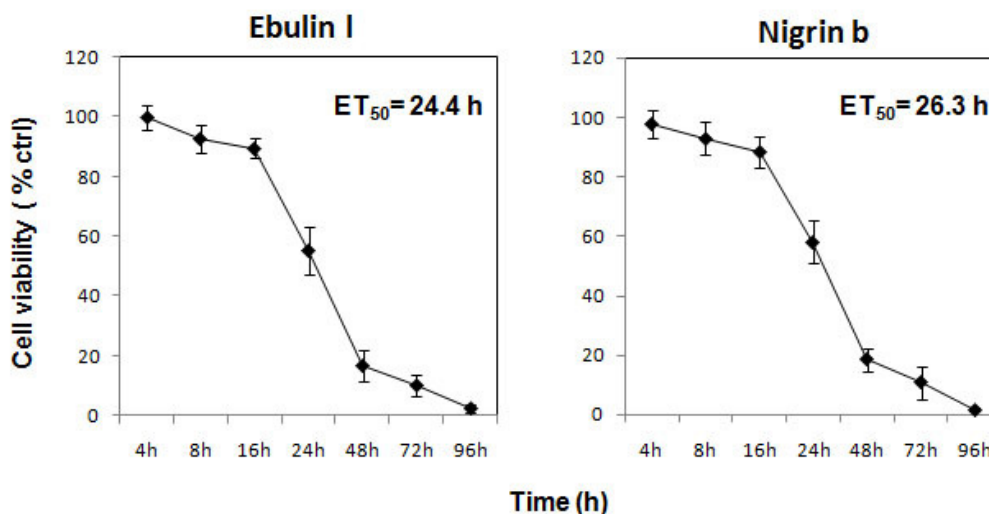


**Fig. 3.1.** Time-response curve. Viability of NB100 cells ( $2 \times 10^3$  cells/well) treated with ebulin I ( $10^{-7}$ M) and nigrin b ( $10^{-7}$ M) after the indicating times. Viability was evaluated using a colorimetric assay based on MTS reduction. The results are the means of three independent experiments, each performed in triplicate, and are represented as percentage of control values obtained from cultures grown in the absence of RIPs. \*\* $p < 0.01$  (8 hours); \*\*\*\* $p < 0.0001$  (16, 24, 48, 72, 96 hours), Anova/ Bonferroni.

## 3.2. Assessment of apoptosis

### 3.2.1. Microscopic analysis with phase-contrast

The presence of cellular morphological changes in NB100 cells treated for 24 and 48 hours with ebulin I and nigrin b was examined by phase-contrast microscopy. After 24 hours of treatment, NB100 cells showed a lower cell density compared to controls; cells also appeared with a certain cytoplasmic granulation attributable to the presence of vacuoles. After 48 hours of intoxication, apoptotic morphological changes, such as cell shrinkage, formation of membrane vesicles and cytoplasmic condensation, became clearly evident (figure 3.2).

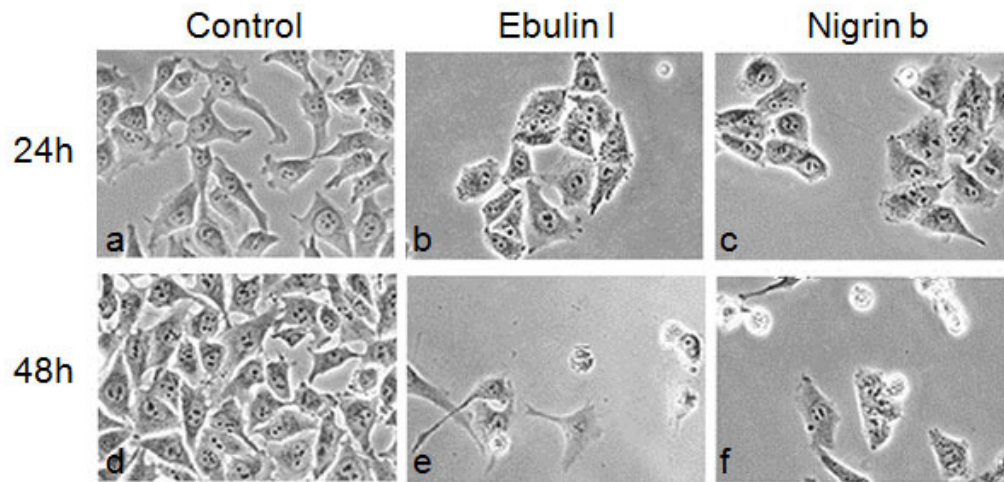


**Fig. 3.2.** NB100 cells morphology by phase-contrast microscopy: untreated (a, d) and treated with ebulin I  $10^{-7}$ M (b, e) and nigrin b  $10^{-7}$ M (c, f) for 24 and 48 hours, respectively (400 $\times$  magnification).

### 3.2.2 Cytofluorimetric analysis

Apoptosis was monitored by double staining with Annexin V/PI through flow cytofluorimetric analysis of NB100 cells. PI-positive cells are in the upper left quadrant, while cells in late apoptosis and early apoptosis are in the upper and lower right quadrants, respectively. After 24 hours of intoxication with RIPs, only about 2% of treated cells were in late stage apoptosis; this percentage increased over time to about 13% at 48 hours for both RIPs (figure 3.3). The positivity to Annexin V/PI in flow cytofluorimetric analysis confirmed the induction of apoptosis after treatment of NB100 cells with ebulin I and nigrin b. Despite the high RIP doses used, no necrosis was detectable.

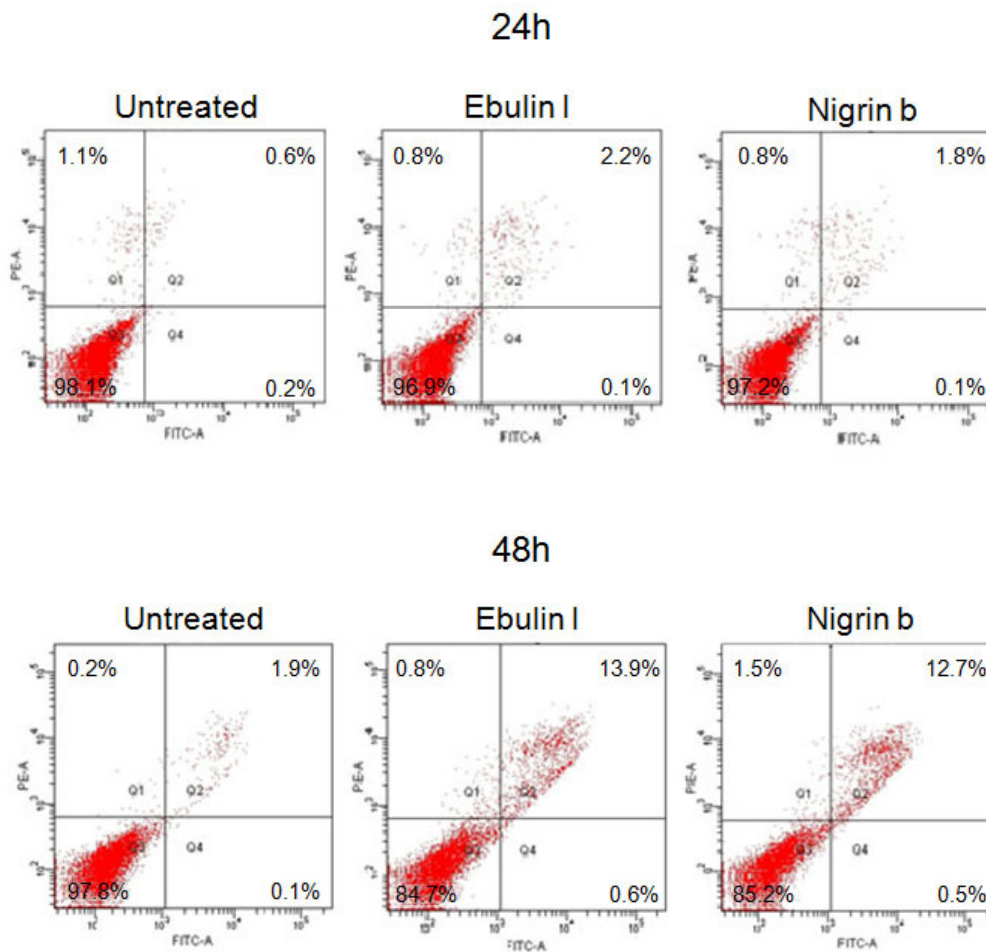


**Fig. 3.3.** Evaluation of apoptosis/necrosis by Annexin V-EGFP/PI staining, followed by flow cytometry analysis. Representative plots of Annexin V (FITC channel)/PI (PE channel) staining of NB100 cells untreated or treated with ebulin I ( $10^{-7}$ M) and nigrin b ( $10^{-7}$ M).

Comparison of cell viability results with those obtained with Annexin V/IP showed a strong discrepancy. In fact, the percentage of dead cells in the samples treated with the two RIPs resulted lower in vitality experiments, obtained by MTS reduction assay (about 40% and 80% at 24 and 48 hours, respectively), compared to the percentage of cells positive to Annexin V and/or to IP (about 3% and 15% at 24 and 48 hours, respectively). For this reason, cell viability was evaluated with alternative methods, such as the Trypan Blue vital exclusion test and the determination of cellular ATP in bioluminescence. Experiments were performed at 24 and 48 hours, expressing data as percentage of controls (as in MTS assay). The results obtained were compared with the values obtained with the MTS reduction assay. The graph showed that the viability of cells treated with ebulin I and nigrin b did not significantly vary when evaluated with the three methods (figure 3.4).

As the Trypan Blue test is the only method, among the three used, that allows to discriminate dead cells from viable cells, it was possible to express the data obtained with this method as percentage of dead cells with respect to the total cells, in order to compare them with those obtained with cytofluorimetric analysis. The percentages of dead cells obtained from the two methods resulted comparable (data not shown). Therefore, the discrepancy between viability data from Trypan Blue or cytofluorimetric analysis and those from MTS or ATP assay might be due to differences related to methodology dissimilarities of the assays.

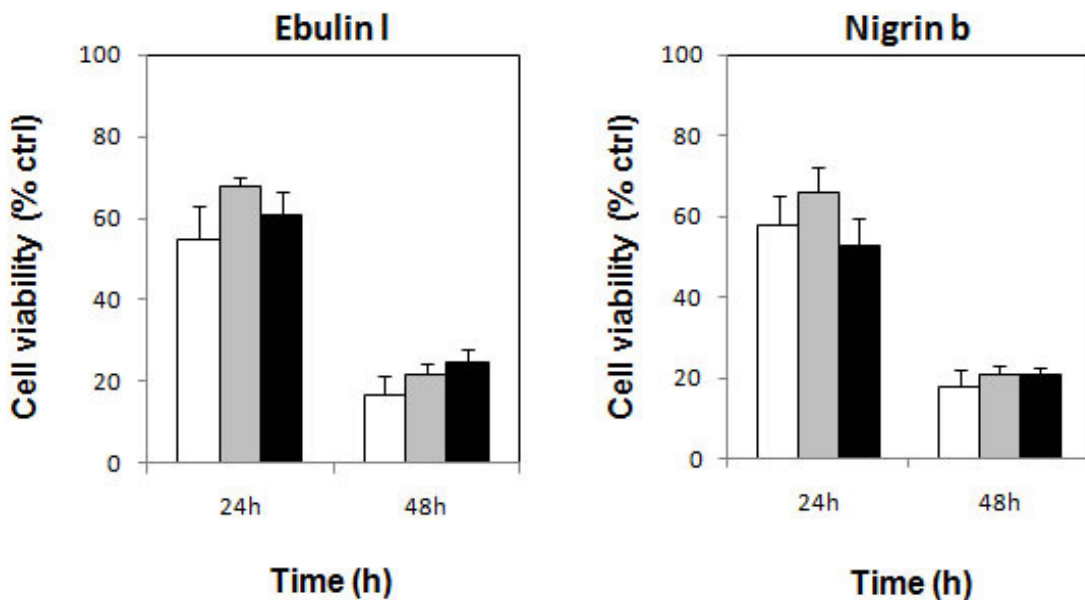


**Fig. 3.4.** Viability of NB100 cells ( $2 \times 10^3$  cells/well) treated with ebulin I ( $10^{-7}$ M) and nigrin b ( $10^{-7}$ M) after 24 and 48 hours. The viability assay based on MTS reduction (white columns) was compared with those based on the determination of the intracellular ATP (grey columns) and on Trypan Blue cell counting (black columns). The results are the means of three independent experiments, each performed in triplicate, and are presented as the percentage of control values obtained from cultures grown in the absence of RIPs. No significant differences were observed (confidence interval 95%, test Anova/Bonferroni).

### 3.2.3 Caspase 3/7 activation

In 2009 Bolognesi and co-workers described ricin and saporin capable to induce apoptotic caspase-dependent death at high concentrations in lymphoma cells (Polito *et al.*, 2009a). To assess the involvement of caspase-dependent apoptosis, caspase 3/7 activation was measured in NB100 cells exposed to  $10^{-7}$ M ebulin I and nigrin b in a time range from 4 to 72 hours. A strong time-dependent activation of caspase 3/7 was

observed, which became significantly higher than in control samples after 8 hours of treatment. The level of caspase activity grew exponentially over time, until reaching a plateau after 48 hours with 1352% and 922% activation values in cells treated with ebulin I and nigrin b, respectively, compared to untreated cells (figure 3.5).

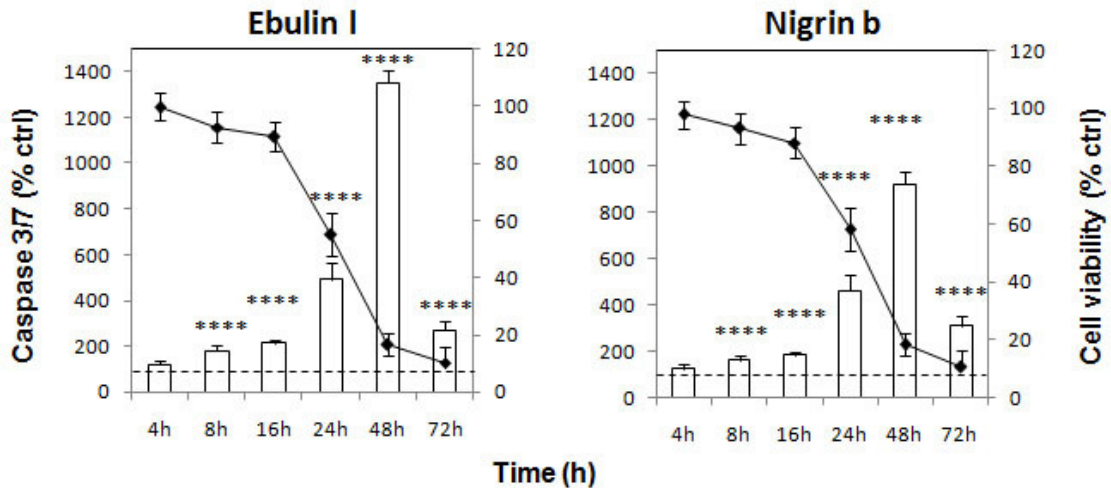


**Fig. 3.5.** Caspase 3/7 activation (columns) in NB100 cells ( $2 \times 10^3$  cells/well) treated with ebulin I ( $10^{-7}$ M) and nigrin b ( $10^{-7}$ M), compared with cell viability ( $\blacklozenge$ ). Caspase activity was expressed as the percentage of control values obtained from cultures grown in the absence of RIPs. The results are the means of three independent experiments, each performed in triplicate. \*\*\*\* $p < 0.0001$ , Anova/ Bonferroni test.

A comparison between non-toxic type 2 RIPs and stenodactylin, ricin and saporin, tested on the same cell line, revealed a strong activation of caspase 3/7 with all these RIPs; however, the extent of activation was lesser in cells treated with ebulin I and nigrin b in the first 24 hours of treatment. After 48 hours of treatment, both ebulin I and nigrin b induced a caspase activation comparable to those obtained after 24 hours with toxic RIPs at much lower concentrations (table 3.3). This demonstrates that the two RIPs from *Sambucus* are able to activate an apoptotic caspase-dependent mechanism of the same magnitude compared with other RIPs, but they need higher concentrations and longer times.

**Table 3.3:** Comparison of caspase 3/7 activation induced by the non-toxic type 2 RIPs ebulin 1 ( $10^{-7}$ M) and nigrin b ( $10^{-7}$ M), the toxic type 2 RIPs ricin ( $10^{-13}$ M) and stenodactylin ( $10^{-14}$ M) and the type 1 RIP saporin ( $10^{-11}$ M), at 24 and 48 hours in NB100 cells.

Caspase 3/7 activation					
	Ebulin 1	Nigrin b	Stenodactylin	Ricin	Saporin
24h	493 %	461%	1484%	1164%	631%
48h	1352%	922%			

### 3.3 Evaluation of cytotoxicity by inhibitors of specific cell death pathways

Further studies have been done in order to evaluate the involvement of the apoptotic process and/or alternative death processes induced by the two RIPs from *Sambucus*. For this purpose cytotoxicity experiments have been conducted in the presence of specific inhibitors of some cell death pathways such as the pan-caspasic inhibitor Z-VAD-fmk (Z-VAD) and the inhibitor of necroptosis, necrostatin-1.

#### 3.3.1. Caspase-dependent apoptosis inhibition by Z-VAD-fmk

To deeper the role of caspase-dependent programmed cell death, the pan-caspase inhibitor Z-VAD was used to selectively inhibit the apoptotic pathway, as the inhibitor irreversibly binds to the catalytic site of caspase. NB100 cells were pretreated and maintained in Z-VAD (100  $\mu$ M) and cell viability was determined with the MTS reduction assay in a time interval from 24 to 96 hours. After 24 hours, a slight but not significant improvement in the survival of cells pretreated with Z-VAD was observed, compared with cells treated with the RIPs alone. However, a significant protective effect of the pan-caspase inhibitor was more evident at longer times of treatment. In particular, after 48 hours the viability increased from 16% to 41% in cells treated with ebulin 1 and from 18% to 46% in cells treated with nigrin b. Cell protection decreased over time: at 72 hours the viability passed from 10% to 35% in cells treated with ebulin 1 and from 10% to 30% in cells treated with nigrin b, while at 96 hours viability resulted 31% and 24% for ebulin 1 and nigrin b, respectively (figure 3.6a).

A comparison of the two non-toxic type 2 RIPs with stenodactylin showed that after 24 hours of treatment with stenodactylin, the presence of the inhibitor gave a total protection to the cells, as the viability increases from 2% to 95%. This total protection of the cell population was not found with ebulin 1 and nigrin b, for which the protection was only partial and became significant only after 48 hours of treatment (figure 3.6b).

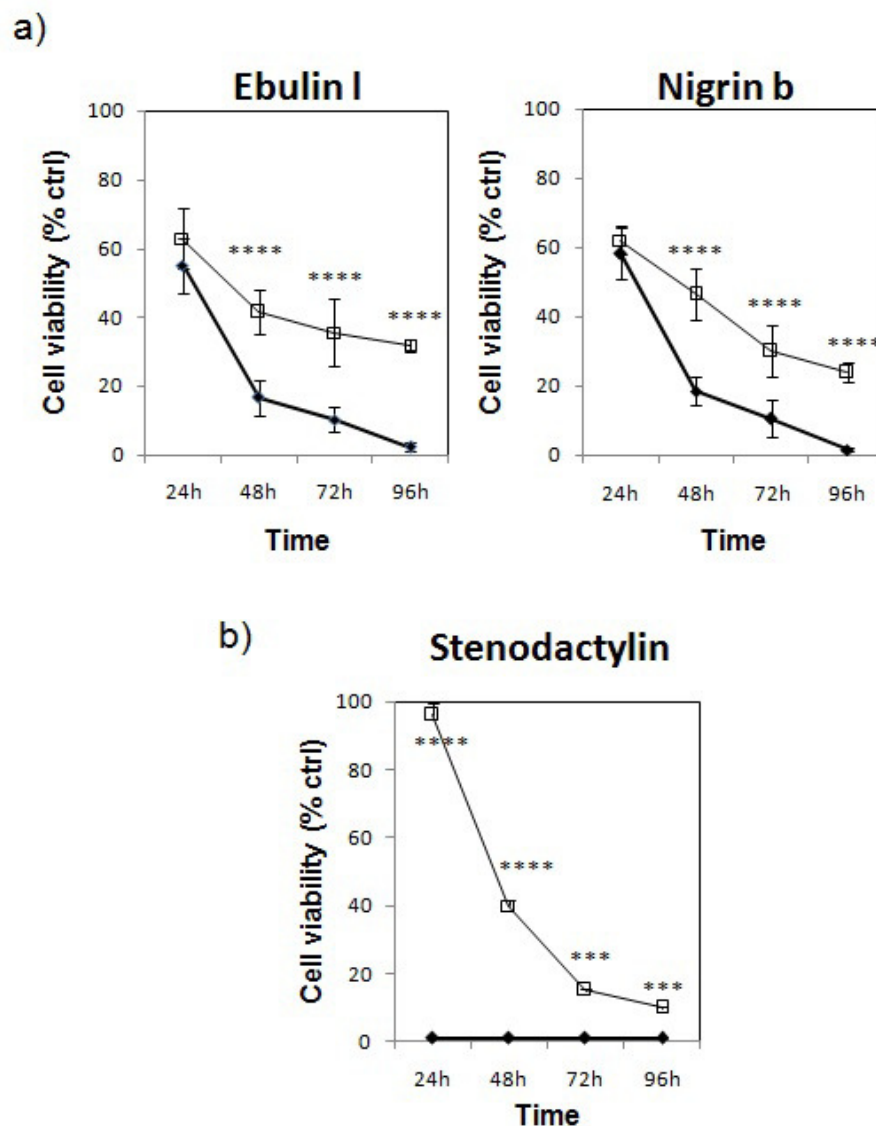


**Fig. 3.6.** Viability of NB100 cells ( $2 \times 10^3$  cells/well) treated with (a) ebulin 1 ( $10^{-7}$ M) and nigrin b ( $10^{-7}$ M) and (b) stenodactylin ( $10^{-12}$ M), alone (◆) or in the presence of 100  $\mu$ M Z-VAD (◻). The pan-caspase inhibitor was added 3 hours before the RIP, and the viability was observed after the indicating times. Viability was evaluated using a colorimetric assay based on MTS reduction. The results are the means of at least three independent experiments, each performed in triplicate, and are presented as the percentage of control values obtained from cultures grown in the absence of RIPs. \*\*\*\* $p < 0.0001$ , Anova/ Bonferroni test.

The lack of a total protection by the pan-caspase inhibitor was not caused by its inactivation. Z-VAD was added every 24 hours, and as reported in figure 3.7, the effector caspase were effectively maintained at the basal level even at long times of treatment.

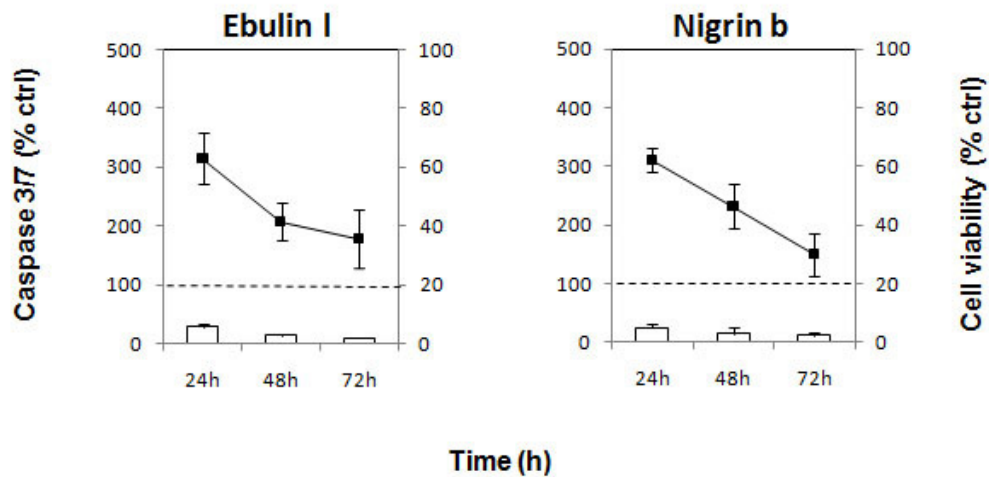


**Fig. 3.7.** Effect of ebulin I ( $10^{-7}$ M) and nigrin b ( $10^{-7}$ M) on cell viability (■) and caspase 3/7 activity (columns) in NB100 cells. Cells were pretreated for 3 hours with 100  $\mu$ M Z-VAD. The viability of NB100 cells was evaluated at the indicate times with a colorimetric assay based on MTS reduction. Caspase 3/7 activity and the cell viability are expressed as the percentage of control values obtained from cultures grown in the absence of RIPs. The results are the means of three independent experiments, each performed in triplicate.

An interesting aspect can be observed at long times of treatment, where the protection given by Z-VAD seems to reach a plateau (about 30% of vitality). This indicates that about 30% of cells does not die if simultaneously incubated with Z-VAD, suggesting that for these cells the activation of another way of cell death is not possible. This may depend on the cell cycle or on metabolic status of the cells, but more probably on the genetic pattern of tumor cells. Genetic alterations could be responsible for the acquirement of cell resistance to death or for a different RIP intracellular routing and compartmentalization, possibly allowing the toxin to reach only a single molecular target.

The morphological analysis of NB100 cells treated with ebulin I and nigrin b in the presence of Z-VAD was assessed by phase-contrast microscopy at 24 and 48 hours. After 24 hours of treatment, no morphological differences were observed between cells

treated with ebulin 1 and nigrin b alone with respect to those pretreated with Z-VAD. However, after 48 hours, there was a greater viability of the cells treated with Z-VAD than those treated with the RIPs alone (figure 3.8).

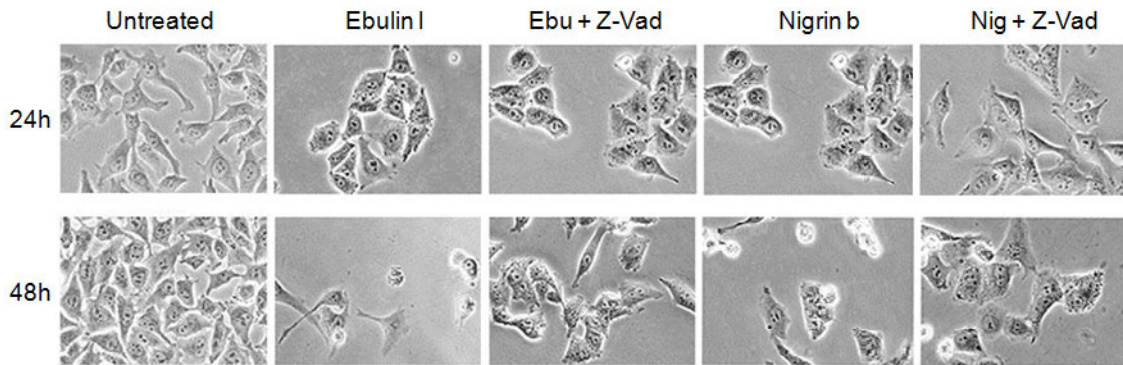


**Fig. 3.8.** NB100 cells morphology by phase-contrast microscopy: untreated and treated with ebulin 1 ( $10^{-7}$ M) and with nigrin b ( $10^{-7}$ M) alone or in the presence of 100  $\mu$ M Z-VAD at 24h and 48h (400 $\times$  magnification). The pan-caspase inhibitor was added 3 hours before the RIP, and the viability was observed after the indicating times.

NB100 cells were subjected to Annexin V/PI double staining after treatment with ebulin 1 and nigrin b in the presence or absence of the inhibitor. At 24 hours, only a slight difference in the number of apoptotic cells among cells treated with the two RIPs alone (2.2% for ebulin 1 and 1.8% for nigrin b) and cells pretreated with Z-VAD (1.4% for ebulin 1 and 0.9% for nigrin b). On the contrary, at 48 hours the difference was more marked with a decrease in the number of cells in advanced apoptosis, passing from 13.9% to 5.1% for ebulin 1 and from 12.7% to 4.9% for nigrin b (figure 3.9).

These results demonstrated the prevalence of apoptosis at 48 hours of treatment and suggested that at 24 hours the apoptotic pathway has still a secondary role in the cell death pathway triggered by the two RIPs from *Sambucus*. This shows a different behavior with respect to toxic type 2 RIPs and supports the hypothesis that *Sambucus* toxins kill cells by activating more than one cell death pathway, which is especially prevalent at 24 hours.

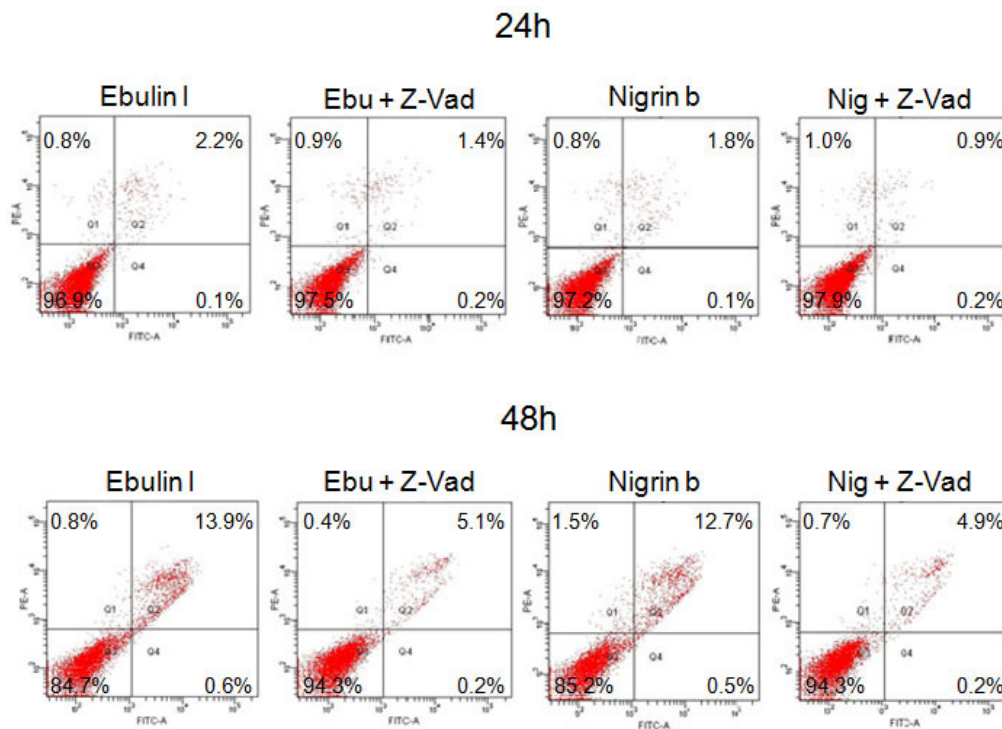


**Fig. 3.9.** Evaluation of apoptosis by Annexin V/PI staining, followed by flow cytometry analysis. Representative plots of Annexin V (FITC channel)/PI (PE channel) staining of NB100 cells cultured untreated or treated with ebulin 1 ( $10^{-7}$ M) and nigrin b ( $10^{-7}$ M) alone or in the presence of 100  $\mu$ M Z-VAD at 24h and 48h. The pan-caspase inhibitor was added 3 hours before the RIP, and the viability was observed after the indicating times.

### 3.3.2 Evaluation of the involvement of necroptosis

Necroptosis is a programmed necrosis that occurs due to tumor necrosis factor receptor (TNF-R) activation. The involvement of necroptosis has been described in the literature for other RIPs such as abrin, a toxic type 2 RIP (Bora *et al.*, 2010). In particular, pretreatment of NB100 cells with the necroptosis inhibitor necrostatin-1 prior to stenodactylin incubation, preserved approximately 70% of cells after 24 h (Polito *et al.*, 2016a). When the apoptotic cell death is inhibited by Z-VAD, cells can still die through necroptosis (Declercq *et al.*, 2009). Therefore, to determine the role of other possible toxic mechanisms induced by ebulin 1 and nigrin b, a set of experiments were performed using the inhibitor of necroptosis necrostatin-1, at a dose previously tested in our laboratory with other RIPs and that was not toxic to the cells, but protected them from necroptosis.

Necroptosis depends on the serin-threonine kinase receptor-interacting proteins 1 (R.I.P1) and 3 (R.I.P3). R.I.P1 is crucial in necroptosis and its activity is inhibited by necrostatin-1 (Christofferson and Yuan, 2010). NB100 cells were treated and maintained in 100  $\mu$ M necrostatin-1 and the cell viability was determined by MTS reduction assay at different times (24, 48 and 72 hours of incubation with the two RIPs). A slight increase of cell viability was observed at all the examined times. However, these differences were not significant for both RIPs. (figure 3.10).

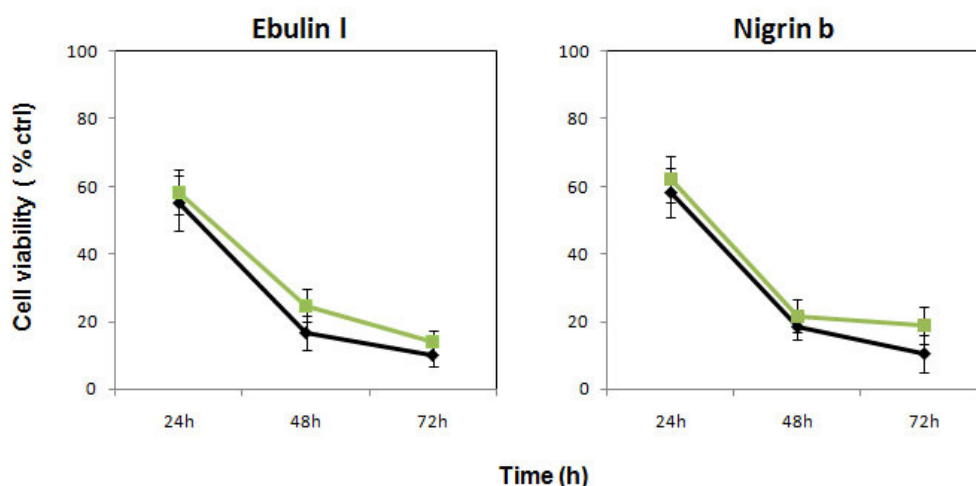


**Fig. 3.10.** Viability of NB100 cells ( $2 \times 10^3$  cells/well) treated with ebulin 1 ( $10^{-7}$ M) and nigrin b ( $10^{-7}$ M) alone (black) or in the presence of 100  $\mu$ M necrostatin-1 (green). The necroptosis inhibitor was added 3 hours before the RIP and the viability was observed after the indicating times using a colorimetric assay based on MTS reduction. The results are the means of at least three independent experiments, each performed in triplicate, and are presented as the percentage of control values obtained from cultures grown in the absence of RIPs. No significant differences were observed (confidence interval 95%, test Anova/Bonferroni).

### 3.4 Cell cycle analysis

In order to assess if the reduced viability in cells treated with ebulin 1 and nigrin b depended on a cytostatic effect of these toxins, cell cycle analysis was performed. This could explain the reduced capacity of NB100 to metabolize the MTS in the first 24 hours. The distribution of NB100 cells was evaluated depending on the cell cycle phase through the flow cytometric analysis after staining with PI. Figure 3.11 showed a very similar pattern of cell cycle between the samples untreated and those treated with the two RIPs. Therefore, it can be excluded a cell cycle block in the residual percentage of cells treated with the two RIPs in the first 24 hours.

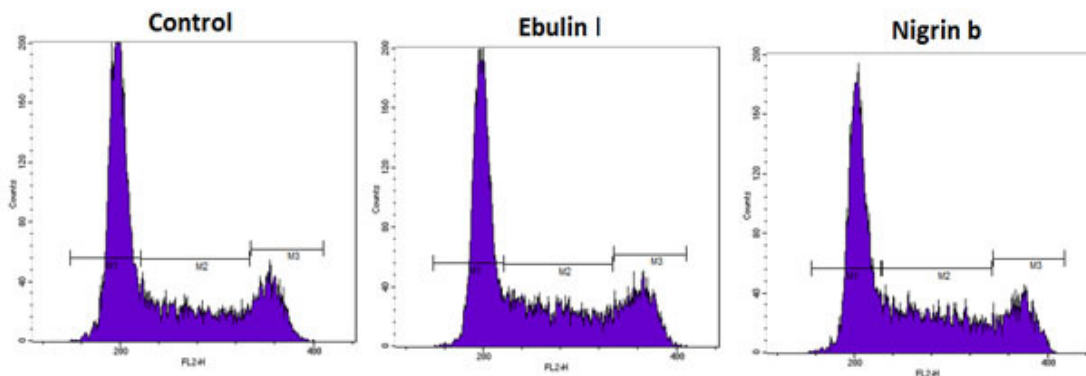


**Fig. 3.11.** Effect on NB100 cell cycle distribution. Flow cytometric cell cycle analysis was performed using PI for the DNA staining of NB100 cells following 24 hours of treatment with ebulin I ( $10^{-7}$ M) and nigrin b ( $10^{-7}$ M).

### 3.5 Assessment of autophagy

In 2015 Shang and co-workers demonstrated that the accumulation in the lysosomes of some *S. nigra* proteins, including SNA-V (nigrin b), in HeLa cells, caused saturation and subsequent activation of alternative degradation pathways, such as autophagy. Autophagy is a cellular degradation process that involves the lysosomal breakdown of cytoplasmic components. It is maintained at basal level in most cells and contributes to the routine turnover of cytoplasmic components. After stress or pathological stimuli, its activation increases. The microtubule-associated protein light chain 3 (LC3) is a marker of autophagy and it is a major constituent of autophagosome. During autophagy, LC3 is cleaved to generate the cytosolic form LC3I, which is subsequently conjugated to phosphatidyl ethanolamine to form LC3II, which is in turn recruited to autophagosomal membranes (Kabeya *et al.*, 2000). Autophagosomes fuse with lysosomes to form autophagolysosomes and intra-autophagosomal components are degraded by lysosomal hydrolases. At the same time, LC3-II located in autophagolysosomal lumen is degraded (Tanida *et al.*, 2008).

Western blot analysis of extracts from NB100 cells treated with ebulin I and nigrin b ( $10^{-7}$ M) revealed the presence of only one band corresponding to LC3I (16 kDa), thus denying a possible involvement of autophagy in the cell death mechanism induced by ebulin I and nigrin b at 24 hours of treatment (figure 3.12). In order to assess the specificity of the antibody used, the autophagic response to chloroquine was also analyzed. Chloroquine inhibits the fusion of the autophagosome with lysosome and, consequently, the lysosomal protein degradation, resulting in accumulation of LC3II

levels. Under chloroquine stress (100  $\mu$ M), there was an increase of the LC3II (14 kDa) of the same intensity, both in untreated and ebulin I-treated NB100 cells. The result confirmed no involvement of autophagy in cell death pathways triggered by *Sambucus* toxins.

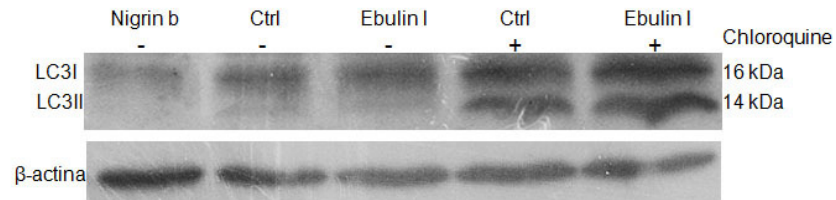


**Fig. 3.12.** Expression of LC3 after 24 hours by western blot analysis of extracts from NB100 cells treated with nigrin b ( $10^{-7}$ M) and with ebulin I ( $10^{-7}$ M) alone (-) or in the presence of 100  $\mu$ M chloroquine (+). The 16 kDa band corresponds to LC3I, while the 14 kDa band corresponds to LC3II. The same blot was hybridized with anti- $\beta$ -actin as loading control.

## **CONCLUSION**

To resume, in the present study ebulin 1 and nigrin b completely abolish neuroblastoma cell viability; however, they need more time and higher concentration to fully carry out their cytotoxic effect ( $10^{-7}$ M, 96h) compared with toxic type 2 RIPs.

The obtained results indicate that ebulin 1 and nigrin b are able to induce caspase-dependent apoptosis, as revealed by the strong time-dependent activation of caspase 3/7. The activation results of the same entity of other toxic type 2 RIPs, but at a RIP concentration much higher and at periods longer than 24 hours. Despite the activation of caspase is highly significant after 8 hours, the pan-caspase inhibitor Z-VAD gave no significant protection to NB100 cells at the first 24 hours. This suggests that at this time the apoptotic pathway has still a secondary role in the cell death pathways triggered by the two RIPs from *Sambucus*, showing a different behavior with the respect to the cell death mechanisms induced by toxic type 2 RIPs. Moreover, an interesting aspect was observed after long time of treatment with *Sambucus* RIPs. In fact, when cells are pre-treated with Z-VAD, about 30% of cells seems to become resistant to death, suggesting that the involvement of another cell death pathway is not possible. It remains unclear if this depends on the cell cycle arrest, on metabolic status of the cells or more probably on the altered genetic pattern of the tumor cells.

In conclusion, the mechanism of cell death induced by ebulin 1 and nigrin b is partly due to caspase-dependent apoptosis and it may assume the existence of a further cell death pathway that would be prevalent at the early 24 hours of intoxication and that is different from necrosis, necroptosis and autophagy, as demonstrated. Moreover, a block of cell cycle can be excluded. After 24 hours, the apoptotic pathway becomes the main route of cell death. Further studies are required to understand other cell death mechanisms probably involved in the cell death pathway triggered by ebulin 1 and nigrin b, in order to clarify what happens at the first 24 hours of intoxication.

*Chapter 4*

# **Materials and methods**



## 4.1 Materials

### RIPs

Stenodactylin was purified from the caudex of *Adenia stenodactyla* as described by Stirpe *et al.*, 2007. Ricin was purified from the seeds of *Ricinus communis* as described by Nicolson *et al.*, 1974. Ebulin I was purified from the leaves of *Sambucus ebulus* as described by Girbés *et al.*, 1993b. Nigrin b was purified from the bark of *Sambucus nigra* as described by Girbés *et al.*, 1993a.

### Plants

Plants were purchased from Exotica Botanical Rarities, Erkelenz-Golkrath, Germany, while *A. kirkii* from Mbuyu–Sukkulenten, Bielefeld, Germany. If not immediately used on arrival, plants were kept in the greenhouse of the Botanical Garden of the University of Bologna.

### Safety precautions

Because other previously investigated *Adenia* plants had shown the presence of high amounts of potent toxins, stringent safety measures are employed during handling of *Adenia* tissues. The plants were carefully handled; direct or indirect contacts with skin or eyes were avoided. The preparation of extracts were conducted in closed equipments under a ventilated fume hood to prevent inhaling toxic aerosols.

### Cell cultures

Human neuroblastoma cells (NB100) and human uterine cervix carcinoma cells (HeLa) were maintained in RPMI 1640 medium (Sigma-Aldrich) containing 10% heat-inactivated foetal bovin serum (FBS), 2 mM L-glutamine, 100 U/ml penicillin and 100 µg/ml streptomycin (Sigma-Aldrich). All cells were cultured at 37°C in a humidified environment with 5% CO<sub>2</sub> in a HeraCell Haereus incubator (Hanau, Germany) and routinely checked for the absence of mycoplasma infection. Trypan Blue and trypsin/EDTA were obtained from BioWhittaker (Vervies, Belgium). Cytotoxicity was

evaluated using L-[4,5-<sup>3</sup>H] leucine purchased by GE Healthcare (Buckingham shire, UK). Flasks and plates were from Falcon (Franklin Lakes, NJ, USA).

## **Antibodies**

Rabbit sera against ricin, volkensin and type 1 RIPs were prepared as described by Strocchi (Strocchi *et al.*, 1992). Rabbit sera against stenodactylin e lanceolin were prepared as described by Stirpe *et al.*, 2007. The alkaline phosphatase-conjugated anti-rabbit IgG used for ELISA was purchased from Sigma, whereas the phosphatase substrate (4-nitrophenyl phosphate disodium salt hexahydrate) was purchased from Merk (Darmstadt, Germany). Western blot was performed with rabbit antibody against LC3 purchased from Cell Signaling Technology, Inc. (Danvers, Massachusetts, USA), while mouse antibody against actin and the horseradish peroxidase-conjugated anti-rabbit or anti-mouse IgG were purchased from Sigma Aldrich. Antibodies were diluted following manufacturer's instructions.

## **Kits**

Caspase activity was evaluated using the luminescent kit Caspase-Glo™3/7 Assay (Promega Corporation, Wisconsin, USA). Morphological membrane changes were detected using Annexin V-EGFP/PI detection kit (Biovision, Mt. View, CA). Viability was measured using the colorimetric CellTiter 96® Aqueous One Solution Cell Proliferation Assay (Promega), which contains a novel tetrazolium compound [3-(4,5-dimethylthiazol-2-yl)-5-(3-carboxymethoxyphenyl)-2-(4-sulfophenyl)-2H-tetrazolium, MTS] and an electron coupling reagent (1-methoxy phenazine methosulfate, PMS). The mitochondrial potential changes were detected using the Mitochondria Staining Kit (Sigma Aldrich). Total DNA was extracted through DNeasy Minikit (Qiagen), while total RNA was isolated using the RNeasy Minikit (Qiagen). The PCR product was purified using the NucleoSpin® Gel and PCR Clean-up kit, while the plasmids were purified using Nucleo Spin Plasmid kit both purchased from MACHEREY-NAGEL. TA Cloning® Kit Dual Promoter used for ligation, the pCR™II cloning vector and the chemically competent *E. coli* INVαF' were purchased from Invitrogen (Life technology-Carlsbad-CA, USA). The reverse transcriptase MuLV, the dNTPs were obtained from GeneAmp RNA PCR kit (Applied Biosystem, Roche, New Jersey, USA).

## Reagents

The scintillation liquid was the Ready-Gel (Beckman Instrument, Fullerton, USA). The reagents and the molecular weight standard were purchased from GE Healthcare. DAPI-Antifade was from Resnova SRL, Genzano di Roma, Italy. The pan-caspase inhibitor Z-VAD-fmk (carbobenzoxy-valyl-alanyl-aspartyl-[O-methyl]fluoromethylketone), was supplied by Vinci-Biochem (Florence, Italy). The Immobilon Western detection Reagent and the nitrocellulose membrane were purchased from Millipore (Milford, MA, USA). The inhibitor of necroptosis, necrostatin-1, was obtained from Sigma-Aldrich. Yeast RNA was purchased from Roche Diagnostics S.L. (Barcelona, Spain). Single-stranded salmon sperm DNA was purchased from Sigma-Aldrich. The reagents, the gels and the standards for electrophoresis were purchased from GE Healthcare, Milan, Italy. The water used was prepared with a Milli-Q apparatus (Millipore, Milford, MA, USA). Other reagents used were from Merck (Darmstadt, Germany), Carlo Erba (Milano, Italy) and Sigma. All reagents were of analytical grade, and when possible RNase-free.

## Instruments

Sepharose CL-6B (an agarose-based, bead-formed matrix, containing 6% agarose) and Sephacryl S-100 (cross-linked copolymer of allyl dextran and N,N'-methylene bisacrylamide) were from GE Healthcare (Buckinghamshire, UK). Protein concentration was determined by UVICON 860 Spectrophotometer (Kontron Instruments, Milano, Italy). The protein were separated on SDS-PAGE using the PhastSystem (GE-Healthcare) and then blotting using the Mini Protean 3 Cell electroblotting apparatus (Bio-Rad). The DNA/RNA content was determined by Beckman DU 640 Spectrophotometer. Cell incorporated radioactivity was measured by a  $\beta$ -counter (Beckman Coulter, Fullerton, CA, USA). Morphological cell analysis was carried out by a phase-contrast microscope with a digital camera from Nikon Eclipse TS100 (Chiyoda, Tokyo, Japan). Fluorescence microscopy was performed with a Nikon Eclipse E600 fluorescence microscope (Nikon instruments, Calenzano, Firenze). The luminescence was read using the Fluoroskan Ascent FL (Labsystem, Finland). Absorbance at 492 nm was measured by a microtiter plate reader Multiskan EX, ThermoLabsystem, (Helsinki, Finland). Flow cytometry analysis was done using the FACS Aria BD analyzer (Franklin Lakes, New Jersey, USA). PCR was conducted using the thermal cycler Gene Amp

PCR system 2400 (Perkin Elmer). DNA and RNA bands were analyzed by UV-transilluminator (254-312 nm) including in the imaging instrument GelDoc (Biorad).

### **DNA sequencing Softwares**

A search for sequence similarity was performed with BLAST program available on-line (<http://www.ncbi.nlm.nih.gov/BLAST>). Sequence alignment was performed using ClustelW available tool, included in Mega 7 program with the default parameters manually modified aligning a number of amino acids characteristic of the sequences, such as those of the active site for the A-chains and the cysteines for the B-chains. The aligned sequences were graphically represented by sequence logos created with WebLogo 3 (Di Maro *et al.*, 2014). Kirkiin 3D structure was predicted using the program I-TASSER, (<http://zhanglab.ccmb.med.umich.edu/I-TASSER/>), which used as comparative models the structures of abrin (1abr), viscumin (2rg9) and ricin (3px8) for kirkiin A-chain and the structures of cinnamomin (2vlc), ricin (2aai) and abrin (1abr) for kirkiin B-chain. The program Discovery Studio 3.5 suite (<http://accelrys.com>) was used for the graphical representation. Docking of the A-chain with adenine and 1 $\alpha$  subdomain with lactose was predicted used COACH program included in I-TASSER; docking of 2 $\gamma$  subdomain was predicted used PATCHDOCK program (<http://bioinfo3d.cs.tau.ac.il/PatchDock/>).

### **Statistical analysis**

Statistical analyses were conducted using the XLSTAT-Pro software, version 6.1.9 (Addinsoft 2003). Results are given as means  $\pm$  SD of three different experiments. Data were analyzed by Anova/Bonferroni test, followed by a comparison with Dunnett's test.

## 4.2 Methods

### 4.2.1 *Adenia lectin purification*

Lectins from *A. epigea*, *A. lindenbergii*, *A. monodelpha* and *A. kirkii* caudices were purified as described in Pelosi *et al.*, 2005. Samples of caudices (4–16 g each, approximately) were decorticated, minced with scissors and homogenized with an Ultra-Turrax with 5 ml/g of phosphate-buffered saline (PBS, 0.14 M NaCl containing 5 mM sodium phosphate buffer, pH 7.4). After overnight stirring at 4°C, each extract was strained through cheesecloth and centrifuged at 18,000 × g for 30 minutes at 4°C. Crude extracts were adjusted to 100% saturation with solid (NH<sub>4</sub>)<sub>2</sub>SO<sub>4</sub> and stored at 4°C until the following step. The (NH<sub>4</sub>)<sub>2</sub>SO<sub>4</sub> precipitated material was collected by centrifugation, resuspended in PBS, dialysed against PBS and loaded into a Sepharose CL-6B column (14cm h × 1cm Ø). The column was previously treated with 0.2 M HCl for 150 min at 50°C to cleave the polysaccharide chains in the matrix, thus exposing additional terminal galactosyl residues; then, the column was extensively washed and equilibrated with PBS. After loading the extract, the column was washed with PBS and the peak was eluted with 0.2 M galactose in PBS. The eluted protein was dialysed against PBS. Lectins were analyzed by 20% SDS-PAGE both under reducing and non-reducing conditions.

### 4.2.2. *Adenia kirkii lectin purification*

About 500g of *A. kirkii* caudex were decorticated and homogenized with an Ultra-Turrax, as previously described for *Adenia* lectins (section 4.2.1). Since the material was very compact, 450 ml of PBS were added. After overnight stirring at 4°C, the extract was strained through cheesecloth and centrifuged at 18,000 × g at 4°C for 30 min. The crude extract was further centrifuged to obtain a clear supernatant. The total recovered volume was 2790 ml, of which 2290 ml were adjusted to 100% saturation with solid (NH<sub>4</sub>)<sub>2</sub>SO<sub>4</sub> and stored at 4°C, whereas the remaining 500 ml were loaded into a Sepharose CL-6B column (7cm h × 5cm Ø) pre-treated with 0.2 M HCl, as previously described. The peak was eluted with 0.2 M galactose. The 38 ml obtained from CL-6B were concentrated to 2 ml on YM10 membrane under nitrogen pressure, and loaded into a Sephacryl S-100 column (94 cm h × 1.5 cm Ø), in order to separate the lectins

according to the size. Representative fractions of the S-100 protein peaks were analyzed on a PhastGel Homogeneous 20 in a Phast System, following the supplier's protocol. The protein fractions corresponding to the two purified lectins were collected and analyzed on a 8-25% PhastGel gradient, in order to obtain a greater resolution and to verify the purity of the bands.

#### **4.2.3. Chemico-physical characterization of lectins**

Lectins were analyzed by SDS-PAGE (see section 4.2.23). The isoelectric point was determined using a 20% polyacrylamide IEF gel 3-9 in a Phast System. The running and staining with Coomassie Brilliant Blue were performed following the supplier's protocol.

The determination of the protein content of crude extract and not retained material by Sepharose CL-6B was performed by spectrophotometric analysis at 230 nm, 260 nm and 320 nm, using the Kalb and Bernlohr method, which reduces the interference of the polyphenols present in the plant extract (Kalb and Bernlohr, 1977). The protein content of Sephacryl S-100 fractions was determined by spectrophotometric analysis at 280 nm.

#### **4.2.4. Haemagglutinating activity**

Haemagglutinating activity was determined in 96 wells microtiter plates. Each well contained 50  $\mu$ l of a 2% suspension of human erythrocytes (group 0, Rh+) and 2-fold serial dilutions of the lectins, in a final volume of 100  $\mu$ l. The plates were gently shaken and after about 1 hour at room temperature (25°C) the presence/absence of agglutination was visually examined.

#### **4.2.5 Enzyme-linked immunosorbent assay (ELISA)**

The cross-reactivity of kirkiin was performed by Enzym Linked Immunosorbent Assay (ELISA), using antibodies against several RIPs both type 1 and type 2. In 96-well microtiter plates 2  $\mu$ g per well of kirkiin were added in 100  $\mu$ l of 50 mM carbonate buffer pH 9.0 containing 15 mM sodium carbonate and 35 mM sodium bicarbonate. The plate was left overnight at 4°C so that the RIP could adhere to the well. After 5 washes with 200 ml PBS/Tween (137 mM NaCl, 1.5 mM KH<sub>2</sub>PO<sub>4</sub>, 8 mM Na<sub>2</sub>HPO<sub>4</sub>\*12H<sub>2</sub>O,

0.05% (v/v) Tween 20), 200  $\mu$ l of 0.5 mg/ml BSA (bovine serum albumin) were added, in order to saturate the charges of the well. After 1 hour of incubation at 37°C, 5 washes were performed with 200  $\mu$ l of PBS/Tween and then reciprocal serum dilutions (from 1:100 to 1:12800) were added (100  $\mu$ l/well). The dilutions were prepared in 50 mM lactose, 50 mM mannose and 0,05% Tween 20. After 3 hours of incubation at 37°C and 5 washes with 200  $\mu$ l of PBS/Tween, 100  $\mu$ l of anti-rabbit secondary antibody (1:7000) conjugated to alkaline phosphatase were added and incubated 1 hour at 37 °C. After 5 washes with 200  $\mu$ l PBS/Tween, 100  $\mu$ l of 1 mg/ml enzyme substrate (4-nitrophenyl phosphate disodium) dissolved in buffer containing 1 M diethalonamine, 0.5 M  $MgCl_2 \cdot 6H_2O$  and 3 mM  $NaN_3$  were added. The absorption was measured at 405 nm with a Multiskan EX microtiter plate reader.

#### 4.2.6 rRNA glycosylase activity

N-glycosylase activity of kirkiin was assessed by analysing the release of the diagnostic fragment upon treatment with acid aniline. Rabbit reticulocytes lysate (40  $\mu$ l) and S-30 lysate from yeast (25  $\mu$ l) were incubated with 3 $\mu$ g of RIP at 37°C for 1 hour. 2  $\mu$ l of 0.5 M EDTA pH 8 and 500  $\mu$ l of 50 mM Tris-HCl (pH 7.8) and 0.5% SDS (p/v) were added and the samples were vigorously vortexed for 30 seconds to dissociate the ribosomal proteins. After a phenol extraction, in order to eliminate the proteins, the samples were centrifuged for 5 minutes at 10,000 x g and the aqueous phase was recovered. The RNA was precipitate at -80°C overnight by adding 0.1 volumes of 3 M sodium acetate pH 5.2 and 3 volumes of absolute ethanol. RNA was centrifuged for 15 minutes at 10,000 x g at 4°C and the pellet was washed with 70% ethanol (v/v) and then centrifuged again. The pellet was dried at room temperature and then resuspended in 20 $\mu$ l of sterile  $H_2O$  Mill Q. RNA was treated with 20  $\mu$ l of 2 M aniline acetate pH 4.5 on ice for 10 minutes in the dark. After adding 200  $\mu$ l of sterile water, RNA was extracted with ether saturated with water. The aqueous phase was precipitated at -80°C overnight by adding 0.1 volumes of 3 M sodium acetate pH 5.2 and 3 volumes of absolute ethanol. RNA was centrifuged for 15 minutes at 10,000 x g at 4°C and the pellet was washed with 70% ethanol (v/v) and then centrifuged again. The pellet was resuspended in 20  $\mu$ l of sterile water and the concentration was determined by spectrophotometer. The RNAs were subjected to electrophoresis on 5% (w/v) polyacrylamide-7 M urea gel at 15 mA for a

suitable time (from 1 hour 30 min to 1 hour 50min) in order to better differentiate the Endo's fragment, and stained with ethidium bromide.

#### **4.2.7 Polynucleotide:adenosine glycosylase (PNAG) activity assay**

##### PNAG activity on salmon sperm DNA

PNAG activity was determined by measuring the amount of adenine release from salmon sperm DNA (ssDNA). The assay was performed by incubation of 10 µg of ssDNA with 3 µg of RIP in 300 µl of a reaction mixture containing 1 M KCl and 0.5 M sodium acetate (pH 4.5) at 30 °C for 1 hour. DNA was precipitate at -80°C overnight by adding 0.1 volumes of 3 M sodium acetate pH 5.2 and 3 volumes of absolute ethanol. DNA was centrifuged for 15 minutes at 10,000 x g at 4°C and the adenine released from RIP-treated DNA were determined in the obtained supernatants by spectrophotometer at 260 nm.

##### PNAG activity on tobacco mosaic virus (TMV)

The breakage of the virus capsid was performed by vigorously vortexing 100 µl of TMV (20 mg/ml) in 500 µl of 50 mM Tris-HCl (pH 7.8) and 0.5% SDS. RNA samples were extracted by phenolization and centrifuged for 10 minutes at 10,000 x g at room temperature. The surnatant was precipitated overnight at -80°C by adding 0.1 volumes of 3 M sodium acetate pH 5.2 and 3 volumes of absolute ethanol. RNA was centrifuged for 15 minutes at 10,000 x g at 4°C and the pellet was washed with 70% ethanol (v/v) and then centrifuged again. The pellet was dried at room temperature and then resuspended in 20 µl of sterile water. Then, 15 µg of TMV RNA were incubated with 3 µg of the RIP at 37°C for 1 hour in a final volume of 25 µl TE buffer (10 mM Tris-HCl and 1 mM EDTA) pH 7.2.

RNA was treated with 25 µl of 2 M aniline acetate pH 4.5 on ice for 10 minutes in the dark and then extracted with ether saturated with water. The aqueous phase was precipitated at -80°C over night by adding 0.1 volumes of 3 M sodium acetate pH 5.2 and 3 volumes of absolute ethanol. RNA was centrifuged for 15 minutes at 10,000 x g at 4°C and the pellet was washed with 70% ethanol (v/v) and then centrifuged again. The pellet was resuspended in 15 µl of steril water and the concentration was determined by spectrophotometer. RNA samples were subjected to electrophoresis at 15 mA for 1 hour

15 minutes in 5% (w/v) polyacrylamide-7 M urea gel and stained with ethidium bromide.

#### **4.2.8 Endonuclease activity on supercoiled plasmid DNA**

For the detection of the endonuclease activity of the RIP on circular DNA, pCR 2.1 was used. This plasmid was obtained in laboratory by purification from *E. coli* INV $\alpha$ F' bacterial cells (Invitrogen). 200 ng of the plasmid were incubated at 37°C for 1 hour with 3  $\mu$ g of RIP in a final volume of 10  $\mu$ l of 10 mM Tris-HCl (pH 7.8), 50 mM NaCl and 50 mM KCl in presence/absence of 5 mM MgCl<sub>2</sub>. The samples were analyzed on 0.8% agarose gel electrophoresis.

#### **4.2.9 Synthesis of DNA**

The caudex of *A.kirkii* was disrupted using mortar and pestle and grinded to a fine powder under liquid nitrogen. Total DNA was extracted through DNeasy Minikit (Qiagen), according to the manufacturer's instruction.

#### **4.2.10 Synthesis of cDNA via reverse transcription (RT)**

The caudex of *A.kirkii* was disrupted using mortar and pestle and grinded to a fine powder under liquid nitrogen. Total RNA was extracted through RNeasy Minikit (Qiagen), according to the manufacturer's instruction. Poly(A)-rich RNA was reverse transcribed using the synthetic oligonucleotide J1 (5'CGTCTAGAGTCGACTAGTGC(T)<sub>20</sub>3'). Approximately 1  $\mu$ g of total RNA and 1  $\mu$ l of RNase inhibitor were incubated in a thermal cycler first at 65°C for 5 minutes and then at 23°C for 20 minutes. It was later cooled on ice for 1 minute and 15  $\mu$ l of reaction mixture were added containing: 1 $\times$ PCR Buffer II, 5 mM of MgCl<sub>2</sub>, 1 mM of each dNTP, 10  $\mu$ M of J1, and 4 U/ $\mu$ l of MuLV reverse transcriptase (Roche). The reaction mixture was incubated 20 minutes at 23°C, 20 minutes at 42°C, 5 minutes at 99°C to inactivate the enzyme and finally 5 minutes at 5°C.

#### 4.2.11 Selection of the oligonucleotides for PCR amplification

Gene-specific primers for full-length of kirkiin were designed and synthesized on volkensin sequence (CAD61022) and N-terminal sequences available for other *Adenia* RIPs. The alignment of N-terminal amino acid sequences of the A-chains showed that lanceolin A1 shared 15/18 amino acids residues with modeccin and both had a Phe as N-terminal amino acid. Volkensin A-chain showed a homology of 15/21 amino acids with both stenodactylin and lanceolin A2, whereas stenodactylin A-chain shared 21/21 amino acids with that of lanceolin A2. Even B-chain N-terminal identity was very high, with the exception of the first three amino acid residues, which are identical only in stenodactylin and volkensin (Asp-Pro-Val) (Stirpe *et al.*, 2007) (figure 4.1).

Alignment:	
Lanceolin A1	-FPKVILDCTRATVERYTQFI 20
Lanceolin A2	VFPKVIFDCTRATVERYTQFI 21
Stenodactylin A chain	VFPKVIFDCTRATVERYTQFIM 22
Modeccin A chain	-FPKVTLDDTRATVESYTT
Volkensin A chain	VFPKVPFDVVPKATVESYTRFIR 22
	**** : .:**** **:**
Lanceolin B1	D--CPFGETTAYIVGRDXXCV 19
Lanceolin B2	D--CPSGETTAYIVGRDXXCV 19
Stenodactylin B chain	DPVCPSGETTAYIVGRDXXXV 21
Modeccin B chain	EMICPSGETTAYIVGRKGGXV
Volkensin B chain	DPVCPSGETTAFIVGRDGRCV 21
	** *****:****

**Fig. 4.1.** Amino acid alignment of the N-terminal of lanceolin A1, lanceolin A2, stenodactylin, modeccin and volkensin A- and B-chains. The single letter code represents amino acids. Identical residues (\*), conserved substitutions (:), and semiconserved (.) substitutions are reported. X, unassigned amino acid positions. Data from Stirpe *et al.*, 2007

Three couple of primers were used to detect the full-length amino acid sequence of kirkiin (A2 degenerated and B1R for A-chain and part of the B-chain; B1 and B5 reverse for B-chain; A2 and B5 reverse for the complete sequence). Another primer was designed in proximity of the N-terminal end of A-chain (A1), but it did not produced amplification. Primers were synthesized by Integrated DNA Technologies (Belgium). The primer sequences are reported in table 4.1.

**Table 4.1.** Primers sequences.

A1	5' GTTTTCCCCAAGGTCATHHTTCGAC 3'
A2	5' GCCACGGTAGAGAGRTACACT 3'
B1R	5' AAGTCGTCTCCCCGGAAGGGC 3'
B1	5' TGCCCTTCCGGGGAGACGACT3'
B5R	5' TAGGAACCATTGCTGGTTGGA3'

#### 4.2.12 Kirkiin gene amplification

For kirkiin gene amplification 2  $\mu$ l of the above-synthesize cDNA (diluted 1:10) or 40 ng/ $\mu$ l of total DNA were used, and 16  $\mu$ l of master mix and 0.5  $\mu$ M of each primers were added. A typical reaction master mix included 1 $\times$ PCR buffer/Mg<sup>2+</sup>, 0.25 mM dNTPs Mix, 0.5 U/ $\mu$ l Taq Polymerase (Biotools, Madrid, Spain). PCR amplification was carried out as reported in table 4.2.

**Table 4.2.** PCR condition.

Step	Temperature °C	Time	N°. of cycles
Initial denaturation	94	3 min	1
Denaturation	94	30 sec	} 40
Annealing	55	40 sec	
Extension	72	1-2 min	
Final extension	72	10 min	1
Hold	15		

Differences in PCR amplification are in the annealing temperature, which is based on the fusion temperature of each primers and in the extension time at 72°C, which depends on the size of the fragment of interest.

About 5 µl of the amplified products from each tube along with 3 µl of loading dye were separated on 0.8% agarose gel using 1X TAE buffer. *HindIII/EcoRI* double digest was used as DNA molecular weight marker.

#### 4.2.13 cDNA and DNA cloning

The PCR product was purified using the NucleoSpin® Gel and PCR Clean-up kit (MACHEREY-NAGEL), according to the manufacturer's instruction.

The purified PCR product was ligated into the pCR<sup>TM</sup>II cloning vector (figure 4.2) using the TA Cloning® Kit Dual Promoter (Invitrogen). For ligation, optimal molar ratio is 1:3 of vector:insert. The components of ligation mixture was mixed into a 0.5 ml microcentrifuge tube and incubated at 23°C for 2 hours in a thermal cycler. The vector contains genes for ampicillin resistance and the enzyme β-galactosidase (*lacZ*) that make it possible to select for transformed bacteria. The cloning site is in the *lacZ* gene.

The ligation mixture was used to transform the Chemically Competent *E. coli* INVαF' cells (Invitrogen). The cells were provided as frozen 50 µl aliquots from TA Cloning® kit and were thawed on ice. The ligation mixture (5 µl) was gently pipetted into the competent cells and gently mixed. The samples were incubated on ice for 30 minutes and then heat shocked for 30 seconds in 42°C water bath and then placed on ice for 2 minutes. After the heat shock, 250 µl of SOC medium, provided from the kit, was added onto each sample. SOC medium was previously prewarmed at room temperature. The samples were incubated at 37°C horizontally shaking at 225 rpm for 1 hour. 50 and 100 µl of each sample was spreaded onto a prewarmed LB/amp plate with 40 µl of XGal from the 20 mg/ml stock. After 15 minutes, the plates were inverted and incubated at 37°C overnight.

Cells transformed with vectors containing recombinant DNA produced white colonies; cells transformed with plasmids that not have DNA insert interrupting the *LacZ* gene (i.e. only the vector) grew into blue colonies. The white colonies (*lacZ*-negative transformants ) were screened by PCR, dipping the colony into a PCR tube with a yellow tip and then streaking it onto a fresh agar plate using a numbered template. PCR was performed by using the appropriate couple of primers (M13 and M13R universal primers). The PCR mix included: 1×PCR Buffer, 0.25 mM dNTPs, 1 µM of each primers, 5 U/µl Taq Polymerase (Biotools). PCR amplification was performed with the PCR conditions reported in table 4.2. The hybridization temperature was 60°C for 30

seconds and the extension time at 72°C was 1 minute 30 seconds for A- and B-chains and 2 minutes 30 seconds for the entire sequence amplifications.

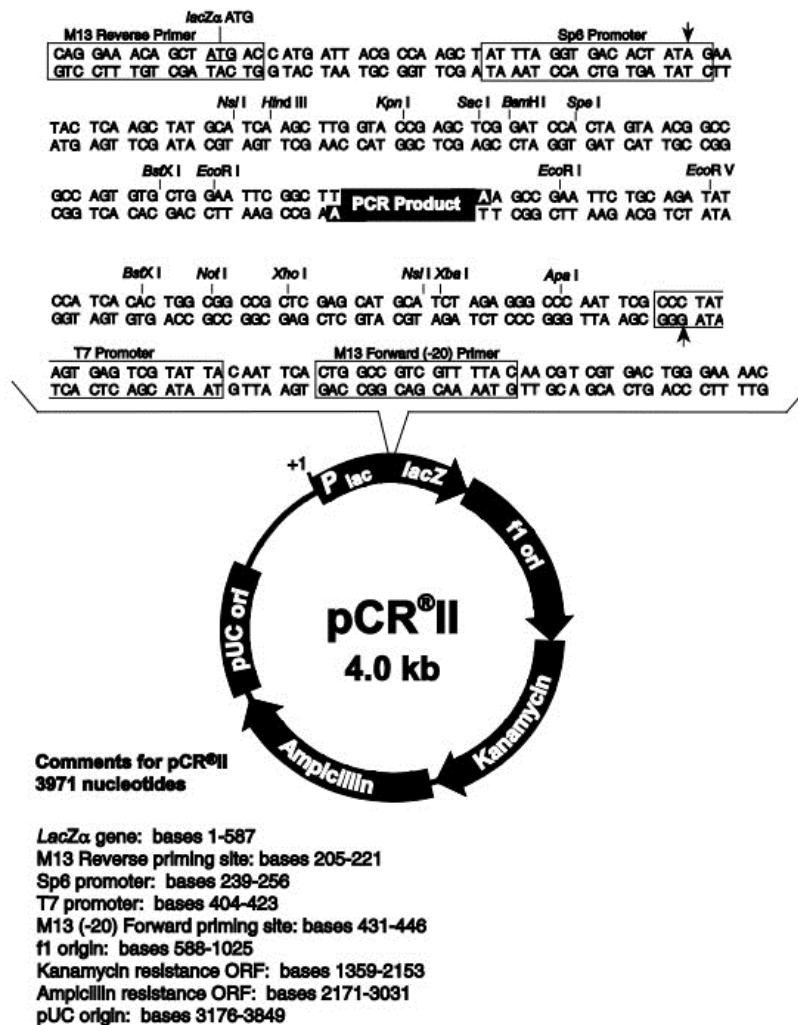


**Fig. 4.2.** Map of the linearized vector pCR®II. Image from TA Cloning® Kit manual (Invitrogen).

#### 4.2.14 Purification of the plasmids

The positive white colonies (LacZ-negative) were transferred from the agar plates to a Falcon tube each, containing 10 ml LB-medium with 100 µg/ml ampicillin, and incubated overnight at 37°C at 225 rpm. The cells were collected by centrifugation (2800 rpm for 10 minutes) and the plasmids were then purified using Nucleo Spin Plasmid kit (MACHEREY-NAGEL), according to the manufacturer's instruction. The DNA content was determined by measuring the absorbance at 260 nm. The plasmid

quality and the presence of sequence fragment were checked by running the samples on a 0.8% agarose gel analysis by digestion with *EcoRI* enzyme.

#### **4.2.15 DNA sequence**

The purified plasmids were sequenced by CENIT Support system of Villamayor (Salamanca, Spain). The samples were prepared according to the manufacturer's recommendations.

#### **4.2.16 Protein synthesis inhibition assay**

##### Cell-free system

Cell-free protein synthesis for *Adenia* lectins was determined *in vitro* using a rabbit reticulocyte lysate system. 25  $\mu$ l of rabbit reticulocyte lysate (prepared as described by Allen e Schweet, 1962) and 12.5  $\mu$ l of a reaction mixture composed of 10 mM TrisHCl pH 7.4, 100 mM ammonium acetate, 2 mM Mg-acetate, 1 mM ATP, 0.2 mM GTP, 15 mM creatine phosphate, 12  $\mu$ U creatine kinase, 0.05 mM amino acids (without leucine), 0.75  $\mu$ Ci L-[<sup>3</sup>H]leucine were added to appropriate dilutions of the lectins. The reaction tubes were incubated at 28°C under stirring for 7 minutes and blocked with 1 ml 0.1M KOH. After adding 25  $\mu$ l of hydrogen peroxide to the tubes, 1 ml of 20% trichloroacetic acid (TCA) was added when the liquid was decolorized, in order to precipitate the proteins. The protein precipitate was collected on Whatman filters GF/C in suitable ampoules with 5% TCA. Then, 5 ml of Ready-Gel scintillation fluid (Beckman) containing 0.7% of acetic acid were added to the vials to break down any chemiluminescence. The radioactivity of L-[<sup>3</sup>H]leucine incorporated into new synthesized proteins was measured by  $\beta$ -counter. The same experiment was carried out under reducing conditions, with the addition of 1% 2-mercaptoethanol for 30 minutes at 37°C. The experiments were conducted in duplicate and the inhibitory effect of proteins were represented as IC<sub>50</sub> value, which is defined as the amount of inhibitory protein that gives 50% of protein synthesis inhibition, calculated by linear regression.

### Cell lines

NB100 and HeLa cells ( $1 \times 10^4$  cells in 500  $\mu\text{l}$ /well of complete medium RPMI) were seeded in 24-well plates. After 24 hours of incubation, the medium was removed and 300  $\mu\text{l}$  of kirkiin were added to the appropriate dilutions (from  $10^{-15}\text{M}$  to  $10^{-11}\text{M}$ ), while the control samples were incubated only with the complete medium. After 72 hours of incubation with the RIP, the medium was removed and substituted with RPMI without leucine and containing 0.125  $\mu\text{Ci}$ /well of [ $^3\text{H}$ ]leucine. After 6 hours of incubation at  $37^\circ\text{C}$ , 1 ml of 20% TCA per well was added. The plate was left for 30 minutes at  $4^\circ\text{C}$  to precipitate the proteins and subsequently, 3 washes with 5% TCA were performed. The cells were detached with 200  $\mu\text{l}$  KOH 1 M for 10 minutes at  $37^\circ\text{C}$ . After a further wash with 0.1 M KOH, the content of each well was transferred in suitable vials and 5 ml of scintillation fluid were then added to each. The radioactivity of the [ $^3\text{H}$ ]leucine incorporated into the new synthesized proteins was determined by  $\beta$ -counter. The experiments were conducted in duplicate and  $\text{IC}_{50}$  values were calculated by linear regression.

### **4.2.17 Cell viability assay**

#### Cell viability by MTS assay

Cell viability was evaluated with the colorimetric assay CellTiter 96® Aqueous One Solution Cell Proliferation. The kit is a colorimetric assay which allows to measure the number of metabolically active cells, thus still viable. The MTS tetrazolium compound presents a yellow color and it is bioreduced by cells into a red colored formazan product, soluble in RPMI medium. The enzyme responsible for the reaction is a mitochondrial dehydrogenase that is present only in metabolically active cells. The compound conversion is presumably accomplished by NADPH or NADH produced by the enzyme. The quantity of formazan product is measured by measuring the absorbance at 490 nm and it is proportional to the number of viable cells.

NB100 and HeLa cells ( $2 \times 10^3$  cells in 100  $\mu\text{l}$ /well of complete medium RPMI) were seeded in 96-well microtiter plates. After 24 hours, cells were incubated with scalar dilutions of kirkiin (from  $10^{-15}\text{M}$  to  $10^{-11}\text{M}$ ) and left for 72 hours. In addition, time-course experiments were conducted on cells exposed to kirkiin ( $10^{-11}\text{M}$ ), ebulin 1 ( $10^{-7}\text{M}$ ) and nigrin b ( $10^{-7}\text{M}$ ) in a range between 4 and 96 hours. After the indicated times, the medium was removed and CellTiter 96 Aqueous One Solution Reagent diluted 1: 6

was added in a final volume of 120  $\mu\text{l}$ /well. After 1 hour of incubation at 37°C, the absorbance at 492 nm was measured. The results are the means of at least three experiments performed in triplicate.

#### Cell viability by ATP assay

This assay is based on the measurement of intracellular ATP produced by viable cells. The kit used is the CellTiter-Glo™ Luminescent Cell Viability Assay (Promega). It is based on the luciferin/luciferase reaction that generates the luminescent compound oxyluciferin in the presence of ATP. The luminescent signal is stable and linear (from 0 to 50000 living cells) and directly proportional to the amount of ATP produced.

NB100 cells ( $2 \times 10^3$  cells in 100  $\mu\text{l}$ /well of complete RPMI) were seeded in 96-well microtiter plates. After 24 hours, cells were incubated with ebulin I ( $10^{-7}\text{M}$ ) and nigrin b ( $10^{-7}\text{M}$ ). After the indicated times, the medium was removed and 100  $\mu\text{l}$  of CellTiter-Glo™ diluted 1:2 in complete RPMI were added. Plates were shaken at 420 rpm and incubated for 20 minutes in the dark at room temperature. The luminescence was measured by Fluoroskan Ascent FL (integration time 10 sec).

#### Cell viability by trypan blue exclusion test

Trypan Blue is a vital dye used to selectively stain viable cells. It is a negatively charged chromophore which is not able to cross the membrane of intact cells, but in dead cells it can easily penetrate, making them distinguishable from living cells with a rapid analysis with a simple microscopic observation. For the counting of the cells the Neubauer chamber was used and a solution containing 30  $\mu\text{l}$  of 0.1% trypan blue, 65  $\mu\text{l}$  RPMI and 5  $\mu\text{l}$  cell suspension was prepared.

#### Viability in the presence of cell-death inhibitors

RIP toxicity was evaluated in association with the pan-caspase inhibitor Z-VAD-fmk (100  $\mu\text{M}$ ) and the necroptosis inhibitor necrostatin-1 (100  $\mu\text{M}$ ). The reagents were added to the culture 3 hours before RIP treatment and every 24 hours after RIP treatment.

#### 4.2.18 Cell and nuclear morphology

NB100 cells ( $2 \times 10^3$  cells in 100  $\mu\text{l}$ /well of complete RPMI) were seeded in 24-well plates and after 24 hours, cells were incubated with kirkiin ( $10^{-11}\text{M}$ ), ebulin 1 ( $10^{-7}\text{M}$ ) and nigrin b ( $10^{-7}\text{M}$ ) in a range between 16, 24 and 48 hours at  $37^\circ\text{C}$ . Morphological analysis was assessed by phase contrast microscopy.

For nuclear analysis, NB100 cells ( $2 \times 10^4$  in 500  $\mu\text{l}$ /well of complete RPMI) were seeded directly on a coverslip in 24-well plates 48 hours prior the experiment. After treatment with kirkiin ( $10^{-11}\text{M}$ ) for 24 and 48 hours, cells were washed with PBS and fixed with methanol/acetic acid 1:3 for 20 minutes. After washing with PBS, the cells were incubated with 7  $\mu\text{l}$  DAPI/antifade (4',6-diamidino-2-phenylindole) and visualized under Nikon Eclipse E600W fluorescence microscope.

#### 4.2.19 Analysis of the mitochondrial membrane electrical potential gradient

The mitochondrial membrane potential ( $\Delta\psi\text{m}$ ) was measured using the cationic, lipophilic dye JC-1 (5,5',6,6'-tetrachloro-1,1',3,3'-tetraethylbenzimidazolocarboyanine iodide) contained in Mitochondria Staining Kit (Sigma). JC-1 selectively enters the mitochondria and reversibly change color from green to red as the membrane potential increases. In healthy cells with high  $\Delta\psi\text{m}$ , JC-1 forms J-aggregates yielding red fluorescence. In apoptotic or unhealthy cells the mitochondrial membrane potential dissipates and JC-1 remains in the monomeric form with green fluorescence.

Cells ( $2 \times 10^4$  in 500  $\mu\text{l}$ /well of complete RPMI) were seeded directly on a coverslip in 24-well plates 48 hours prior the experiments. After treatment with kirkiin ( $10^{-11}\text{M}$ ) for 24 and 48 hours cells were stained with 500  $\mu\text{l}$  of JC-1 dye (1:100 in RPMI) and incubated at room temperature for 10 minutes in the dark. The cells were then washed three times with staining buffer purchased from the kit. The coverslips were inverted on glass slide and the cells were observed under Nikon Eclipse E600W fluorescence microscope.

#### 4.2.20 Assessment of apoptosis

Apoptotic cell death was examined by flow cytometry using Annexin V-EGFP/PI detection kit and by luminometer measuring of caspase activation. Apoptosis inhibitor

Z-VAD was added 3 hours before treatment with the RIP.

#### Quantification by flow cytometry

Apoptotic cell death was examined by flow cytometry using Annexin V-EGFP/PI detection kit. Annexin V is a molecule able to bind to phosphatidylserine residues which are exposed on the cell membrane with the activation of apoptosis, while propidium iodide (PI) is a fluorescent DNA-intercalating molecule.

NB100 cells ( $2 \times 10^6/3$  ml RPMI complete) were seeded in  $25\text{cm}^2$  flasks and then treated with kirkiin ( $10^{-11}\text{M}$ ), ebulin 1 ( $10^{-7}\text{M}$ ) and nigrin b ( $10^{-7}\text{M}$ ). After the indicated times, the cells were centrifuged at  $400 \times g$  for 5 minutes, washed 2 times with cold PBS, centrifuged again and then resuspended in  $294 \mu\text{l}$  binding buffer supplied with the kit. Annexin V-EGFP ( $3 \mu\text{l}$ ) and propidium iodide ( $3 \mu\text{l}$ ) were added and the tubes were incubated for 10 minutes in the dark at room temperature. The cells were analyzed by flow cytometry FACS Aria (BD) using the FACSDiva software.

#### Caspase 3/7 activation

Caspase 3/7 activation was assessed by the luminescent assay Caspase-Glo™. The kit provides a luminogenic caspase substrate, which contains the tetrapeptide sequence specific for caspase 3/7 (DEVD). The caspase cleaves its substrate generating a luminescent signal, produced by luciferase. Luminescence is proportional to the amount of caspase activity present.

NB100 cells ( $2 \times 10^3$  in  $100 \mu\text{l}$ /well of complete RPMI) were seeded 96-well microtiter plates and after 24 hours, cells were incubated with kirkiin ( $10^{-11}\text{M}$ ), ebulin 1 ( $10^{-7}\text{M}$ ) and nigrin b ( $10^{-7}\text{M}$ ). After the indicated times, the medium was removed and  $50 \mu\text{l}$  of Caspase-Glo™3/7 diluted 1:2 in complete RPMI were added. Plates were shaken at 420 rpm and incubated for 20 minutes in the dark at room temperature.

The luminescence was measured by Fluoroskan Ascent FL (integration time 10 seconds) and the values were normalized for the viability.

#### **4.2.21 Cell cycle analysis by flow cytometry with PI**

The distribution of cell population in the different phases of the cell cycle was examined by flow cytometric analysis after staining with PI.

NB100 cells ( $2 \times 10^5$  in 3 ml of RPMI complete) were seeded in 25cm<sup>2</sup> flasks and then treated with ebulin I ( $10^{-7}$ M) and nigrin b ( $10^{-7}$ M). After 24 hours of treatment, the cells were centrifuged at 400xg for 5 minutes, washed 2 times with cold PBS, centrifuged again and fixed by adding 70% cold ethanol drop by drop, vortexing the samples. The samples were then stained with a solution containing 5 µg/ml PI, 0.1% Triton and 50 µg/ml RNAsi. The solution was boiled for 5 minutes to obtain a DNase free solution. The cells were analyzed by flow cytometry FACS Aria (BD) using the FACSDiva software. The intensity of the fluorescent is proportional to the amount of DNA within the cells: cells in G2 and M phases have a double DNA amount compared to cells in G1 phase, while cells in S phase have an intermediate amount of DNA, as they are in the replication process.

#### **4.2.22 Assessment of autophagy**

Cells ( $1 \times 10^6$ /20 ml RPMI complete) were seeded in 75 cm<sup>2</sup> flasks and after 24 hours, were treated with ebulin I ( $10^{-7}$ M) and nigrin b ( $10^{-7}$ M). At 24 hours of treatment, cells were centrifuged at  $500 \times g$  for 5 minutes at room temperature. Cell pellets were lysed by adding 100 µl of Cell Lytic-M (Sigma-Aldrich) supplemented with protease inhibitor cocktail (1:100), phosphatase inhibitor cocktail 1 (1:100) and sodium-orthovanadate (1:500). After 45 minutes on ice, vortexing every 5 minutes, the samples were centrifuged at  $12,000 \times g$  for 25 minutes at 4°C in order to remove the insoluble material. Protein supernatant (cell lysate) was collected and stored at -20°C. Protein content was quantified by spectrophotometer by Bradford assay. The protein (50 µg/lane) were separated by 10% SDS-PAGE and blotted for 45 minutes at 100V to nitrocellulose membrane (Millipore). Non-specific antibody binding sites were blocked by incubation with blocking buffer, containing TBS/Tween (TRIS buffered saline, 0.1% Tween 20) and 5% milk powder for 1 hour at room temperature. After 3 washes with TBS/Tween, membranes was incubated overnight at 4°C with the primary antibodies anti-LC3 (1:500), direct against LC3I (16 kDa) and LC3II (14 kDa), and monoclonal anti-β-actin (1:6000), which detects β-actin (42 kDa) used as protein loading control. All antibodies were diluted in TBS/Tween with 5% bovine serum albumin. After 3 washes with TBS/Tween, membranes were incubated for 1 hour at room temperature with horseradish peroxidase-conjugated anti-rabbit or anti-mouse secondary antibody (Sigma) (diluted 1:6000 for LC3 and 1:13000 for β-actin) in blocking buffer. After

further 3 washes, proteins were detected by incubating the membrane with Immobilon Western detection Reagent (Millipore), according to manufacturer's protocol and the image was taken on Kodak® BioMax light Film.

#### **4.2.23 SDS- PAGE**

Proteins were incubated in sample buffer (40 mM Tris/HCl pH 6.8, 2% SDS, 0.005% bromophenol blue) containing 0.5% (v/v) 2-mercaptoethanol (reducing conditions), or 1 mg/ml iodoacetamide (non-reducing conditions) for 20 minutes at 37°C. The gel was stained with 0.1% (w/v) Coomassie Brilliant Blue G250 in 50% methanol and 10% acetic acid, following the protocol recommended by the manufacturer (GE Healthcare).

#### **4.2.24 RNA electrophoresis on 5% polyacrylamide-7M urea gel**

Ribosomal RNA was analyzed using 5% (w/v) polyacrylamide in denaturing conditions with 7 M urea. RNA samples were incubated in loading buffer containing 150 mg/ml sucrose, 7 M urea, 0.4 µg/ml bromophenol blue and 1XTBE buffer (45 mM Tris, 45 mM boric acid, 1 mM EDTA pH 8). After boiling the samples for 30 seconds, the run was performed at 15 mA for 1h 15 min/1h 50 min, approximately, using TBE buffer. The gel was stained with 10 µl ethidium bromide (20 mg/ml) in 10 ml TBE buffer for 20-30 minutes and RNA bands were analyzed by UV-transilluminator (254-312 nm) including in the imaging instrument GelDoc (Biorad).

#### **4.2.25 DNA electrophoresis on agarose gel**

DNA was analyzed using 0.8% agarose gel in TAE (0.04 M Tris, 0.04 M acetate, 1 mM EDTA, pH 8.0) buffer. The samples were incubated in loading buffer (containing 45% glycerol (v/v), 10% of 10XTAE and 0.025% bromophenol blue). The run was performed at 90 V for 50 minutes, approximately, using TAE buffer. The gel was stained with a fluorescent solution, containing 10 µl GelRed (10000X) in 100 ml TAE buffer for 20-30 minutes. DNA bands were analyzed by UV-transilluminator (254-312 nm) including in the imaging instrument GelDoc (Biorad).

# **Bibliography**



- Aceto S, Di Maro A, Conforto B, Siniscalco GG, Parente A, Delli Bovi P, Gaudio L. Nicking activity on pBR322 DNA of ribosome inactivating proteins from *Phytolacca dioica* L. leaves. *Biol Chem.* 2005;386(4):307-17.
- Agoreyo BO, Okoro NC, Choudhary MI. Preliminary phytochemical analyses of two varieties of *Adenialobata* (jacq) and the antioxidant activity of their various solvent fractions. *Bayero Journal of Pure and Applied Sciences.* 2012; 5(1): 182–186
- Akendengue B, Lemamy GJ, Bourobou HB. and Laurens A. Bioactive natural compounds from medico-magic plants of Bantu area. *Studies in Natural Product Chemistry.* 2005; 32:803-820.
- Alewine C, Hassan R, Pastan I. Advances in anticancer immunotoxin therapy. *Oncologist.* 2015 Feb;20(2):176-85. Review.
- Allen EH, Schweet RS. Synthesis of hemoglobin in a cell-free system. I. Properties of the complete system. *J Biol Chem.*1962; 237:760–767.
- Bagga S, Seth D, Batra JK. The cytotoxic activity of ribosome-inactivating protein saporin-6 is attributed to its rRNA N-glycosidase and internucleosomal DNA fragmentation activities. *J Biol Chem.* 2003; 278(7):4813-20.
- Balint GA. Ricin: the toxic protein of castor oil seeds. *Toxicology.* 1974; 2(1):77-102.
- Baluna R, Coleman E, Jones C, Ghetta V, Vitetta ES. The effect of a monoclonal antibody coupled to ricin A chain-derived peptides on endothelial cells in vitro: insights into toxin-mediated vascular damage. *Exp Cell Res.* 2000; 258(2):417-24.
- Barbieri L, Brigotti M, Perocco P, Carnicelli D, Ciani M, Mercatali L, Stirpe F. Ribosome-inactivating protein depurinate poly(ADP-ribosyl)ated poly(ADPribose) polymerase and have transforming activity for 3T3 fibroblasts. *FEBS Lett.* 2003; 538,178-182
- Barbieri L, Ciani M, Girbés T, Liu WY, Van Damme EJ, Peumans WJ, Stirpe F. Enzymatic activity of toxic and non-toxic type 2 ribosome-inactivating proteins. *FEBS Lett.* 2004;563(1-3):219-22.
- Barbieri L, Falasca AI, Stirpe F. Volkensin, the toxin of *Adenia volkensii* (kilyambiti plant). *FEBS Lett.* 1984; 171, 277–279.
- Barbieri L, Gasperi-Campani A, Derenzini M, Betts CM, Stirpe F. Selective lesions of acinar pancreatic cells in rats poisoned with abrin. A morphological and biochemical study. *Virchows Arch B Cell Pathol.* 1979; 30:15–24. 43.
- Barbieri L, Polito L, Bolognesi A, Ciani M, Pelosi E, Farini V, Jha A.K, Sharma N, Vivanco J.M, Chambery A, Parente A, Stirpe F. Ribosome-inactivating proteins in edible plants and purification and characterization of a new ribosome-inactivating protein from *Cucurbita moschata*. *BiochimBiophysActa.* 2006; 1760(5):783-92.
- Barbieri L, Valbonesi P, Bondioli M, Alvarez ML, Dal Monte P, Landini MP, Stirpe F. Adenine glycosylase activity in mammalian tissues: an equivalent of ribosome-inactivating proteins. *FEBS Lett.* 2001; 505(1):196-7.
- Barbieri L, Valbonesi P, Gorini P, Pession A. and Stirpe F. Polynucleotide: adenosine glycosidase activity of ribosome-inactivating proteins: effect on DNA, RNA and poly(A). *NucleicAcids Res.* 1997; 25(3): 518–522.

- Barbieri L, Zamboni M, Montanaro L, Sperti S. and Stirpe F. Purification and Properties of Different Forms of Modeccin, the Toxin of *Adeniadigitata*. *Biochem. J.* 1980; 185, 203-210.
- Barbieri L, Battelli MG, Stirpe F. Ribosome-inactivating proteins from plants. *Biochim. Biophys. Acta.* 1993; 1154: 237-282.
- Barbieri L, Gorini P, Valbonesi P, Castiglioni P, Stirpe F. Unexpected activity of saporins. *Nature.* 1994; 372, 624.
- Battelli MG, Barbieri L, Stirpe F. Toxicity of, and histological lesions caused by, ribosome-inactivating proteins, their IgG-conjugates, and their homopolymers. *ActaPatholMicrobiolImmunol Scand.* 1990; 98:585–593.
- Battelli MG, Scicchitano V, Polito L, Farini V, Barbieri L, Bolognesi A. Binding and intracellular routing of the plant-toxic lectins, lanceolin and stenodactylin. *BiochimBiophys Acta.* 2010; 1800(12):1276-82.
- Battelli MG, Citores L, Buonamici L, Ferreras JM, de Benito FM, Stirpe F, Girbés T. Toxicity and cytotoxicity of nigrin b, a two-chain ribosome-inactivating protein from *Sambucus nigra*: comparison with ricin. *Arch Toxicol.* 1997; 71(6):360-4.
- Battelli MG, Musiani S, Buonamici L, Santi S, Riccio M, Maraldi NM, Girbés T, Stirpe F. Interaction of volkensin with HeLa cells: binding, uptake, intracellular localization, degradation and exocytosis. *Cell Mol Life Sci.* 2004; 61(15):1975-84.
- Battelli MG. Cytotoxicity and toxicity to animals and humans of ribosome-inactivating proteins. *Mini Rev. Med. Chem.* 2004; 4, 513-521.
- Battelli, MG., Buonamici, L., Bolognesi, A., Stirpe, F. In vivo and in vitro uptake of an anti-CD30/saporin immunotoxin by rat liver parenchymal and non parenchymal cells. *Hepatology* 1994; 20, 940-947.
- Benítez J, Ferreras JM, Muñoz R, Arias Y, Iglesias R, Córdoba-Díaz M, del Villar R, Girbés T. Cytotoxicity of an ebulin l-anti-human CD105 immunotoxin on mouse fibroblasts (L929) and rat myoblasts (L6E9) cells expressing human CD105. *MedChem.* 2005; 1(1):65-70.
- Bergamaschi G, Perfetti V, Tonon L, Novella A, Lucotti C, Danova M, Glennie M.J, Merlini G, Cazzola M. Saporin. A ribosome-inactivating protein used to prepare immunotoxins, induces cell death via apoptosis. *Br J Haematol.* 1996; 93(4):789-94.
- Bhaskar AS, Deb U, Kumar O, Lakshmana Rao PV. Abrin induced oxidative stress mediated DNA damage in human leukemic cells and its reversal by N-acetylcysteine. *Toxicol In Vitro.* 2008; 22(8):1902-8.
- Bolognesi A, Bortolotti M, Maiello S, Battelli MG, Polito L. Ribosome-Inactivating Proteins from Plants: A Historical Overview. *Molecules.* 2016; 21(12).
- Bolognesi A, Polito L, Scicchitano V, Orrico C, Pasquinelli G, Musiani S, Santi S, Riccio M, Bortolotti M, Battelli M.G. Endocytosis and intracellular localisation of type 1 ribosome-inactivating protein saporin-s6. *J BiolRegulHomeost Agents.* 2012; 26(1):97-109.

- Bolognesi A, Polito L. Immunotoxins and other conjugates: pre-clinical studies. *Mini Rev Med Chem.* 2004; 4(5):563-83.
- Bolognesi A, Tazzari P, Olivieri F, Polito L, Falini B, Stirpe F. Induction of apoptosis by ribosome-inactivating proteins and related immunotoxins. *Int J Cancer.* 1996; 68(3):349-55.
- Bolognesi A, Tazzari P.L, Tassi C, Gromo G, Gobbi M, Stirpe F. A comparison of anti-lymphocyte immunotoxins containing different ribosome-inactivating proteins and antibodies. 1992 *Clin. Exp. Immunol.* 89, 341-346.
- Bora N, Gadadhar S, Karande AA. Signaling different pathways of cell death: Abrin induced programmed necrosis in U266B1 cells. *Int J Biochem Cell Biol.* 2010; 42(12):1993-2003.
- Brigotti M, Alfieri R, Sestili P, Bonelli M, Petronini PG, Guidarelli A, Barbieri L, Stirpe F, Sperti S. Damage to nuclear DNA induced by Shiga toxin 1 and ricin in human endothelial cells. *FASEB J.* 2002; 16(3):365-72.
- Büssing A, Suzart K, Bergmann J, Pfüller U, Schietzel M, Schweizer K. Induction of apoptosis in human lymphocytes treated with *Viscum album L.* is mediated by the mistletoe lectins. *Cancer Lett.* 1996; 99(1):59-72.
- Büssing A, Multani AS, Pathak S, Pfuller U, Schietze, M. Induction of apoptosis by the N-acetyl-galactosamine-specific toxic lectin from *Viscum album L.* is associated with a decrease of nuclear p53 and Bcl-2 proteins and induction of telomeric associations. *Cancer Lett.* 1998; 130(1-2):57-68.
- Byers VS, Levin AS, Malvino A. A phase II study of effect of addition of trichosanthin to zidovudine in patients with HIV disease and failing antiretroviral agents. *AIDS Research and Human Retroviruses.* 1994; 10(4), 413-420.
- Carzaniga R, Sinclair L, Fordham-Skelton AP, Harris N, Croy RRD. Cellular and subcellular distribution of saporins, type-1 ribosome-inactivating proteins in soapwort (*Saponaria officinalis L.*). *Planta.* 1994 ;194:461- 470.
- Cavallaro U, Soria MR. Targeting plant toxins to the urokinase and alpha 2-macroglobulin receptors. *Semin Cancer Biol.* 1995; 6(5):269-78.
- Chambery A, Pisante M, Di Maro A, Di Zazzo E, Ruvo M, Costantini S, Colonna G, Parente A. Invariant Ser211 is involved in the catalysis of PD-L4, type I RIP from *Phytolacca dioica* leaves. *Proteins.* 2007; 67:209–218.
- Chambery A, Di Maro A, Monti MM, Stirpe F, Parente A. Volkensin from *Adenia volkensii* Harms (kilyambitiplant), a type 2 ribosome-inactivating protein. *Eur J Biochem.* 2004; 271(1):108-17.
- Christiansen SP, Peterson D, To T, Youle R, McLoon L. Long-term effects of ricin-mAb 35 on extraocular muscles of rabbits: potential treatment for strabismus. *Invest Ophthalmol Vis Sci.* 2002; 43(3):679-85.
- Christofferson DE, Yuan J. Necroptosis as an alternative form of programmed cell death. *Curr Opin Cell Biol.* 2010; 22(2):263-8.

- Citores L, Ferreras JM, Muñoz R, Benítez J, Jiménez P, Girbés T. Targeting cancer cells with transferring conjugates containing the non-toxic type 2 ribosome-inactivating proteins nigrin b or ebulin l. *Cancer Lett.* 2002; 184(1):29-35.
- Citores L, Muñoz R, De Benito FM, Iglesias R, Ferreras JM, Girbes T. Differential sensitivity of HELA cells to the type 2 ribosome-inactivating proteins ebulin l, nigrin b and nigrin f as compared with ricin. *Cell MolBiol (Noisy-le-grand).* 1996; 42(4):473-6.
- Citores L, Muñoz R, Rojo MA, Jiménez P, Ferreras JM, Girbés T. Evidence for distinct cellular internalization pathways of ricin and nigrin b. *Cell MolBiol (Noisy-le-grand).* 2003; 49.
- Das MK, Sharma RS, Mishra V. Induction of apoptosis by ribosome inactivating proteins: importance of N-glycosidase activity. *Appl Biochem Biotechnol.* 2012; 166(6):1552-61.
- de Virgilio M, Lombardi A, Caliandro R, Fabbrini M.S. Ribosome-inactivating proteins: from plant defense to tumor attack. *Toxins (Basel).*2010; 2(11):2699-737.
- Declercq W, Vanden Berghe T, Vandenabeele P. RIP kinases at the crossroads of cell death and survival. *Cell.* 2009; 138(2):229-32. Review.
- Di Maro A, Citores L, Russo R, Iglesias R, Ferreras JM. Sequence comparison and phylogenetic analysis by the Maximum Likelihood method of ribosome-inactivating proteins from angiosperms. *Plant Mol Biol.* 2014; 85(6):575-88.
- Dosio F, Stella B, Cerioni S, Gastaldi D, Arpicco S. Advances in anticancer antibody-drug conjugates and immunotoxins. *Recent Pat Anticancer Drug Discov.*2014; 9(1):35-65. Review.
- Dowd PF, Zuo WN, Gilliki JW, Johnso ET, Boston RS. Enhanced resistance to *Helicoverpa zea* in tobaccoexpressing an activated form of maize ribosome-inactivatingprotein. *J. Agric. Food Chem.* 2003; 51, 3568–3574.
- Duggar BM, Armstrong JK. The effect of treating the virus of tobacco mosaic with the juices of various plants. *Ann Mo Bot Gard* 1925; 12:359–366.
- Eggl U, Newton LE. *Etymological Dictionary of Succulent Plant Names.* Springer 2013; 3:127.
- Endo Y, Tsurugi K. The RNA N-glycosidase activity of ricin A-chain. The characteristics of the enzymatic activity of ricin A-chain with ribosomes and with rRNA. *J Biol Chem* 1988; 263:8735–8739.
- Endo Y, Mitsui K, Motizuki M, Tsurugi K. The mechanism of action of ricin and related toxic lectins on eukaryotic ribosomes. The site and the characteristics of the modification in 28 S ribosomal RNA caused by the toxins. *J Biol Chem.* 1987; 262(12):5908-12.
- Endo Y, Gluc, A, Wool IG. Ribosomal RNA identity elements for ricin A-chain recognition and catalysis. *J. Mol. Biol.* 1991; 254, 848-855.
- Fang EF, Zhang CZ, Wong JH, Shen JY, Li CH, Ng TB. The MAP30 protein from bitter melon (*Momordica charantia*) seeds promotes apoptosis in liver cancer cells in vitro and in vivo. *Cancer Lett.* 2012; 324(1):66-74.

- Feng J, Li M, Huang Y, Xiao Y. Symmetric key structural residues in symmetric proteins with beta-trefoil fold. *PLoS One*. 2010; 5:e14138
- Fernández-Puentes C, Carrasco L. Viral infection permeabilizes mammalian cells to protein toxins. *Cell*. 1980 Jul; 20(3):769-75.
- Ferreras JM, Barbieri L, Girbés T, Battelli MG, Rojo MA, Arias FJ, Rocher MA, Soriano F, Mendéz E, Stirpe F. Distribution and properties of major ribosome-inactivating proteins (28 S rRNA N-glycosidases) of the plant *Saponaria officinalis* L. (Caryophyllaceae) *BiochimBiophysActa*.1993; 1216(1):31-42.
- Ferreras JM, Citores L, Iglesias R, Jiménez P, Girbés T. Sambucus Ribosome-Inactivating Proteins and Lectins. *Toxic Plant Proteins. Plant Cell Monographs*. 2010, 18:107-131.
- Ferreras JM, Citores L, Iglesias R, Jiménez P, Girbés T. Use of ribosome-inactivating proteins from sambucus for the construction of immunotoxins and conjugates for cancer therapy. *Toxins (Basel)*. 2011; 3(5):420-41.
- Foà-Tomasi L, Campadelli-Fiume G, Barbieri L, Stirpe F. Effect of ribosome-inactivating proteins on virusinfected cells. Inhibition of virus multiplication and of protein synthesis. *Arch Virol*. 1982; 71(4):323-32.
- Fodstad O, Olsnes S, Pihl A. Inhibitory effect of ricin and abrin on the growth of transplantable murine tumours and of abrin on human cancers in nude mice. *Cancer Res*. 1977; 37, 4559-4567.
- Fracasso G, Stirpe F, Colombatti M. Ribosome-Inactivating Protein- containing conjugates for therapeutic use. In: Lord J.M., Hartley R.M., editors. *Toxic Plant Proteins, Plant Cell Monographs*. Springer-Verlag; Heidelberg, Berlin, German: 2010; pp. 225–263.
- Frankel A, Welsh P, Richardson J, Robertus JD. Role of arginine 180 and glutamic acid 177 of ricin toxin A chain in enzymatic inactivation of ribosomes. *Mol Cell Biol*. 1990; 10(12):6257-63.
- Frigerio L, Jolliff, NA, Di Cola A, Felip DH, Paris N, Neuhaus JM, Lord JM; Ceriotti A, Roberts LM. The internal propeptide of the ricin precursor carries a sequence-specific determinant for vacuolar sorting. *Plant Physiol*. 2001; 126, 167–175.
- Gayoso MJ, Muñoz R, Arias Y, Villar R, Rojo MA, Jiménez P, Ferreras JM, Aranguéz I, Girbés T. Specific dose-dependent damage of Lieberkühn crypts promoted by large doses of type 2 ribosome-inactivating protein nigrin b intravenous injection to mice. *Toxicol Appl Pharmacol*. 2005; 207(2):138-46.
- Ghosh PC, Wu HC. Enhancement of cytotoxicity of modeccin by nigericin in modeccin-resistant mutant cell lines. *Exp. Cell Res*. 1988; 174: 397–410.
- Giansanti F, Di Leandro L, Koutris I, Pitari G, Fabbrini M.S, Lombardi A, Flavell D.J, Flavell S.U, Gianni S, Ippoliti R. Engineering a switchable toxin: the potential use of PDZ domains in the expression, targeting and activation of modified saporin variants. *Protein Eng Des Sel*. 2010; 23(2):61-8.
- Gilabert-Oriol R, Weng A, Mallinckrodt Bv, Melzig MF, Fuchs H, Thakur M. Immunotoxins constructed with ribosome-inactivating proteins and their enhancers:a lethal cocktail with tumor specific efficacy. *Curr Pharm Des*. 2014; 20(42):6584-643. Review.

- Gill LS. Ethnomedical uses of Plants in Nigeria. University of Benin Press. Benin, Nigeria. 1992; P.276.
- Girbés T, Citores L, Ferreras JM, Rojo MA, Iglesias R, Muñoz R, Arias FJ, Calonge M, García JR, Méndez E. Isolation and partial characterization of nigrin b, a non-toxic novel type 2 ribosome-inactivating protein from the bark of *Sambucusnigra* L. *Plant Mol Biol*. 1993(a); 22(6):1181-6.
- Girbés T, Citores L, Iglesias R, Ferreras JM, Muñoz R, Rojo MA, Arias FJ, García JR, Méndez E, Calonge M. Ebulin 1, a nontoxic novel type 2 ribosome-inactivating protein from *Sambucusebulus* L. leaves. *J Biol Chem*. 1993(b); 268(24):18195-9.
- Girbés T, Ferreras JM, Arias FJ, Stirpe F. Description, distribution, activity and phylogenetic relationship of ribosome-inactivating proteins in plants, fungi and bacteria. *Mini Rev Med Chem*. 2004; 4(5):461-76.
- Girbes T, Ferreras JM, Arias FJ, Muñoz R, Iglesias R, Jimenez P, Rojo MA, Arias Y, Perez Y, Benitez J, Sanchez D, Gayoso MJ. Non-toxic type 2 ribosome-inactivating proteins (RIPs) from *Sambucus*: occurrence, cellular and molecular activities and potential uses. *Cell MolBiol (Noisy-le-grand)*. 2003; 49(4):537-45. Review.
- Glennie MJ, McBride HM, Stirpe F, Thorpe PE, Worth AT, Stevenson GT. Emergence of immunoglobulin variants following treatment of a B cell leukemia with an immunotoxin composed of antiidiotypic antibody and saporin. *J Exp Med*. 1987; 166(1):43-62.
- Griffiths GD, Leek MD, Gee DJ. The toxic plant proteins ricin and abrin induce apoptotic changes in mammalian lymphoid tissues and intestine. *J. Pathol*. 1987; 151, 221–229.
- Gu YJ, Xia ZX. Crystal structures of the complexes of trichosanthin with four substrate analogs and catalytic mechanism of RNA N-glycosidase. *Proteins*. 2000; 39(1):37-46.
- Hajto T, Hostanska K, Frei K, Rordorf C, Gabius HJ. Increased secretion of tumor necrosis factors alpha, interleukin 1, and interleukin 6 by human mononuclear cells exposed to beta-galactoside-specific lectin from clinically applied mistletoe extract. *Cancer Res*. 1990; 50(11):3322-6.
- Hao Q, Van Damme EJ, Hause B, Barre A, Chen Y, Rougé P, Peumans WJ. Iris bulbs express type 1 and type 2 ribosome-inactivating proteins with unusual properties. *Plant Physiol*. 2001; 125(2):866-76.
- Harper CG, Gonatas JO, Mizutani T, Gonatas NK. Retrograde transport and effects of toxic ricin in the autonomic nervous system. *Lab Invest*. 1980; 42(4):396-404.
- Harrison MB, Wiley RG, Wooten GF. Selective localization of striatal D1 receptors to striatonigral neurons. *Brain Res*. 1990; 528(2):317-22.
- Hartley MR, Lord JM. Cytotoxic ribosome-inactivating lectins from plants. *BBA*. 2004; 1701:1–14.
- Hartley MR, Chddock JA, Bonnes MS. The structure and function of ribosomeinactivating proteins. *Trend Plant Sci*. 1996; 1, 254-260.
- Hasegawa N, Kimura Y, Oda T, Komatsu N, Muramatsu T. Isolated ricin B chainmediated apoptosis in U937 cells. *Biosci. Biotechnol. Biochem*. 2000; 64, 1422-1429.

- Hatakeyama T, Yamasaki N, Funatsu G. Identification of the tryptophan residue located at the low-affinity saccharide binding site of ricin D. *J Biochem.* 1986; 100(3):781-8.
- Hearn DJ. *Adenia* (Passifloraceae) and its Adaptive Radiation: Phylogeny and Growth Form Diversification *Systematic Botany.* 2006; 31(4): 805–821.
- Higuchi S, Tamura T, Oda T. Cross-talk between the pathways leading to the induction of apoptosis and the secretion of tumor necrosis factor-alpha in ricin-treated RAW 264.7 cells. *J Biochem.* 2003; 134(6):927-33. PubMed PMID: 14769883.
- Hoogenboom HR, Marks JD, Griffiths AD, Winter G. Building antibodies from their genes. *Immunol Rev.* 1992; 130:41-68.
- Horrix C, Raviv Z, Flescher E, Voss C, Berger M.R. Plant ribosome-inactivating proteins type II induce the unfolded protein response in human cancer cells. *Cell Mol Life Sci.* 2011; 68(7):1269-81.
- Hossann M, Li Z, Shi Y, Kreilinger U, Büttner J, Vogel PD, Yuan J, Wise JG, Trommer WE. Novel immunotoxin: a fusion protein consisting of gelonin and an acetylcholine receptor fragment as a potential immunotherapeutic agent for the treatment of Myasthenia gravis. *Protein Expr Purif.* 2006; 46(1):73-84.
- Hott JS, Dalakas MC, Sung C, Hallett M, Youle RJ. Skeletal muscle-specific immunotoxin for the treatment of focal muscle spasm. *Neurology.* 1998; 50(2):485-91.
- Hudak KA, Dinman JD, Tumer NE. Pokeweed antiviral protein accesses ribosomes by binding to L3. *J. Biol. Chem.* 1999; 274, 3859-3864.
- Hughes JN, Lindsay CD, Griffiths GD. Morphology of ricin and abrin exposed endothelial cells is consistent with apoptotic cell death. *Hum Exp Toxicol.* 1996; 15(5):443-51.
- Husain J, Tickle IJ, Wood SP. Crystal structure of momordin, a type I ribosome inactivating protein from the seeds of *Momordica charantia*. *FEBS Lett.* 1994; 342(2):154-8.
- Iglesias R, Citores L, Di Maro A, Ferreras JM. Biological activities of the antiviral protein BE27 from sugar beet (*Beta vulgaris* L.). *Planta.* 2015; 241(2):421-33.
- Iglesias R, Citores L, Ragucci S, Russo R, Di Maro A, Ferreras JM. Biological and antipathogenic activities of ribosome-inactivating proteins from *Phytolacca dioica* L. *Biochim Biophys Acta.* 2016; 1860(6):1256-64.
- Iordanov MS, Pribnow D, Magun JL, Dinh TH, Pearson JA, Chen SL, Magun BE. Ribotoxic stress response: activation of the stress-activated protein kinase JNK1 by inhibitors of the peptidyl transferase reaction and by sequence-specific RNA damage to the alpha-sarcin/ricin loop in the 28S rRNA. *Mol Cell Biol.* 1997; 17(6):3373-81.
- Irvin J.D. Pokeweed antiviral protein. *Pharmacol. Ther.* 1983; 21 371–387.
- Jiménez P, Gayoso M, Tejero J, Cabrero P, Córdoba-Díaz D, Basterrechea JE, Girbés T. Toxicity in mice of lectin ebulin f present in dwarf Elderberry (*Sambucus ebulus* L.). *Toxicon.* 2013; 61:26-9.
- Johannes L, Popoff V. Tracing the retrograde route in protein trafficking. *Cell.* 2008; 135(7):1175-87.

- Kabeysa Y, Mizushima N, Ueno T, Yamamoto A, Kirisako T, Noda T, Kominami E, Ohsumi Y, Yoshimori T. LC3, a mammalian homologue of yeast Apg8p, is localized in autophagosome membranes after processing. *EMBO J.* 2000; 19(21):5720-8.
- Kahn JO, Kaplan LD, Gambertoglio JG, Bredesen D, Arri CJ, Turin L, Kibort T, Williams RL, Lifson JD, Volberding PA. The safety and pharmacokinetics of GLQ223 in subjects with AIDS and AIDS-related complex: a phase I study. *AIDS.* 1990; 4(12):1197-204.
- Kalb VF Jr, Bernlohr RWA. New spectrophotometric assay for protein in cell extracts. *Anal Biochem.* 1977; 82(2):362-71.
- Katzin B.J, Collins E.J, Robertus J.D. The structure of ricin A chain at 2.5 Å. *Proteins Struct. Funct. Genet.* 1991; 251-259.
- Kim MS, Lee J, Lee KM, Yang SH, Choi S, Chung SY, Kim TY, Jeong WH, Park R. Involvement of hydrogen peroxide in mistletoe lectin-II-induced apoptosis of myeloleukemic U937 cells. *Life Sci.* 2003; 73(10):1231-43.
- KimWH, ParkWB, Gao B, Jung MH. Critical role of reactive oxygen species and mitochondrial membrane potential in Korean mistletoe lectin-induced apoptosis in human hepato carcinoma cells. *Mol.Pharmacol.* 2004; 66,1383–1396.
- Kochi SK, Collier RJ. DNA fragmentation and cytolysis in U937 cells treated with diphtheria toxin or other inhibitors of protein synthesis. *Exp Cell Res.*1993; 208(1):296-302.
- Kurinov IV, Rajamohan F, Venkatachalam TK, Uckun FM. X-ray crystallographic analysis of the structural basis for the interaction of pokeweed antiviral protein with guanine residues of ribosomal RNA. *Protein Sci.* 1999; 8(11):2399-405.
- Lamb FI, Roberts LM, Lord JM. Nucleotide sequence of cloned cDNA coding for preprorcin. *Eur J Biochem.* 1985; 148(2):265-70.
- Lee SY, Lee MS, Cherla RP, Tesh VL. Shiga toxin 1 induces apoptosis through the endoplasmic reticulum stress response in human monocytic cells. *Cell Microbiol.* 2008; 10(3):770-80.
- Lehar SM, Pedersen JT, Kamath RS, Swimmer C, Goldmacher VS, Lambert JM, Blättler WA, Guild BC. Mutational and structural analysis of the lectin activity in binding domain 2 of ricin B chain. *Protein Eng.* 1994; 7(10):1261-6.
- Li J, Xia X, Ke Y, Nie H, Smith MA, Zhu X. Trichosanthin induced apoptosis in HL-60 cells via mitochondrial and endoplasmic reticulum stress signaling pathways. *BiochimBiophysActa.* 2007; 1770(8):1169-80.
- Licastro F, Morini MC, Bolognesi A, Stirpe F. Ricin induces the production of tumour necrosis factor-alpha and interleukin-1 beta by human peripheral-blood mononuclear cells. *Biochem J.* 1993; 294 ( Pt 2):517- 20.
- Lin JY, Tserng KY, Chen CC, Lin LT, Tung TC. Abrin and ricin: new anti-tumour substances. *Nature.* 1970; 18; 227(5255):292-3.
- Ling J, Liu WY, Wang TP. Cleavage of supercoiled double-stranded DNA by several ribosome-inactivating proteins in vitro. *FEBS Lett.* 1994; 345(2-3):143-6.

- Lodg, JK, Kaniewshi WK, Tumer NE. Broad spectrum virus resistance in transgenic plants expressing pokeweed antiviral protein. *Proc. Natl. Acad. Sci.* 1993; 90, 7089–7093.
- Lombardi A, Bursomanno S, Lopardo T, Traini R, Colombatti M, Ippoliti R, Flavell DJ, Flavell SU, Ceriotti A, Fabbrini MS. *Pichia. pastoris* as a host for secretion of toxic saporin chimeras. *FASEB J.* 2010; 24:253–265.
- Lord JM, Roberts LM, Robertus JD. Ricin: structure, mode of action, and some current applications. *FASEB J.* 1994; 8(2):201-8.
- Lu P, Jin Y. Ectopic pregnancy treated with tricosanthin. *Chin. Med. J.* 1989; 102:365-367.
- Madan S, Ghosh PC. Enhancing potency of liposomal monensin on ricin cytotoxicity in mouse macrophage tumor cells. *Biochem Int.* 1992; 28(2):287-95.
- Madhumathi J, Verma RS. Therapeutic targets and recent advances in protein immunotoxins. *Curr Opin Microbiol.* 2012; 15(3):300-9.
- Mansouri S, Choudhary G, Sarzala PM, Ratner L, Hudak KA. Suppression of human Tcell leukemia virus I gene expression by pokeweed antiviral protein. *J Biol Chem.* 2009; 284(45):31453-62
- Mariotti-Lippi L, Bellini C, Mori S. Palaeovegetational reconstruction based on pollen and seeds/fruits from a Bronze Age archaeological site in Tuscany (Italy). *Plant Biosyst.* 2010, 144,902–908.
- Martin L; Jacomet S., Thiebault S. Plant economy during the neolithic in a mountain context: The case of “Le Chenet des Pierres” in the French Alps (Bozel-Savoie, France). *Veg. Hist. Archaeobotany.* 2008, 17, s113–s122.
- Martin S. The Proteids of the Seeds of *Abrus precatorius* (Jequirity). *Proceedings of the Royal Society of London (1854-1905).* 1887; 42:331–334.
- Mayerhofer PU, Cook JP, Wahlman J, Pinheiro TT, Moore KA, Lord JM, Johnson AE, Roberts LM. Ricin A chain insertion into endoplasmic reticulum membranes is triggered by a temperature increase to 37°C. *J. Biol. Chem.* 2009; 284, 10232–10242.
- Mayfield S. Production of anti-cancer immunotoxins in algae: Ribosome inactivating proteins as fusion partners. *Biotechnol. Bioeng.* 2013; 110:2826–2835.
- Montfort W, Villafranca JE, Monzingo AF, Ernst S, Katzin B, Rutenber E, Xuong NH, Hamlin R, Robertu JD. Three-dimensional structure of ricin at 2.8Å. *Biol. Chem.* 1987; 262, 5398-5403.
- Monti B, D’Alessandro C, Farini V, Bolognesi A, Polazzi E, Contestabile A, Stirpe F, Battelli MG. In vitro and in vivo toxicity of type 2 ribosome-inactivating proteins lanceolin and stenodactylin on glial and neuronal cells *NeuroToxicology.* 2007; 28, 637–644.
- Monzingo AF; Robertu, JD. X-ray analysis of substrate analogs in the ricin A-chain active site. *J. Mol. Biol.* 1992, 227, 1136–1145.
- Mshan NR, Abbiw DK, Addae-Mensa I, Adjanouhoun E, Ahyi MRA, Ekpere JA, Enow-Orock EG, Gbile ZO, Noamesi GK, Odei MA, Odunlami H, Oteng-Yeboah AA, Sarpong

- K, Sofowora A, Tackie AN. Traditional Medicine and Pharmacopoeia, Contribution to the revision of Ethnobotanical and Floristic Studies in Ghana, OAU/STRC Technical Report. 2000.
- Muñoz R, Arias Y, Ferreras JM, Rojo MA, Gayoso MJ, Nocito M, Benitez J, Jiménez P, Bernabéu C, Girbés T. Targeting a marker of the tumourneovasculature using a novel anti-human CD105-immunotoxin containing the non-toxic type 2 ribosome-inactivating protein nigrin b. *Cancer Lett.* 2007; 256(1):73-80.
- Narayanan S, Surendranath K, Bora N, Surolia A, Karande A.A. Ribosome inactivating proteins and apoptosis. *FEBS Lett.* 2005; 579(6):1324-31.
- Nicolson GL, Blaustein J, Etzler ME. Characterization of two plant lectins from *Ricinus communis* and their quantitative interaction with a murine lymphoma. *Biochemistry.* 1974; 13(1):196-204.
- Nielsen K, Boston RS. Ribosome-inactivating proteins: a plant perspective. *Annu. Rev. Physiol. Plant Mol. Biol.* 2001; 52:785-816.
- Olmo N, Turnay J, González de Buitrago G, López de Silanes I, Gavilanes JG, Lizarbe MA. Cytotoxic mechanism of the ribotoxin  $\alpha$ -sarcin Induction of cell death via apoptosis. *European Journal of Biochemistry.* 2001; 268, 7, 2113–2123.
- Olsnes S, Pihl A. Different biological properties of the two constituent peptide chains of ricin, a toxic protein inhibiting protein synthesis. *Biochemistry* 1973; 12, 3121–3126.
- Osuagwu GGE, Ibeabuchi IC. The influence of aqueous leaf and stem extracts of *Adenialobata* (Jacq) on the flowering and fruiting of okra (*Abelmoschus esculenta*) and groundnut (*Arachis hypogea*) *African Journal of Biotechnology.* 2010; 9: 3260-3263.
- Palanca-Wessels MC, Press OW. Advances in the treatment of hematologic malignancies using immunoconjugates. *Blood.* 2014; 123(15):2293-301.
- Parikh BA, Baykal U, Di R, Tumer NE. Evidence for retro-translocation of pokeweed antiviral protein from endoplasmic reticulum into cytosol and separation of its activity on ribosomes from its activity on capped RNA. 2005; 44(7):2478-90.
- Pascal JM, Day PJ, Monzingo AF, Ernst SR, Robertus JD, Iglesias R, Pérez Y, Ferreras JM, Citores L, Girbés T. 2.8-Å crystal structure of a nontoxic type-II ribosome-inactivating protein, ebulin I. *Proteins.* 2001; 43(3):319-26.
- Paul I, Devor M. Completeness and selectivity of ricin "suicide transport" lesions in rat dorsal root ganglia. *J Neurosci Methods.* 1987; 22(2):103-11.
- Pelosi E, Lubelli C, Polito L, Barbieri B, Bolognesi A, Stirpe, F. Ribosome-inactivating proteins and other lectins from *Adenia* (Passifloraceae). *Toxicon.* 2005; 46(6), 658–663.
- Peuman, WJ, Hao Q, van Damme EJ. Ribosome-inactivating proteins from plants: More than RNA N-glycosidases? *FASEB J.* 2001, 15, 1493–1506.
- Pincus SH, Smallshaw JE, Song K, Berry J, Vitetta ES. Passive and active vaccination strategies to prevent ricin poisoning. *Toxins (Basel).* 2011; 3(9):1163-84.
- Pincus SH. Therapeutic potential of anti-HIV immunotoxins. *Antivir. Res.* 1996, 33, 1–9.

- Polito L, Bortolotti M, Farini V, Battelli MG, Barbieri L, Bolognesi A. Saporin induces multiple death pathways in lymphoma cells with different intensity and timing as compared to ricin. *Int J Biochem Cell Biol.* 2009(a); 41(5):1055-61.
- Polito L, Bortolotti M, Farini V, Pedrazzi M, Tazzari PL, Bolognesi A. ATG-saporin-S6 immunotoxin: a new potent and selective drug to eliminate activated lymphocytes and lymphoma cells. *Br J Haematol.* 2009(b); 147(5):710-8.
- Polito L, Bortolotti M, Maiello S, Battelli MG, Bolognesi A. Plants Producing Ribosome-Inactivating Proteins in Traditional Medicine. *Molecules.* 2016b; 21(11). Review.
- Polito L, Bortolotti M, Pedrazzi M, Bolognesi A. Immunotoxins and other conjugates containing saporin-s6 for cancer therapy. *Toxins (Basel).* 2011; 3(6):697-720.
- Polito L, Bortolotti M, Pedrazzi M, Mercatelli D, Battelli MG, Bolognesi A. Apoptosis and necroptosis induced by stenodactylin in neuroblastoma cells can be completely prevented through caspase inhibition plus catalase or necrostatin-1. *Phytomedicine.* 2016a; 23(1):32-41.
- Polito L, Bortolotti M, Mercatelli D, Mancuso R, Baruzzi G, Faedi W, Bolognesi A. Protein synthesis inhibition activity by strawberry tissue protein extracts during plant life cycle and under biotic and abiotic stresses. *Int. J. Mol. Sci.* 2013a; 14, 15532-15545.
- Puri M, Kaur I, Perugini MA, Gupta RC. Ribosome-inactivating proteins: current status and biomedical applications. *Drug Discov Today.* 2012; 17(13 14):774-83.
- Rajamohan F, Pugmire MJ, Kurinov IV, Uckun FM. Modeling and alanine scanning mutagenesis studies of recombinant pokeweed antiviral protein. *J Biol Chem.* 2000; 275(5):3382-90.
- Rajamohan F, Kurinov IV, Venkatachalam TK, Uckun FM. Deguanlylation of human immunodeficiency virus (HIV)-1 RNA by recombinant pokeweed antiviral protein. *Biochem. Biophys. Res. Commun.* 1999; 263, 419-424.
- Rao PV, Jayaraj R, Bhaskar AS, Kumar O, Bhattacharya R, Saxena P, Dash PK, Vijayaraghavan R. Mechanism of ricin-induced apoptosis in human cervical cancer cells. *Biochem Pharmacol.* 2005; 69(5):855-65.
- Ready MP, Adams RP, Robertus JD. Dodecandrin, a new ribosome-inhibiting protein from *Phytolacca dodecandra*. *Biochim. Biophys. Acta.* 1984; 791 (3): 314-9.
- Ready MP, Brown DT, Robertus JD. Extracellular localization of pokeweed antiviral protein. *Proc Natl Acad Sci U S A.* 1986; 83(14):5053-6.
- Ready MP, Kim Y, Robertus JD. Site-directed mutagenesis of ricin A-chain and implications for the mechanism of action. *Proteins.* 1991; 10(3):270-8.
- Reinbothe S, Reinbothe C, Lehmann J, Becker W, Apel K, Parthier B. JIP 60 a methyl jasmonate-induced ribosome-inactivating protein involved in plant stress reactions. *Proc Natl Acad Sci USA.* 1994; 91:7012-7016.
- Rennie DP, McGregor AM, Wright J, Weetman AP, Hall R, Thorpe P. An immunotoxin of ricin A chain conjugated to thyroglobulin selectively suppresses the antithyroglobulin autoantibody response. *Lancet.* 1983; 2(8363):1338-40.

- Roberts LM, Lamb FI, Pappin DJ, Lord JM. The primary sequence of Ricinus communis agglutinin. Comparison with ricin. *J Biol Chem.* 1985; 260(29):15682-6.
- Robertus JD, Monzingo AF. The structure of ribosome inactivating proteins. *Mini Rev Med Chem.* 2004; 4(5):477-86. Review.
- Rojo MA, Yato M, IshiiMinami N, Minami E, Kaku H, Citores L, Girbes T, Shybuya N. Isolation, cDNA cloning, biological properties and carbohydrate binding specificity of sieboldin-b, a type II ribosome inactivating protein from the bark of Japanese elderberry (*Sambucus sieboldiana*). *Arch. Biochem. Biophys.* 1997; 340, 185-190.
- Rojo MA, Citores L, Arias FJ, Ferreras JM, Jimenez P, Girbés T. cDNA molecular cloning and seasonal accumulation of an ebulin 1-related dimeric lectin of dwarf elder (*Sambucus ebulus* L) leaves. *Int J Biochem Cell Biol.* 2003; 35(7):1061-5.
- Roncuzzi L, Gasperi-Campani A. DNA-nuclease activity of the single-chain ribosome-inactivating proteins dianthin 30, saporin 6 and gelonin. *FEBS Lett.* 1996; 392(1):16-20.
- Rosenblum M. Immunotoxins and toxin constructs in the treatment of leukemia and lymphoma. *Adv. Pharmacol.* 2004;51: 209–228.
- Rutenber E, Ready M, Robertus JD. Structure and evolution of ricin B chain. *Nature.* 1987; 326(6113):624-6. PubMed PMID: 3561502.
- Rutenber E, Katzin BJ, Collins EJ, Mlsna D, Ready MP, Robertus JD. Crystallographic refinement of ricin to 2.5 Å. *Protein.* 1991; 240-250.
- Sandvig K, van Deurs B. Delivery into cells: lessons learned from plant and bacterial toxins. *Gene Ther.* 2005; 12(11):865-72.
- Sandvig K, van Deurs B. Endocytosis, intracellular transport, and cytotoxic action of Shiga toxin and ricin. *Physiol Rev.* 1996; 76(4):949-66. Review.
- Saxena N, Rao PV, Bhaskar AS, Bhutia YD. Protective effects of certain pharmaceutical compounds against abrin induced cell death in Jurkat cell line. *Int Immunopharmacol.* 2014; 21(2):412-25.
- Schmelzer GH, Gurib-Fakim. *A Plant Resources of Tropical Africa. Medicinal plants* PROTA Foundation, Backhuys Publishers, Leiden, Netherlands/CTA, Wageningen. 2008; 34-37.
- Schrot J, Weng A and Melzig F.M. Ribosome-Inactivating and Related Proteins. *Toxins* 2015; 7, 1556-1615.
- Sestili P, Alfieri R, Carnicelli D, Martinelli C, Barbieri L, Stirpe F, Bonelli M, Petronini PG, Brigotti M. Shigatoxin 1 and ricin inhibit the repair of H<sub>2</sub>O<sub>2</sub>-induced DNA single strand breaks in cultured mammalian cells. *DNA Repair (Amst).* 2005; 4(2):271-7.
- Shahidi-Noghabi S, Van Damme EJ, Iga M, Smagghe G. Exposure of insect midgut cells to *Sambucus nigra* L. agglutinins I and II causes cell death via caspase-dependent apoptosis. *J Insect Physiol.* 2010; 56(9):1101-7.
- Shih SF, Wu YH, Hung CH, Yang HY, Lin JY. Abrin triggers cell death by inactivating a thiol-specific antioxidant protein. *J. Biol. Chem.* 2001; 276, 21870-21877.

- Siena S, Lappi DA, Bregni M, Formosa A, Villa S, Soria M, Bonadonna G, Gianni AM. Synthesis and characterization of an antihuman T-lymphocyte saporin immunotoxin (OKT1-SAP) with in vivo stability into nonhuman primates. *Blood*. 1988; 72(2):756-65.
- Sikiwal D, Ghosh P, Batra JK. Ribosome inactivating protein saporin induces apoptosis through mitochondrial cascade, independent of translation inhibition. *Int J Biochem Cell Biol*. 2008; 40(12):2880-8.
- Skyler JS, Lorenz TJ, Schwartz S, Eisenbarth GS, Einhorn D, Palmer JP, Mark JB, Greenbaum C, Saria E., Byers V. Effects of an anti-CD5 immunoconjugate (CD5-plus) in recent onset type I diabetes mellitus: A preliminary investigation. The CD5 Diabetes Project Team. *J. Diabetes Complicat*. 1993, 7, 224–232.
- Smith WE, Kane AV, Campbell ST, Acheson DW, Cochran BH, Thorpe CM. Shiga toxin 1 triggers a ribotoxic stress response leading to p38 and JNK activation and induction of apoptosis in intestinal epithelial cells. *Infect Immun*. 2003; 71(3):1497-504.
- Soler-Rodríguez AM, Ghetie MA, Oppenheimer-Marks N, Uhr JW, Vitetta ES. Ricin A-chain and ricin A-chain immunotoxins rapidly damage human endothelial cells: implications for vascular leak syndrome. *Exp Cell Res*. 1993; 206(2):227-34.
- Stafford FJ, Fleisher TA, Lee G, Brown M, Strand V, Austin HA, Balow JE, Klippel JH. A pilot study of anti-CD5 ricin A chain immunoconjugate in systemic lupus erythematosus. *J. Rheumatol*. 1994, 21, 2068–2070.
- Stillmark HP. Über Ricin, eingiftiges Ferment aus den Samen von Ricinus comm. L. und einigen anderen Euphorbiaceen. Inaug. Dissert. Dorpat. Estonia. 1888.
- Stirpe F, Bolognesi A, Bortolotti M, Farini V, Lubelli C, Pelosi E, Polito L, Dozza B, Strocchi P, Chambery A, Parente A, Barbieri L. Characterization of highly toxic type 2 ribosome-inactivating proteins from *Adenialanceolata* and *Adeniastenodactyla* (Passifloraceae). *Toxicon*. 2007; 50(1):94-105.
- Stirpe F, Battelli MG. Ribosome-inactivating proteins: progress and problems. *Cell. Mol. Life Sci*. 2006; 63: 1850–1866.
- Stirpe F. On the action of ribosome-inactivating proteins: are plant ribosomes species-specific? *Biochem J*. 1982; 202(1):279-80.
- Stirpe F. Ribosome-inactivating proteins. *Toxicon*. 2004; 44(4):371-83.
- Stirpe F. Ribosome-inactivating proteins: from toxins to useful proteins. *Toxicon*. 2013; 67:12-6. Review.
- Stirpe F, Bolognesi A, Bortolotti M, Farini V, Lubelli C, Pelosi E, Polito L, Dozza B, Strocchi P, Chambery A, Parente A, Barbieri L. Characterization of highly toxic type 2 ribosome-inactivating proteins from *Adenia lanceolata* and *Adenia stenodactyla* (Passifloraceae). *Toxicon*. 2007; 50(1):94-105.
- Stirpe F, Barbieri L, Gorini P, Valbonesi P, Bolognesi A, Polito L. Activities associated with the presence of ribosome-inactivating proteins increase in senescent and stressed leaves. *FEBS Lett*. 1996; 382, 309–312.
- Strand V, Lipsky PE, Cannon GW, Calabrese LH, Wiesenhutter C, Cohen SB, Olsen NJ, Lee ML, Lorenz TJ, Nelson B. Effects of administration of an anti-CD5 plus

- immunoconjugate in rheumatoid arthritis. Results of two phase II studies. The CD5 plus rheumatoid arthritis investigators group. *Arthritis Rheum.* 1993, 36, 620–630.
- Strocchi P, Barbieri L, Stirpe F. Immunological properties of ribosome-inactivating proteins and a saporin immunotoxin. *J Immunol Methods.* 1992; 155(1):57-63.
- Szalai K, Scholl I, Forster-Waldl E, Polito L, Bolognesi A, Untersmayr E, et al. Occupational sensitization to ribosome-inactivating proteins in researchers. *ClinExp Allergy.* 2005; 35:1354–60.
- Talkmore N, van'tKlooster CIEA, deJong JTVM, VanderWesthuizen JH. Medicinal plants used by traditional healers for the treatment of malaria in the Chipinge district in Zimbabwe. *Journal of Ethnopharmacology.* 2015; 224–237.
- Tanida I, Ueno T, Kominami E. LC3 and Autophagy. *Methods Mol Biol.* 2008; 445:77-88.
- Tazzari PL, Polito L, Bolognesi A, Pistillo MP, Capanni P, Palmisano GL, Lemoli RM, Curti A, Biancone L, Camussi G, Conte R, Ferrara GB, Stirpe F. Immunotoxins containing recombinant anti-CTLA-4 single-chain fragment variable antibodies and saporin: in vitro results and in vivo effects in an acute rejection model. *J Immunol.* 2001; 167(8):4222-9.
- Tejero J, Jiménez P, Quinto EJ, Cordoba-Diaz D, Garrosa M, Cordoba-Diaz M, Gayoso MJ, Girbés T. Elderberries: A Source of Ribosome-Inactivating Proteins with Lectin Activity. *Molecules.* 2015; 20(2):2364-2387. Review.
- Tomlinson JA, Walker VM, Flewett TH, Barclay GR. The inhibition of infection by cucumber mosaic virus and influenza virus by extracts from *Phytolacca americana*. *J Gen Virol.* 1974; 22(2):225-32.
- Tumer NE, Hwang DJ, Bonness M. C-terminal deletion mutant of pokeweed antiviral protein inhibits viral infection but does not dephosphorylate host ribosomes. *Proc. Natl. Acad. Sci.* 1997; 94, 3866–3871.
- Tumer NE, Hudak K, Di R, Coetzer C, Wang P, Zoubenko O. Pokeweed antiviral protein and its applications. *Curr. Top. Microbiol. Immunol.* 1999; 240, 139–158.
- Uckun FM, Rajamohan F, Pendergrass S, Ozer Z, Waurzyniak B, Mao C. Structure based design and engineering of a nontoxic recombinant pokeweed antiviral protein with potent anti-human immunodeficiency virus activity. *Antimicrob Agents Chemother.* 2003; 47(3):1052-61.
- Vago R, Marsden CJ, Lord JM, Ippoliti R, Flavell DJ, Flavell SU, Ceriotti A, Fabbrini MS. Saporin and ricin A chain follow different intracellular routes to enter the cytosol of intoxicated cells. *FEBS J.* 2005; 272(19):4983-95.
- Vallera DA, Ash RC, Zanjani ED, Kersey JH, LeBien TW, Neville DM Jr, Youle RJ. Anti-T-cell reagents for human bone marrow transplantation: Ricin linked to three monoclonal antibodies. *Science.* 1983, 222, 512–515.
- Vallera DA, Youle RJ, Neville DM Jr, Kersey JH. Bone marrow transplantation across major histocompatibility barriers. V. Protection of mice from lethal graft-vs.-host disease by pretreatment of donor cells with monoclonal anti-Thy-1.2 coupled to the toxin ricin. *J. Exp. Med.* 1982, 155, 949–954.

- Van Damme EJ, Hao Q, Charels D, Barre A, Rougé P, Van Leuven F, Peumans WJ. Characterization and molecular cloning of two different type 2 ribosome-inactivating proteins from the monocotyledonous plant *Polygonatum multiflorum*. *Eur J Biochem*. 2000; 267(9):2746-59.
- Van Damme EJM, Hao Q, Chen Y, Barre A, Vandebussche F, Desmyter S, Rougé P, Peumans WJ. Ribosome-inactivating proteins: a family of plant proteins that do more than inactivate ribosomes. *Crit Rev Plant Sci*. 2001; 20:395-465.
- Van Deurs B, Sandvig K, Petersen OW, Olsnes S, Simons K, Griffiths G. Estimation of the amount of internalized ricin that reaches the trans-Golgi network. *J Cell Biol*. 1988; 106(2):253-67.
- Vater CA, Bartle LM, Leszyk JD, Lambert JM, Goldmacher VS. Ricin A chain can be chemically cross-linked to the mammalian ribosomal proteins L9 and L10e. *J Biol Chem*. 1995; 270, 12933-12940.
- Villafranca JE, Robertus JD. Ricin B chain is a product of gene duplication. *J Biol Chem*. 1981; 256(2):554-6.
- Vivanco JM, Savary BJ, Flores HE. Characterization of two novel type I ribosome-inactivating proteins from the storage roots of the Andean crop *Mirabilis expansa*. *Plant Physiol*. 1999; 119, 1447-1456.
- Volkman DJ, Ahmad A, Fauci AS, Neville DM Jr. Selective abrogation of antigen-specific human B cell responses by antigen-ricin conjugates. *J Exp Med*. 1982; 156(2):634-9.
- Walsh MJ, Dodd JE, Hautbergue GM. Ribosome-inactivating proteins: potent poisons and molecular tools. *Virulence*. 2013; 4(8):774-84.
- Walsh TA, Morgan AE, Hey TD. Characterization and molecular cloning of a proenzyme form of a ribosome-inactivating protein from maize. Novel mechanism of proenzyme activation by proteolytic removal of a 2.8-kilodalton internal peptide segment. *J Biol Chem*. 1991; 5;266(34):23422-7.
- Wang BZ, Zou WG, Liu WY, Liu XY. The lower cytotoxicity of cinnamomin (a type II RIP) is due to its B-chain. *Arch Biochem Biophys*. 2006; 451(1):91-6.
- Wang D, Li Q, Hudson W, Berven E, Uckun F, Kersey JH. Generation and characterization of an anti-CD19 single-chain Fv immunotoxin composed of Cterminal disulfide-linked dgRTA. *Bioconjug Chem*. 1997;8:878-884.
- Wang H, Song S, Kou G, Li B, Zhang D, Hou S, Qian W, Dai J, Tian L, Zhao J, Guo Y. Treatment of hepatocellular carcinoma in a mouse xenograft model with an immunotoxin which is engineered to eliminate vascular leak syndrome. *Cancer Immunol Immunother*. 2007; 56(11):1775-83.
- Weldon JE, Xiang L, Zhang J, Beers R, Walker DA, Onda M, Hassan R, Pastan I. A recombinant immunotoxin against the tumor-associated antigen mesothelin reengineered for high activity, low off-target toxicity, and reduced antigenicity. *Mol Cancer Ther*. 2013; 12(1):48-57.
- Weyergang A, Selbo PK, Berstad ME, Bostad M, Berg K. Photochemical internalization of tumor-targeted protein toxins. *Lasers Surg Med*. 2011; 43(7):721-33.

- Wiley RG, Kline RH IV. Neuronal lesioning with axonally transported toxins. *Neurosci Methods* 2000; 103:73–82.
- Wiley RG, Oeltmann TN. Anatomically selective peripheral nerve ablation using intraneural ricin injection. *J Neurosci Methods*. 1986; 17(1):43-53.
- Wiley RG. Neural lesioning with ribosome-inactivating proteins: Suicide transport and immunolesioning. *Trends Neurosci*. 1992, 15, 285–290.
- Wiley RG. Substance P receptor-expressing dorsal horn neurons: Lessons from the targeted cytotoxin, substance P-saporin. *Pain*. 2008, 136, 7–10.
- Wiley RG.; Stirpe, F. Modeccin and volkensin but not abrin are effective suicide transport agents in rat CNS. *Brain Res*. 1988, 438, 145–154.
- Xu X, Yan H, Chen J, Zhang X. Bioactive proteins from mushrooms. *Biotechnol Adv*. 2011; 29(6):667-74.
- Yadav RK, Chae SW, Kim HR, Chae HJ. Endoplasmic reticulum stress and cancer. *J Cancer Prev*. 2014; 19(2):75-88.
- Yamamoto T, Iwasaki Y, Konno H, Kudo H. Primary degeneration of motor neurons by toxic lectins conveyed from the peripheral nerve. *J. Neurol. Sci*. 1985; 70, 327-337.
- Yamasaki C, Nishikawa K, Zeng X.T, Katayama Y, Natori Y, Komatsu N, Oda T, Natori Y. Induction of cytokines by toxins that have an identical RNA N-glycosidase activity: Shiga toxin, ricin, and modeccin. *BiochimBiophysActa*. 2004; 1671:44–50.
- Yan X, Hollis T, Svinth M, Day P, Monzingo AF, Milne GW, Robertus JD. Structure-based identification of a ricin inhibitor. *J Mol Biol*. 1997; 266(5):1043-9.
- Zamboni M, Brigotti M, Rambelli F, Montanaro L, Sperti S. High-pressure-liquid-chromatographic and fluorimetric methods for the determination of adenine released from ribosomes by ricin and gelonin. *Biochem J*. 1989; 259(3):639-43.
- Zarling JM, Moran PA, Haffar O, Sias J, Richman DD, Spina CA, Myers DE, Kuebelbeck V, Ledbetter JA, Uckun FM. Inhibition of HIV replication by pokeweed antiviral protein targeted to CD4+ cells by monoclonal antibodies. *Nature*. 1990; 347(6288):92-5.
- Zhang B, Huang H, Xie J, Xu C, Chen M, Wang C, Yang A, Yin Q. Cucurmosin induces apoptosis of BxPC-3 human pancreatic cancer cells via inactivation of the EGFR signaling pathway. *Oncol Rep*. 2012; 27(3):891-7.
- Zhang C., Gong Y., Ma H., An C., Chen D., Chen Z.L. Reactive oxygen species involved in trichosanthin-induced apoptosis of human choriocarcinoma cells. *Biochem J*. 2001; 355(Pt3),653-661.
- Zhou X, Li XD, Yuan JZ, Tang ZH, Liu WY. Toxicity of cinnamomin a new type II ribosome-inactivating protein to bollworm and mosquito. *Insect Biochem. Mol. Biol*. 2000; 30, 259–264.
- Zoubenko O, Uckun F, Hur Y, Chet I, Tumer N. Plant resistance to fungal infection induced by nontoxic pokeweed antiviral protein mutants. *Nat Biotechnol*. 1997; 15(10):992-6.